Mathematical Biosciences and Engineering

http://www.aimspress.com/journal/MBE

MBE, 23(8): 2516–2580.
DOI: 10.3934/mbe.2026092
Received: 21 April 2026
Revised: 17 June 2026
Accepted: 06 July 2026
Published: 18 August 2026

Research article

Multi-seasonal modelling of Carica papaya and *Paracoccus marginatus* interactions under climate change

Martin Dountio[1,2,3,*], **Maximilien Onana**[1] **and Samuel Bowong**[1,2,3]

[1] Faculty of Science, Dept. of Mathematics and Computer Science, University of Douala, PO Box 24157, Douala, Cameroon

[2] IRD, Sorbonne University, UMMISCO, F-93143, Bondy, France

[3] Living Systems Modelling Group (LiSMoG), University of Douala, PO Box 24157, Douala, Cameroon

* **Correspondence:** Email: martinodountio@gmail.com; Tel: +237698316350.

Abstract: The papaya mealybug, *Paracoccus marginatus*, has emerged as a formidable threat to global tropical agriculture, capable of inducing devastating yield losses through its invasive sap-sucking behavior. While conventional models often overlook environmental complexities, in this study, we introduced a sophisticated multi-seasonal mathematical framework designed to unravel the intricate interplay between mealybug population dynamics, fluctuating climatic conditions, and the persistence of off-season natural reservoirs. Sensitivity analysis highlighted how parameter influences shift across seasons, while our qualitative analysis revealed a dual-threshold mechanism, governed by the local offspring number $\mathcal{N}_0$ and the global stability threshold $\mathcal{N}_g$, as the definitive driver of the system's long-term evolution. While $\mathcal{N}_0 < 1$ analytically ensures local asymptotic stability, our theoretical discussion suggested the existence of a conjectured regime of bistability within the threshold range $\mathcal{N}_g < \mathcal{N}_0 < 1$. This finding highlighted a critical regime where the success of eradication efforts is strictly contingent upon the initial infestation levels. Furthermore, by employing uniform persistence theory, we proved that the pest inevitably establishes a permanent foothold whenever $\mathcal{N}_0 > 1$. To mitigate these agricultural losses, we evaluated the efficacy of two distinct intervention frameworks: (i) Pulsed biological control via impulsive parasitoid releases and (ii) a synergistic integrated pest management (IPM) strategy combining biopesticides with natural enemies. Our simulations demonstrated that while impulsive parasitoid releases alone achieved substantial suppression, reducing immature and mature female populations by 89.35% and 93.04%, respectively, and recovering 75.92% of papaya production, the integrated approach proved transformative. By synchronizing biopesticide applications with parasitoid pulses, mealybug populations were nearly decimated, with reduction rates reaching 99.70% for immatures and an exhaustive 99.90% for adults. Although this intensive suppression yielded a 44.92% increase in net productivity, its primary value

lies in providing a robust, non-linear pathway toward total pest eradication, effectively breaking the cycle of reinfestation.

Keywords: *Paracoccus marginatus*; parasitoids; multi-seasonal model; papaya reservoir; stability; bistability

1. Introduction

Papaya (*Carica papaya*) is a tropical fruit that has commercial importance because of its high nutritional and medicinal value. Papaya cultivation had its origin in southern Mexico and Costa Rica. Total annual world production is estimated at 6 million tonnes of fruits.

India leads the world in papaya production with an annual output of about 3 million tonnes. Other leading producers include Brazil, Mexico, Nigeria, Indonesia, China, Peru, Thailand, and the Philippines [1]. In Cameroon, *C. papaya* is cultivated primarily in the humid forests of the littoral zone (Njombe-Pendja), where ecological conditions, including an equatorial climate, altitudes of 20 to 500 m, average temperatures around 30°C, rainfall of approximately 2350 mm, and volcanic soils, are highly favorable. Despite its potential, national production remains limited, estimated at 700 tonnes over 25 hectares. Exports are minimal (36 tonnes, according to Eurostat, 2020), consisting mainly of dried products, even though the fruit is included in government strategies for agricultural export diversification [2].

Papaya production faces numerous constraints, among which insect pests represent a major biotic challenge. These pests adversely affect crop growth, development, and yield, often leading to plant decline and necessitating intensive pesticide use [3]. Although several insects infest papaya, the papaya mealybug, *Paracoccus marginatus*, a sap-sucking insect belonging to the order Hemiptera, is now considered one of the most serious threats to its cultivation worldwide [4]. First reported in India in 2008 in Tamil Nadu (Coimbatore, Thiruppur, Erode, and Dindigul districts) [5], *P. marginatus* has since spread rapidly to other key papaya-growing states, including Kerala, Karnataka, Andhra Pradesh, Maharashtra, Tripura, and Odisha [6]. The pest damages papaya by feeding on sap from leaves, stems, and fruits using its piercing-sucking mouthparts. This feeding weakens the plant, stunts its growth, and reduces fruit production [7].

The damage caused by *P. marginatus* is multifaceted. Direct sap extraction leads to plant weakening, stunted growth, yield loss, and, in severe cases, plant death. In addition, mealybugs excrete honeydew, a sugary substance that promotes the growth of sooty mold. This black fungal coating interferes with photosynthesis, further compromising plant health and productivity [8]. The economic impact of *P. marginatus* infestations in India has been severe. Studies report yield losses ranging from 10% to 60% in various regions, reaching as high as 91% under heavy infestation pressure [9]. These losses, combined with increased control costs and reduced fruit quality, result in considerable economic damage to growers.

Given its rapid spread and destructive potential, *P. marginatus* poses a persistent threat to sustainable papaya production in India and other affected regions. While multiple control options including biopesticides are available, a deeper understanding of the pest's population dynamics remains essential [8].

There are several ways of controlling papaya mealybug, including the use of biopesticides. Biopesticides are products derived from natural sources, such as plant extracts, essential oils, or microorganisms, which are used to control pests in an environmentally friendly way. One biopesticide commonly used against papaya mealybug is neem oil. Neem oil is extracted from the seeds of the neem tree (*Azadirachta indica*) and contains compounds that act as insecticides. They can be sprayed on infested parts of the plant to kill mealybugs and prevent their reproduction [10]. Another biopesticide used against papaya mealybug is pyrethrum, extracted from the flowers of certain chrysanthemum species. Pyrethrum acts as an insecticide by disrupting the insects' nervous system. However, the use of biopesticides also has certain disadvantages. They may be less persistent than chemical pesticides, meaning they need to be applied more frequently to maintain their effectiveness. Their effectiveness can also vary according to environmental conditions and pest susceptibility, and some biopesticides can be costly to produce and apply [11].

In addition to biopesticides, biological control using natural enemies has proven to be one of the most sustainable and effective strategies against *P. marginatus*. Several parasitoid species, particularly *Acerophagus papayae*, *Anagyrus loecki*, and *Pseudleptomastix mexicana*, have been introduced and successfully established in various regions, including India, the Caribbean, and West Africa, resulting in significant reductions of mealybug populations [12, 13]. These parasitoids attack the immature stages (mainly nymphs and young females) of the mealybug, thereby naturally regulating their populations without harmful impacts on the environment [11]. The integration of these parasitoids with biopesticide applications represents an effective integrated pest management (IPM) strategy for sustainable papaya production.

Climate change plays a crucial role in the development and reproduction of *P. marginatus*. Like many organisms, this bacterium has an optimum temperature range within which it develops and reproduces optimally: *P. marginatus* can develop and complete its life cycle between 18 $^{\circ}C$ and 30 $^{\circ}C$. The estimated minimum temperature thresholds for the adult males and females are 14.5 $^{\circ}C$ and 13.9 $^{\circ}C$, respectively, while the estimated optimum and maximum temperature thresholds are 28.7 $^{\circ}C$ and 31.9 $^{\circ}C$, respectively, for males and for adult females they are 28.4 $^{\circ}C$ and 32.1 $^{\circ}C$ respectively [14]. Rainfall also has an impact on plant growth dynamics. Papaya plants are very sensitive to drought, and water stress results in a lack of fruiting. Requirements vary from 50 to 120 mm per month [1].

Mathematical modeling has become an essential tool for studying plant-insect interactions. Moreover, mathematical models help analyze the underlying mechanisms of plant-insect interactions, study the impact of environmental factors on these interactions, and assess the effectiveness of control strategies [15]. In this respect, multi-seasonal mathematical models are particularly useful for studying plant-insect interactions throughout several seasons. These models take into account seasonal variations in insect and plant density, as well as interactions between these populations over time. There is a study in the literature entailing multi-seasonal modeling of pest dynamics [16]. In particular, the researchers in [16] proposed and analyzed a mathematical multi-seasonal model in which the dynamics of *Radopholus similis* were controlled through the use of fallow periods and pesticide applications. In addition, other semi-discrete frameworks based on impulsive differential equations have been developed to capture pest-fruit interactions over successive cropping seasons. However, the models available in the literature, including that of [16], do not account for important ecological aspects such as the fruit maturation period, the presence of natural pest reservoirs, and their

natural enemies.

The dynamics of *P. marginatus* is complex due to its adaptability and resistance to environmental stresses, such as drought, heat, and pesticides. Mathematical models studying the population dynamics of *P. marginatus* are scarce. There are only two works in the literature entailing this: [17, 18]. The researchers in [17] proposed a mathematical model to understand the influence of temperature variation on the dynamics of this papaya mealybug. They showed that temperature is crucial in the evolution of this population. However, this model does not incorporate biocontrol strategies, and simplifies the feedback between pests and plants. In reference [18], the researchers proposed a model integrating the effects of temperature and biocontrol strategies on the population dynamics of *P. marginatus*. They demonstrated that control strategies implemented against this papaya mealybug can contribute to a substantial reduction in population size within a papaya plantation. However, these works are limited to a single season and do not take into account other climatic variables, such as humidity and precipitation, the link between the production of flowers by papaya plants that give papaya fruits, and the crown of papaya plants (the upper cluster of young leaves and growing point) and the reservoir of *P. marginatus* (alternative host plants serving as refuge and breeding sites for the mealybug). These ecological facts cannot be neglected in the mathematical modeling of the interaction between papaya plants and *P. marginatus*.

Our objective of this paper is to study the complex interaction between *P. marginatus*, papaya plants over multiple cropping seasons, the natural reservoir, and parasitoids of mealybugs and biopesticides. To achieve this goal, we first propose a delay mathematical multi-seasonal model that takes into account the temperature and rainfall variations and the time delay during the maturity of fruits. We present the theoretical and numerical analysis of the model. More precisely, we study the well-posedness of the model, such as the existence and uniqueness of solutions, the positivity of solutions, and the boundedness of trajectories. We employ the eFAST method to conduct a global sensitivity analysis, pinpointing the key seasonal parameters that dictate system behavior. We derive the pest-free periodic solution and characterize its stability through the local offspring number, $\mathcal{N}_0$, alongside a global dissipative threshold, $\mathcal{N}_g$. Our analysis establishes that the pest-free equilibrium is globally asymptotically stable within the feasible region Γ whenever the condition $\mathcal{N}_0 \leq \mathcal{N}_g < 1$ is satisfied, ensuring absolute eradication. However, we identify a more complex dynamical landscape in the regime where $\mathcal{N}_g < \mathcal{N}_0 < 1$. In this case, a regime of bistability is conjectured, where the long-term outcome depends strictly on the initial infestation level. Furthermore, by employing uniform persistence theory, we prove that the pest population persists indefinitely in the field whenever $\mathcal{N}_0 > 1$, signaling the irreversible establishment of the infestation. Our results show that the reservoir plays a crucial role in the pest's persistence, enabling insects to survive and reproduce during the intercropping period. In the absence of a reservoir, the pest population can be significantly reduced during the following harvest season. Numerical studies have revealed that the use of papaya mealybug parasitoids during the cropping period leads to a substantial reduction in the pest population, an increase in papaya production, and a decrease in mealybug density in the reservoir. We also define and implement two targeted control strategies based on the releases of parasitoids and the use of biopesticides aimed at reducing or eliminating the pest in a papaya plantation. We found that impulsive releases increased papaya production by 75.92% and reduced the number of immature and mature females by 89.35% and 93.04%, respectively. The combination of parasitoids and the use of biopesticides increased papaya production by 44.92% and reduced adult and immature pests

by 99.70% and 99.90%, respectively. This strategy shows promise in the fight against scale insects. Concerning the results obtained in [17] and [18], we overcome some limitations observed in these works by integrating full seasonal cycles with multiple climatic variables and considering more complex ecological dynamics. We introduce the feedback between the plant growth and infestation over multiple agricultural cycles while exploring the long-term effects of climate change, such as extreme weather events and their cumulative impacts on ecosystems. Furthermore, this model has been used to optimize seasonal management strategies, such as ideal windows for parasitoids release or biopesticide application, and we provide recommendations based on robust projections validated by multi-seasonal data series.

This paper is structured as follows: Section 2 outlines the model formulation, followed by a parametric sensitivity analysis in Section 3. Section 4 provides the mathematical analysis alongside numerical simulations that validate the analytical findings and highlight the role of the reservoir. Section 5 investigates the deployment of dual control strategies involving parasitoid release and biopesticide application. Section 6 concludes the paper.

2. Model framework

In this section, we provide the biological backgrounds of papaya and papaya mealybug that we use to formulate a multi-seasonal model of the complex interaction between papaya, *P. marginatus* and climate change.

2.1. Biological background

The growth of papaya (*Carica papaya*) is a complex dynamic process characterized by rapid development and continuous phenological overlap. While sophisticated physiological models exist to capture its intricate dynamics [19, 20], we distill the lifecycle into key functional stages to contextualize its interactions with the papaya mealybug, *P. marginatus*. As a large, herbaceous perennial, papaya exhibits a growth pattern that is indeterminate yet phenologically structured, making the understanding of its stages crucial for pest management modeling.

2.1.1. Seed germination and early seedling establishment

The cycle begins with seed germination, a phase highly dependent on temperature (optimal range of 20–30 $^{\circ}C$) and moisture. Germination typically occurs within 2 to 3 weeks post-sowing in a well-drained, sterile medium [21]. The seedling stage that follows is a critical period of high vulnerability. Lasting 3 to 4 months, the plant develops its initial root system and first true leaves. During this phase, seedlings are highly sensitive to abiotic stresses like waterlogging, drought, and extreme temperatures, as well as biotic threats such as damping-off fungi [21, 22]. The plant's resource allocation is primarily directed toward root establishment and leaf expansion, with minimal reserve capacity to withstand stress or pest attack.

2.1.2. Juvenile vegetative growth and canopy development

Following transplantation, the plant enters a phase of vigorous juvenile growth. Over the next 4–6 months, the papaya plant undergoes rapid apical growth, developing a semi-woody, hollow stem and a

large, palmate-leaf canopy. This stage is metabolically demanding, with high requirements for water, nutrients (particularly nitrogen and potassium), and solar radiation to support high photosynthetic rates [23]. The architecture of the canopy, specifically the density and size of the leaves in the crown, is formed during this period. This dense canopy not only defines the plant's productive potential but also creates the microhabitat characterized by shelter and high sap availability that is highly favorable for the establishment and proliferation of phloem-feeding pests like *P. marginatus*.

2.1.3. Reproductive phase transition and flowering

The transition to the reproductive phase is a pivotal moment in the papaya lifecycle, often occurring as early as 5–6 months after planting. This transition is regulated by internal hormonal cues and external environmental factors, particularly photoperiod and temperature [21]. Papaya exhibits a complex array of sexual systems, primarily dioecy (separate male and female plants) and hermaphroditism. The flowers are borne in axillary inflorescences. Pollination is entomophilous (primarily by hawkmoths and bees) or anemophilous, and the success of fruit set is heavily influenced by the interplay between the plant's sexual type and pollinator activity [24]. The plant now partitions resources between continued vegetative growth and the development of reproductive structures.

2.1.4. Fruit development, maturation, and source-sink dynamics

The fruiting phase represents the longest and most resource-intensive period. After successful pollination, fruit development takes approximately 5 to 9 months to reach full maturity. This phase is governed by strong source-sink relationships, where the leaves (sources) produce photoassimilates that are allocated to the developing fruits (major sinks) [20]. The fruits mature acropetally (from the base of the stem upwards), leading to a staggered harvest. The presence of developing fruit creates a strong draw on the plant's resources, which can reduce vegetative growth and potentially increase the plant's susceptibility to sap-sucking insects by altering the nutrient composition and pressure of the phloem sap [25]. The physical and physiological status of the plant during this stage is a key determinant of pest population dynamics and the economic impact of an infestation.

2.1.5. Senescence and ratooning (in perennial systems)

In commercial cultivation, papaya is often managed as an annual or a short-term perennial crop. Under perennial management, plants can undergo a phase of senescence and may be ratooned (cut back) to stimulate a new flush of vegetative growth for a second production cycle. However, yield and fruit quality typically decline in subsequent cycles, and pest pressures, including those from borers that attack the main stem, often intensify [26].

2.2. Model construction

Herein, we develop a multi-seasonal model for papaya-mealybug dynamics. The model construction is based on the following key assumptions, which are grounded in the biological background of the papaya plant and standard agricultural practices:

(1) **Seasonal climate pattern:** The papaya cultivation area experiences a clearly defined tropical climate with two distinct seasons: A wet season conducive to crop growth, and a dry season where cultivation activities are minimal.

(2) **Crop cycle synchronization:** The agricultural calendar is synchronized with the climate. The year of length $\mathcal{T}$ is subdivided into two periods:
   - The **cropping season** (wet season), of length $\eta < \mathcal{T}$, during which papaya plants are in the field. This period encompasses the later stages of the plant's development, from recently transplanted juveniles with established crowns through to the fruit-bearing adult phase, as described in Section 2.1.
   - The **inter-cropping season** (dry season), of length $\mathcal{T} - \eta$, which begins post-harvest and is a fallow period with no productive plants in the field.

(3) **Model state initialization:** The model initiates its simulation at the beginning of a cropping season, with the field populated by young papaya plants that have already developed a crown structure. This initial condition represents the transplanting of established seedlings from a nursery (typically 3–4 months old), making them immediately susceptible to mealybug infestation and aligning with the "Juvenile Vegetative Growth" stage described in the biological background.

(4) **Discrete management events:** The transitions between seasons are marked by discrete agricultural events:
   - At time $t = n\mathcal{T} + \eta$ (end of the n-th cropping season), a final harvest occurs.
   - Immediately following the harvest, at time t^+, a field cleaning event (e.g., destruction of crop residues) takes place. This practice is crucial for integrated pest management, as it drastically reduces the pest population by removing its primary habitat and food source, thereby breaking the pest's life cycle between cropping seasons.

Let $t_n = n\mathcal{T}$, where $n \in \mathbb{N}$ is the year index. The timeline for one annual cycle (n-th year) is thus: - **Cropping season:** $t \in [t_n, t_n + \eta)$ - **Harvest & Field cleaning:** $t = t_n + \eta$ (discrete event) - **Inter-cropping season:** $t \in (t_n + \eta, t_{n+1}]$.

2.2.1. The cropping season

The cropping season is initiated by the emergence of mealybugs in the field. We consider four major phenological phases of the papaya plant: leaves ($L_1(t)$), flowers ($F(t)$), healthy fruits ($S(t)$), and infected fruits ($I(t)$). The pest population is structured into immature ($L(t)$) and adult ($A(t)$) stages, while $P_r(t)$ represents the parasitoids population.

The model is based on the following biological assumptions:

(i) The number of eggs laid is proportional to the number of adult females present.
(ii) Egg development is regulated by a carrying capacity dependent on available resources.
(iii) Mealybugs primarily feed on fruits during the cropping season.
(iv) Fruit consumption reduces mealybug mortality but does not eliminate it completely.
(v) Papaya harvesting occurs predominantly once a year.
(vi) We assume that the parasitoids recruitment term, Λ_p, which corresponds to the introduction of new sexually mature parasitoïds into the population, occurs through a series of periodic releases over the year. The total annual recruitment is uniformly divided into m releases of size Λ_p/m, with a constant time interval of $(\mathcal{T} - \eta)/m$ between consecutive releases.

(vii) During the active growing season, the commercial papaya plantation provides an optimal and abundant food resource. Due to the highly localized and sedentary nature of *P. marginatus* feeding clusters once established on premium hosts, directional emigration from the natural reservoir back to the field is assumed to be biologically negligible compared to the explosive, internal demographic dynamics within the crop.

The leaf compartment $L_1(t)$ represents the photosynthetic engine of the papaya plant. Its growth is driven by a precipitation-dependent rate $\alpha(P(t))$, where $P(t)$ denotes the time-dependent rainfall, reflecting the crucial influence of water availability on vegetative development [27]. The logistic growth term, $\alpha(P(t))L_1(t)\left(1-\frac{L_1(t)}{K_{L_1}}\right)$, models self-shading and competition for internal resources (e.g., nutrients, space), where K_{L_1} is the maximum sustainable leaf biomass. Losses occur due to natural senescence and abiotic stress at a temperature-dependent rate $\mu_{L_1}(T(t))$, where $T(t)$ represents the ambient temperature over time [28]. These considerations lead to the following differential equation:

$$\frac{dL_1}{dt} = \alpha(P(t))L_1(t)\left(1-\frac{L_1(t)}{K_{L_1}}\right) - \mu_{L_1}(T)L_1(t). \tag{2.1}$$

The flower population, $F(t)$ is produced from the leaf biomass at a temperature-dependent rate $\beta(T(t))$. The logistic term, $\beta(T(t))L_1(t)\left(1-\frac{F(t)}{K_F}\right)$, captures the finite carrying capacity for flowers, K_F, constrained by the plant's energy budget and physical space for inflorescences. Flowers either mature into fruits at a temperature-dependent rate $\nu_F(T(t))$ or are abscised due to poor pollination or environmental stress at a rate $\mu_F(T(t))$ [27, 28]. Thus, the evolution of flowers biomass over time is given by :

$$\frac{dF}{dt} = \beta(T(t))L_1(t)\left(1-\frac{F(t)}{K_F}\right) - (\nu_F(T(t)) + \mu_F(T(t)))F(t). \tag{2.2}$$

The healthy fruit population, $S(t)$, increases due to the maturation of flowers at a temperature-dependent rate $\nu_F(T(t))$, where $T(t)$ represents the ambient temperature over time, which heavily dictates the conversion efficiency from flowers to harvestable fruits [27]. The primary loss mechanism is infestation by mealybugs. The force of infection is modeled by the term $\frac{\gamma\psi A(t-\tau)S(t-\tau)}{N(t-\tau)}$, where $N(t) = S(t) + I(t)$ is the total number of fruits. This represents a frequency-dependent transmission process: γ is the sting probability, ψ is the sting efficiency, and $A(t-\tau)/N(t-\tau)$ is the proportion of infective mealybugs per fruit at time $t-\tau$ [28]. The delay τ accounts for the latency period between the initial sting and the visible manifestation of infection. Healthy fruits also experience a natural loss or physiological drop at a temperature-dependent rate $\mu_S(T(t))$. The net dynamics of healthy fruits are therefore given by the following differential equation:

$$\frac{dS}{dt} = \nu_F(T(t))F(t) - \frac{\gamma\psi A(t-\tau)S(t-\tau)}{N(t-\tau)} - \mu_S(T(t))S(t). \tag{2.3}$$

The infected fruit population, $I(t)$, is recruited from healthy fruits that were successfully infested τ time units ago, as given by the force of infection term. Infected fruits experience two sources of loss: A baseline rate μ_I, and an additional density-dependent loss due to direct damage from feeding mealybugs, modeled by $\frac{dA(t)}{D+I(t)}$. This functional form represents a saturation effect, where d is the

maximum damage rate and D is the infected fruit density at which the damage is half-maximal, leading to the following expression:

$$\frac{dI}{dt} = \frac{\gamma\psi A(t-\tau)S(t-\tau)}{N(t-\tau)} - \left(\mu_I + \frac{dA(t)}{D+I(t)}\right)I(t). \tag{2.4}$$

The recruitment of immature mealybugs $L(t)$ follows a logistic growth function to reflect intra-specific competition for feeding and oviposition sites. The term $\varepsilon a A(t)\left(1 - \frac{L(t)}{K_L(T(t)) + \lambda_1 N(t)}\right)$ is central to this dynamic. The carrying capacity is dynamically augmented by the total fruit biomass, $N(t) = S(t) + I(t)$, becoming $K_L(T(t)) + \lambda_1 N(t)$. This formulation models the biological fact that host fruit availability directly increases the environmental capacity to support a larger immature pest population, where λ_1 quantifies this enhancement [28]. Losses occur due to maturation into adults at a temperature-dependent rate $\nu_L(T(t))$, natural mortality at a rate $\mu_L(T(t))$, and parasitism. Parasitism by *Acerophagus papayae* is modeled with a Holling Type II functional response, $\frac{\sigma L(t) P_r(t)}{L(t) + K_P}$, accounting for the handling time and saturating attack rate of the parasitoids, which represents the primary biological control agent regulating mealybug outbreaks [29]. Consequently, the larva population follows the dynamics given by the following differential equation:

$$\frac{dL}{dt} = \varepsilon a A(t)\left(1 - \frac{L(t)}{K_L(T(t)) + \lambda_1 N(t)}\right) - (\nu_L(T(t)) + \mu_L(T(t)))L(t) - \frac{\sigma L(t) P_r(t)}{L(t) + K_P}. \tag{2.5}$$

The adult mealybug population, $A(t)$, is fueled by the maturation of immatures at a temperature-dependent rate $\nu_L(T(t))$. The mortality rate of adults is modulated by resource availability and host plant quality. The baseline mortality $\mu_A(T(t))$ is reduced by fruit availability, modeled by the term $\frac{\mu_A(T(t))}{1 + \lambda_2 N(t)}$, where λ_2 represents the mortality reduction benefit from feeding on optimal host tissue. Conversely, adult mortality is increased by the term $\frac{edI(t)}{D + I(t)}$, which models the fitness cost or elevated mortality experienced by adults feeding on low-quality, infected fruits, where e acts as a conversion scaling parameter, and D is the half-saturation constant for infected fruit density [29]. As a result, the adult mealybug dynamics are governed by the following differential equation:

$$\frac{dA}{dt} = \nu_L(T(t))L(t) - \left(\frac{\mu_A(T(t))}{1 + \lambda_2 N(t)} - \frac{edI(t)}{D + I(t)}\right)A(t). \tag{2.6}$$

The parasitoid dynamics, $P_r(t)$, include a constant external release rate, Λ_P. Their population grows via the numerical response to parasitism, $\frac{\nu\sigma L(t) P_r(t)}{L(t) + K_P}$, where ν is the conversion efficiency of hosts into new parasitoids. They experience a constant natural mortality rate, μ_{P_r}, yielding the final equation:

$$\frac{dP_r}{dt} = \Lambda_P + \frac{\nu\sigma L(t) P_r(t)}{L(t) + K_P} - \mu_{P_r} P_r(t). \tag{2.7}$$

Additionally, discrete control measures (e.g., sacking) are applied at times t_n, instantaneously reducing the pest and parasitoid populations by a factor ϕ_0:

$$P_r(t_n^+) = \phi_0 P_r(t_n), \quad L(t_n^+) = \phi_0 L(t_n), \quad A(t_n^+) = \phi_0 A(t_n). \tag{2.8}$$

The structure of the model is depicted in Figure 1.

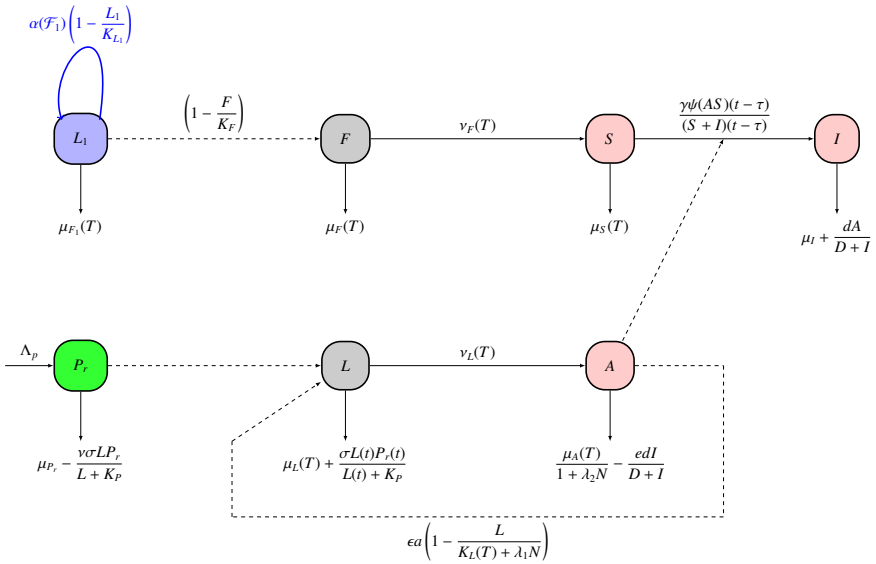

Figure 1. Structure of the model for $t \in [t_n,\ t_n + \eta)$.

Thus, from Figure 1, the infestation dynamics of *Carica papaya* by *P. marginatus* under the influence of parasotoids is described by the following hybrid system:

As illustrated in the flowchart of Figure 1, the infestation dynamics of *Carica papaya* by *P. marginatus* under the influence of parasitoids during the main cropping interval $t \in [t_n, t_n + \eta]$ is described by the following system:

$$\begin{cases} \dot{L_1}(t) &= \alpha(P(t))L_1(t)\left(1-\dfrac{L_1(t)}{K_{L_1}}\right)-\mu_{L_1}(T(t))L_1(t), \\ \dot{F}(t) &= \beta(T(t))L_1(t)\left(1-\dfrac{F(t)}{K_F}\right)-(\nu_F(T(t))+\mu_F(T(t)))F(t), \\ \dot{S}(t) &= \nu_F(T(t))F(t)-\dfrac{\gamma\psi A(t-\tau)S(t-\tau)}{N(t-\tau)}-\mu_S(T)S, \\ \dot{I}(t) &= \dfrac{\gamma\psi A(t-\tau)S(t-\tau)}{N(t-\tau)}-\left(\mu_I+\dfrac{dA(t)}{D+I(t)}\right)I(t), \\ \dot{L}(t) &= \varepsilon aA(t)\left(1-\dfrac{L(t)}{K_L(T(t))+\lambda_1(S(t)+I(t))}\right)-(\nu_L(T(t))+\mu_L(T(t)))L(t)-\dfrac{\sigma L(t)P_r(t)}{L(t)+K_P}, \\ \dot{A}(t) &= \nu_L(T(t))L(t)-\left(\dfrac{\mu_A(T(t))}{1+\lambda_2(S(t)+I(t))}-\dfrac{edI(t)}{D+I(t)}\right)A(t), \\ \dot{P}_r(t) &= \Lambda_P+\dfrac{\nu\sigma L(t)P_r(t)}{L(t)+K_P}-\mu_{P_r}P_r(t), \\ P_r(t_n^+) &= \phi_0 P_r(t_n),\ L(t_n^+) = \phi_0 L(t_n),\ A(t_n^+) = \phi_0 A(t_n). \end{cases} \tag{2.9}$$

For biological reasons, the initial conditions of the system (2.9) are chosen to be

$$\begin{aligned} &L_1(\theta)=\phi_1(\theta),\ F(\theta)=\phi_2(\theta),\ S(\theta)=\phi_3(\theta),\ I(\theta)=\phi_4(\theta), \\ &L(\theta)=\phi_5(\theta),\ A(\theta)=\phi_6(\theta) \text{ and } P_r(\theta)=\phi_7(\theta),\ \text{for } \theta\in[-\tau,t_n], \end{aligned} \tag{2.10}$$

where $\phi = (\phi_1(\theta), \phi_2(\theta), \phi_3(\theta), \phi_4(\theta), \phi_5(\theta), \phi_6(\theta), \phi_7(\theta)) \in C([-\tau, t_n], \mathbb{R}^7_{+0})$, with $C([-\tau, t_n], \mathbb{R}^7_{+0})$ is the

Banach space of continuous functions mapping the interval $[-\tau, t_n^+]$ into $\mathbb{R}^7_{+0}$ and

$$\mathbb{R}^7_{+0} = \left\{(x_1, x_2, x_3, x_4, x_5, x_6, x_7) \in \mathbb{R}^7 : \ x_i > 0, \ i = 1, 2, 3, 4, 5, 6, 7\right\}.$$

2.2.2. Transition from cropping season to inter-cropping season

Herein, we describe the associated physiological process.

The harvesting period represents a critical phase in the agricultural cycle, characterized by significant physiological changes in the papaya crop and associated pest populations. During the time intervals $t \in \left(t_n + \frac{j(\mathcal{T}-\eta)}{m}, t_n + \eta + \frac{j(\mathcal{T}-\eta)}{m}\right]$ for $j \in \{1, \ldots, m-1\}$, systematic harvesting operations are conducted. This phase involves substantial perturbations to the system, resulting in: Selective removal of fruits (both healthy and infected), mechanical damage to vegetative structures (leaves and flowers), and direct and indirect effects on pest populations across different life stages.

The population dynamics during harvesting are characterized by proportional reductions across compartments, as illustrated in Figure 2. The surviving fractions are defined as follows:

- π_{L_1}: Proportion of leaves remaining after harvesting-induced damage.
- π_F: Proportion of flowers remaining after harvesting-induced damage.
- ϕ_h: Control efficiency representing the fraction of pests eliminated during harvesting operations.
- ϕ_{P_r}: Survival rate of parasitoids during harvesting activities.

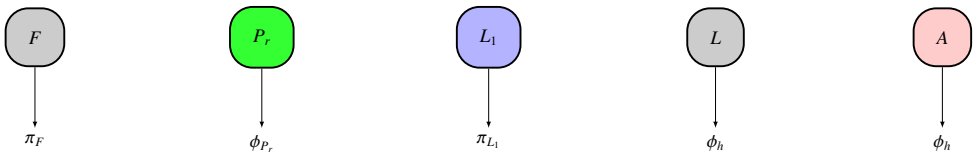

Figure 2. Structure of the model for $t = t_{n+\eta}$).

With this in mind, one obtains the following discrete equations:

$$\begin{cases} L_1((t_n+\eta)^+) = \pi_{L_1} L_1(t_{n+\eta}), \\ F((t_n+\eta)^+) = \pi_F F(t_{n+\eta}), \\ S((t_n+\eta)^+) = 0, \\ I((t_n+\eta)^+) = 0, \\ L((t_n+\eta)^+) = \phi_h L(t_{n+\eta}), \\ A((t_n+\eta)^+) = \phi_h A(t_{n+\eta}), \\ P_r\left(\left(t_{n+\eta} + \dfrac{j(\mathcal{T}-\eta)}{m}\right)^+\right) = \phi_{P_r} P_r\left(t_{n+\eta} + \dfrac{j(\mathcal{T}-\eta)}{m}\right) + \dfrac{\Lambda_p}{m}, \ \ j \in \{1, \ldots, m-1\}. \end{cases} \tag{2.11}$$

2.2.3. The inter-cropping season

The inter-cropping season, defined temporally as $t \in (t_n + \eta, t_{n+1}]$, represents an ecologically distinct period characterized by suboptimal environmental conditions that fundamentally alter the physiological and population dynamics of the papaya-mealybug-parasitoid system. As illustrated in Figure 3, this phase is marked by significant reductions in plant growth rates, increased mortality

across all trophic levels, and a critical shift in resource utilization by pest populations. During the inter-cropping season, photosynthetic efficiency is substantially compromised due to limiting environmental factors such as reduced solar radiation, suboptimal temperatures, and potential water stress. This physiological constraint manifests as a reduced growth rate α_1^i, where $\alpha_1^i < \alpha$ reflects the diminished carbon assimilation capacity. Concurrently, the carrying capacity for leaf biomass $K_{L_1}^i$ decreases due to limited nutrient availability and overall resource constraints. The combined effect of environmental stressors also elevates leaf mortality to $\mu_{L_1}^i > \mu_{L_1}$, primarily through accelerated senescence and increased susceptibility to abiotic damage. These dynamics are captured by:

$$\dot{L}_1(t) = \alpha_1^i(P(t))L_1(t)\left(1 - \frac{L_1(t)}{K_{L_1}^i}\right) - \mu_{L_1}^i(T(t))L_1(t). \tag{2.12}$$

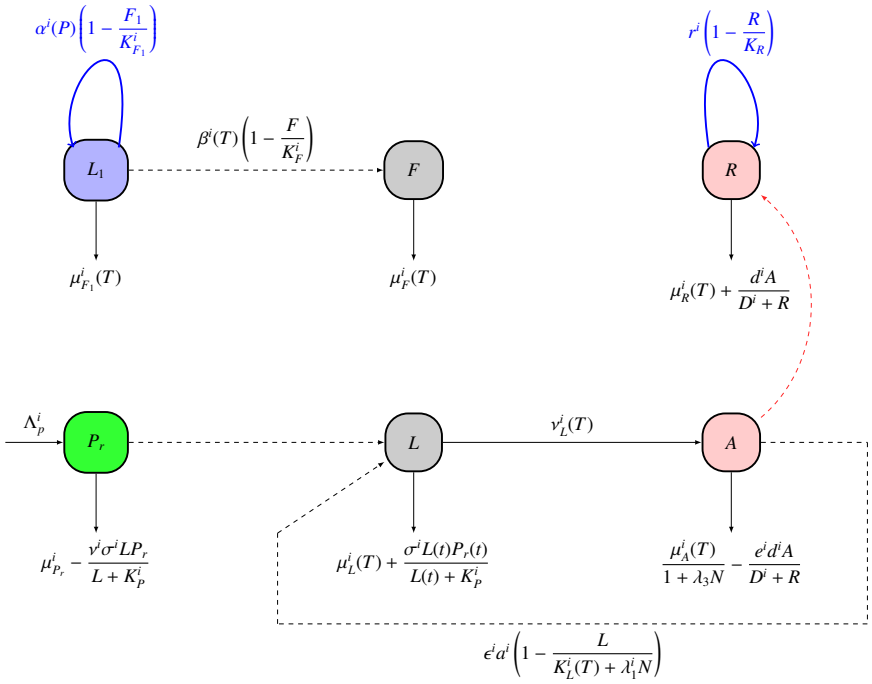

Figure 3. Conceptual framework of the tri-trophic interactions during the inter-cropping season ($t \in (t_n + \eta, t_{n+1}]$).

The transition from vegetative to reproductive growth is significantly inhibited during this period. The flower production rate β^i is reduced ($\beta^i < \beta$) due to limited photoassimilate allocation and hormonal signaling alterations under stress conditions. The floral carrying capacity K_F^i contracts, reflecting the plant's strategic resource conservation. Furthermore, flower mortality μ_F^i increases substantially ($\mu_F^i > \mu_F$) due to accelerated abscission processes and failed pollination events. The fruit development rate ν_F^i becomes negligible as the plant enters a reproductive diapause-like state. These physiological responses are modeled as:

$$\dot{F}(t) = \beta^i(T(t))L_1(t)\left(1 - \frac{F(t)}{K_F^i}\right) - (\mu_F^i(T(t)) + \nu_F^i(T(t)))F(t). \tag{2.13}$$

The complete absence of both healthy $S(t)$ and infected fruits $I(t)$ during this season represents a fundamental ecological bottleneck:

$$\dot{S}(t) = 0, \quad \dot{I}(t) = 0. \tag{2.14}$$

This null state arises from the combined effects of prior harvest removal and the cessation of new fruit development due to unfavorable pollination conditions and resource limitation.

With the disappearance of cultivated fruits, mealybug populations $L(t)$ face severe resource limitation, triggering several adaptive responses. The intrinsic egg-laying rate declines to $a^i < a$ due to nutritional constraints affecting oogenesis. The fertilization efficiency ε^i decreases ($\varepsilon^i < \varepsilon$) as mate-finding becomes more challenging at lower population densities. Critically, the carrying capacity for immature stages undergoes a fundamental shift rather than depending on fruit availability ($N(t) = S(t) + I(t)$), which now correlates with alternative food sources in the natural reservoir, expressed as $K_L^i(T) + \gamma_R^i R(t)$. The development rate ν_L^i slows due to suboptimal nutrition, while mortality μ_L^i increases ($\mu_L^i > \mu_L$) due to resource scarcity and persistent parasitism, though at a reduced attack rate $\sigma^i < \sigma$, reflecting lower parasitoid efficiency under inter-cropping conditions:

$$\dot{L}(t) = \varepsilon^i a^i A(t)\left(1 - \frac{L(t)}{K_L^i(T) + \gamma_R^i R(t)}\right) - (\nu_L^i(T(t)) + \mu_L^i(T(t)))L(t) - \frac{\sigma^i L(t) P_r(t)}{L(t) + K_P^i}. \tag{2.15}$$

Adult mealybugs, $A(t)$, employ two contrasting survival strategies during this resource-limited period. First, they experience elevated baseline mortality, $\mu_A^i > \mu_A$, due to physiological stress and accumulated damage. However, this mortality is partially mitigated through consumption of reservoir resources, modeled by the reduction term $(1 + \lambda_3 R(t))^{-1}$, where λ_3 represents the efficiency with which reservoir consumption translates into reduced adult mortality. Second, feeding on suboptimal reservoir resources incurs fitness costs, represented by the additional mortality term $\frac{e^i d^i R(t)}{D^i + R(t)}$, where d^i quantifies the damage rate from consuming lower-quality food, e^i represents the efficiency of this resource utilization, and D^i is the half-saturation constant:

$$\dot{A}(t) = \nu_L^i(T(t))L(t) - \left(\frac{\mu_A^i(T)}{1 + \lambda_3 R(t)} - \frac{e^i d^i R(t)}{D^i + R(t)}\right)A(t). \tag{2.16}$$

The reservoir $R(t)$ serves as a critical alternative food source during the inter-cropping season, though its dynamics are constrained by slower growth, $r^i < r$, due to seasonal limitations and consumption pressure from mealybugs. The functional response term $\frac{d^i A(t)}{D^i + R(t)}$ captures the consumption dynamics, where mealybugs increasingly utilize this suboptimal resource as fruit availability declines:

$$\dot{R}(t) = r^i R(t)\left(1 - \frac{R(t)}{K_R}\right) - \left(\mu_R + \frac{d^i A(t)}{D^i + R(t)}\right)R(t). \tag{2.17}$$

Parasitoid populations face substantial challenges during the inter-cropping season. The absence of supplemental releases and reduced host densities lead to declining populations through multiple mechanisms: The host encounter rate drops to $\sigma^i < \sigma$ due to lower mealybug densities and reduced parasitoid activity; the conversion efficiency, ν^i, decreases as parasitoids may produce fewer offspring per host under suboptimal conditions; and natural mortality, $\mu_{P_r}^i$, may increase due to the absence of sugar resources previously available from fruits. In addition, Λ_p^i denotes the baseline recruitment of

parasitoids during the inter-cropping season, reflecting residual survival or natural immigration in the absence of intentional releases, and is expected to be significantly lower than the recruitment during the cropping season ($\Lambda_p^i \ll \Lambda_p$). Parameter K_P^i represents the half-saturation constant of the functional response during the inter-cropping period, accounting for reduced host accessibility and parasitoid foraging efficiency under low host-density conditions. The resulting parasitoid dynamics are therefore governed by :

$$\dot{P}_r(t) = \Lambda_p^i + \frac{\nu^i \sigma^i L(t) P_r(t)}{L(t) + K_P^i} - \mu_{P_r}^i P_r(t). \tag{2.18}$$

Thus, for $t \in (t_n + \eta, t_{n+1}]$, we have the continuous system:

$$\begin{cases} \dot{L}_1(t) &= \alpha_1^i(P(t))L_1(t)\left(1 - \dfrac{L_1(t)}{K_{L_1}^i}\right) - \mu_{L_1}^i(T(t))L_1(t), \\ \dot{F}(t) &= \beta^i(T(t))L_1(t)\left(1 - \dfrac{F(t)}{K_F^i}\right) - (\mu_F^i(T(t)) + \nu_F^i(T(t)))F(t), \\ \dot{S}(t) &= 0, \\ \dot{I}(t) &= 0, \\ \dot{L}(t) &= \varepsilon^i a^i A(t)\left(1 - \dfrac{L(t)}{K_L^i(T) + \gamma_R^i R(t)}\right) - (\nu_L^i(T) + \mu_L^i(T))L(t) - \dfrac{\sigma^i L(t) P_r(t)}{L(t) + K_P^i}, \\ \dot{A}(t) &= \nu_L^i(T(t))L(t) - \left(\dfrac{\mu_A^i(T)}{1 + \lambda_3 R(t)} - \dfrac{e^i d^i R(t)}{D^i + R(t)}\right)A(t), \\ \dot{R}(t) &= r^i R(t)\left(1 - \dfrac{R(t)}{K_R}\right) - \left(\mu_R + \dfrac{d^i A(t)}{D^i + R(t)}\right)R(t), \\ \dot{P}_r(t) &= \Lambda_P^i + \dfrac{\nu^i \sigma^i L(t) P_r(t)}{L(t) + K_P^i} - \mu_{P_r}^i P_r(t). \end{cases} \tag{2.19}$$

2.2.4. Transition from the inter-cropping season to the new cropping season

The transition between cropping cycles represents a critical management intervention that fundamentally resets the ecological conditions of the papaya plantation. As illustrated in Figure 4, at the temporal boundary $t = t_{n+1}^+$, farmers implement comprehensive field cleaning procedures to eliminate accumulated biological debris and create optimal conditions for the subsequent cropping season.

This agricultural practice serves multiple ecological functions: It physically removes weed competition, reduces inoculum potential of pathogens, eliminates pest refuge habitats, and enhances resource availability for the new papaya crop. The cleaning process selectively affects different biological compartments through mechanical removal and habitat disruption, with varying efficiency across population types.

The cleaning process intentionally preserves a proportion of existing vegetative structures to maintain the plant's photosynthetic capacity while removing senescent and diseased tissues. Parameters ψ_{L_1} and ψ_F represent the survival fractions of leaves and flowers, respectively, where $0 \leq \psi_{L_1}, \psi_F \leq 1$. These values reflect the balance between removing potentially pathogenic materials and conserving the plant's functional biomass. Higher values indicate more conservative pruning strategies, while lower values correspond to more aggressive field clearing. This selective

preservation is mathematically represented by the discrete transition equations:

$$\begin{cases} L_1(t_{n+1}^+) &= \psi_{L_1} L_1(t_{n+1}), \\ F(t_{n+1}^+) &= \psi_F F(t_{n+1}). \end{cases} \tag{2.20}$$

All remaining fruits from the previous cycle are systematically removed to prevent resource competition and eliminate potential sources of mealybug infestation. This complete elimination ensures that the new cropping cycle begins without carryover of infected fruits that could serve as initial inoculum for mealybug populations. The reset mechanism is defined by the equations:

$$\begin{cases} S(t_{n+1}^+) &= 0, \\ I(t_{n+1}^+) &= 0. \end{cases} \tag{2.21}$$

The cleaning process directly targets pest populations through physical removal and habitat destruction. Parameters ψ_L and ψ_A quantify the efficiency of these control measures against immature and adult mealybugs, respectively. Typically, $\psi_L < \psi_A$ reflects the greater vulnerability of sessile immature stages to mechanical disruption compared to mobile adults that may escape the cleaning process. This differential impact is captured by the impulsive equations:

$$\begin{cases} L(t_{n+1}^+) &= \psi_L L(t_{n+1}), \\ A(t_{n+1}^+) &= \psi_A A(t_{n+1}). \end{cases} \tag{2.22}$$

The alternative food source for mealybugs is deliberately reduced through the removal of weed hosts and crop residues. The parameter ψ_R represents the proportion of the reservoir resource that persists after cleaning, where lower values indicate more effective elimination of alternative host plants. This management action is formulated as:

$$R(t_{n+1}^+) = \psi_R R(t_{n+1}). \tag{2.23}$$

While the cleaning process inevitably affects natural enemy populations, parameter ψ_P acknowledges that some parasitoids may survive in protected microhabitats or through rapid recolonization from surrounding areas. The conservation of these biological control agents is described by:

$$P_r(t_{n+1}^+) = \psi_P P_r(t_{n+1}). \tag{2.24}$$

Figure 4. Population transitions during field cleaning at cycle initiation ($t = t_{n+1}^+$).

The complete discrete reset system that governs the transition between cropping cycles is therefore given by:

$$\begin{cases} L_1(t_{n+1}^+) = \psi_{L_1} L_1(t_{n+1}), \\ F(t_{n+1}^+) = \psi_F F(t_{n+1}), \\ S(t_{n+1}^+) = 0, \\ I(t_{n+1}^+) = 0, \\ L(t_{n+1}^+) = \psi_L L(t_{n+1}), \\ A(t_{n+1}^+) = \psi_A A(t_{n+1}), \\ R(t_{n+1}^+) = \psi_R R(t_{n+1}), \\ P_r(t_{n+1}^+) = \psi_P P_r(t_{n+1}). \end{cases} \tag{2.25}$$

2.3. Mathematical modeling of climate change

Climate change is a complex phenomenon affecting various ecosystem aspects, including temperature, precipitation patterns, and humidity. In this study, we investigate the impacts of climate change on critical variables of systems (2.9) and (2.19). We present a comprehensive analysis of the relationships between climate variables and these variables, aiming to better understand the potential consequences of climate change on systems (2.9) and (2.19).

The temperature data depicted in Figure 5 are fitted using a Piecewise Cubic Hermite Interpolating Polynomial (`pchip`) procedure in Matlab R2015a. Among several candidate models, this shape-preserving piecewise formulation provides the optimal fit to the observed multi-year oscillations in Douala's climate from 2000 to 2023, effectively capturing the seasonal thermal amplitudes without introducing numerical artifacts.

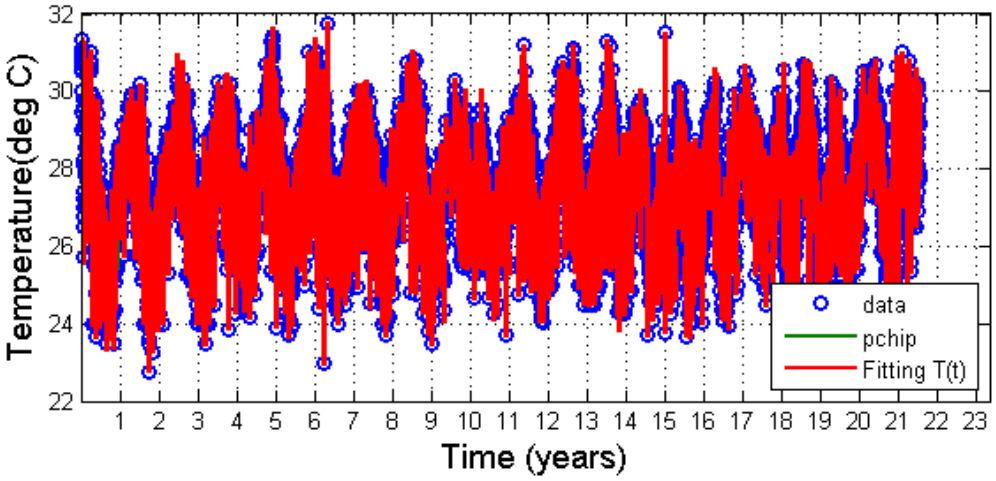

Figure 5. Temperature variations in Douala-Cameroon from 2000 to 2023 (Source: https://www.tutiempo.net/ampen/climate/ws-649100.html).

The resulting continuous temperature profile $T(t)$ is differentiable (C^1) and is defined on each subinterval $t \in [t_i, t_{i+1}]$ by a local cubic polynomial of the form:

$$T(t) = \sum_{k=0}^{3} c_{k,i}(t - t_i)^k, \tag{2.26}$$

where i denotes the index of the specific weather record interval, and t_i represents the discrete time nodes of the historical weather records. Let $h_i = t_{i+1} - t_i$ be the length of the subinterval, T_i and T_{i+1} be the temperature values at the boundaries, and d_i and d_{i+1} be the assigned tangents (derivatives) at these nodes.

The local coefficients $c_{k,i}$ (for $k = 0, 1, 2, 3$) are uniquely determined to interpolate the data points while strictly preserving monotonicity and preventing artificial overshoots. By applying the boundary conditions $T(t_i) = T_i$, $T(t_{i+1}) = T_{i+1}$, $T'(t_i) = d_i$, and $T'(t_{i+1}) = d_{i+1}$, these coefficients are explicitly expressed as:

$$\begin{aligned} c_{0,i} &= T_i, \\ c_{1,i} &= d_i, \\ c_{2,i} &= \frac{3\Delta_i - 2d_i - d_{i+1}}{h_i}, \\ c_{3,i} &= \frac{d_i + d_{i+1} - 2\Delta_i}{h_i^2}, \end{aligned} \tag{2.27}$$

where $\Delta_i = \frac{T_{i+1} - T_i}{h_i}$ represents the secant slope of the interval. The derivatives d_i are computed using a monotonicity-preserving limiter (such as the Fritsch-Carlson algorithm) to eliminate any non-physical oscillations.

The precipitation data presented in Figure 6 are modeled employing Matlab R2015a's curve fitting tools. After evaluating multiple mathematical forms, a Piecewise Cubic Hermite Interpolating Polynomial (`pchip`) formulation emerges as providing the most accurate representation of Douala's multi-year rainfall variability observed between 2000 and 2023, effectively capturing the zero-precipitation thresholds and heavy downpours without inducing numerical oscillations.

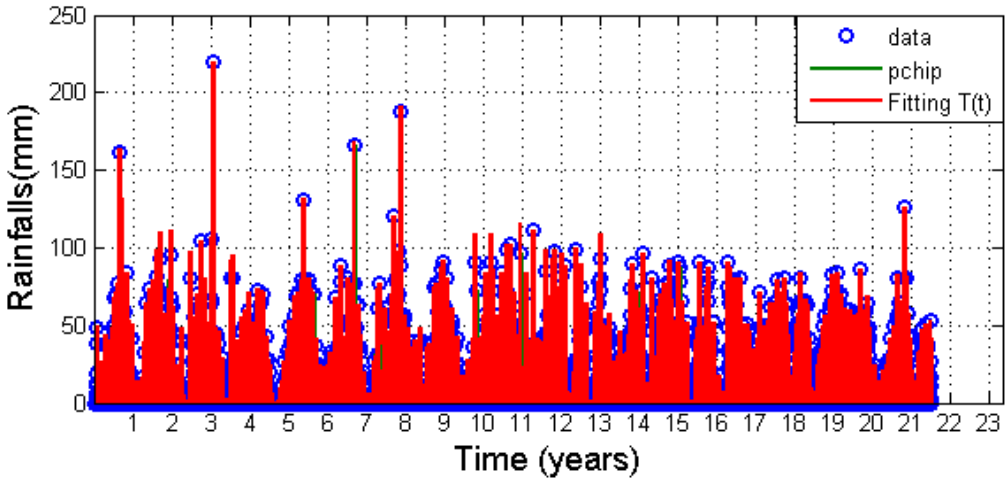

Figure 6. Rainfalls in Douala-Cameroon from 2000 to 2023 (Source: https://www.tutiempo.net/ampen/climate/ws-649100.html).

The resulting multi-seasonal rainfall profile $R_a(t)$ is analytically expressed on each subinterval $t \in$

$[t_i, t_{i+1}]$ by the following piecewise function:

$$R_a(t) = \begin{cases} 0 & \text{if } t \in \tilde{T}_d, \\ \sum_{k=0}^{3} c_{k,i}(t - t_i)^k & \text{if } t \in \tilde{T}_r, \end{cases} \tag{2.28}$$

where $\tilde{T}_d$ and $\tilde{T}_r$ correspond to the periods of the dry and rainy seasons, respectively. Here, i denotes the index of the weather record interval, t_i represents the discrete time nodes, and the local polynomial coefficients $c_{k,i}$ are explicitly calculated according to the analytical expressions given in (2.27), adapted for the rainfall data.

Taking into account the correlation between the leaf development and precipitation, as well as the effects of temperature on the growth and mortality of flowers, fruits, eggs, and adult stages of *P. marginatus*, we define the parameter α based on precipitation, and the parameters β, μ_L, μ_F, ν_F, ν_E, μ_A, μ_E, K_E, and μ_S based on temperature variations. We assume that the mortality rate of leaves, flowers, fruits, eggs, and adults of *P. marginatus* is minimized at optimal temperature and increases as weather conditions become unfavourable. Additionally, we assume that the mortality rate is independent of the seasons.

The mortality rate is modeled as follows:

$$\mu_i(T(t)) = \mu_{i_{\max}} + (\mu_{i_{\min}} - \mu_{i_{\max}}) \exp\left(-\left(\frac{T(t) - T_{\text{opt}}}{\mathcal{A}_T}\right)^2\right), \tag{2.29}$$

where $\mu i_{\max}$ and $\mu_{i_{\min}}$ denote respectively the maximum and minimum mortality rates, respectively, for $i \in L, F, S, E, A$. The amplitude is $\mathcal{A}_T = \dfrac{T_{\max} - T_{\min}}{2}$, with $T_{\max}$ and $T_{\min}$ representing the maximum and minimum temperatures of the region, respectively. This formulation is inspired by the Gaussian thermal performance function commonly used to describe temperature-dependent biological rates [30].

We assume that the growth and development rate of eggs, leaves, flowers, and fruits are maximal when the temperature is favourable for the development of the plant and decrease when the temperature deviates from the optimum. This is modeled as:

$$p(T(t)) = p_{\min} + (p_{\max} - p_{\min}) \exp\left(-\left(\frac{T(t) - T_{\text{opt}}}{\mathcal{A}_T}\right)^2\right), \tag{2.30}$$

where $p \in \beta, \nu_F, \nu_E$, $p$max is the maximal growth and reproduction rate, and $p_{\min}$ is the minimum growth and reproduction rate. As before, $\mathcal{A}_T = \dfrac{T_{\max} - T_{\min}}{2}$. Similar Gaussian-type equations have been widely applied to model temperature-dependent development rates in insects and other ectotherms [30, 31].

When the temperature is optimal, a considerable number of eggs can be found inside the ovisac. Consequently, the carrying capacity of the spawning site is given by:

$$K_E(T) = K_{E_{\min}} + (K_{E_{\max}} - K_{E_{\min}}) \exp\left(-\left(\frac{T(t) - T_{\text{opt}}}{\mathcal{A}_T}\right)^2\right), \tag{2.31}$$

where $K_{E_{\min}}$ and $K_{E_{\max}}$ are the minimum and maximum capacities, respectively, of the spawning site. This approach is consistent with established thermodynamic models for temperature-dependent biological processes [30, 32].

We also assume that rainfall between 200 mm and 1400 mm favors good leaf growth, while low rainfall leads to poor growth. Hence, parameter α is modeled as:

$$\alpha(t) = \alpha_{\min} + (\alpha_{\max} - \alpha_{\min})\frac{R_a(t)}{R_{\max}}, \tag{2.32}$$

where $\alpha_{\max}$ and $\alpha_{\min}$ are the maximal and minimal values of α. This linear relationship between biological parameters and precipitation has been widely used in ecological modeling to account for the effect of water availability on plant growth and development [33].

Tables A.1–A.3, presented in Appendix A.3, describe the model variables and the ranges and values of the parameters used to simulate the impact of climate change in systems (2.9) and (2.19).

3. Sensitivity analysis

Herein, we perform a global sensitivity analysis to identify the most influential parameters on the model state variables during the growing season and the inter-season.

Sensitivity analysis is a crucial step in the mathematical modeling of dynamical systems, as it enables the identification of parameters that most strongly control model behavior. Unlike local approaches that vary one parameter at a time, the Extended Fourier Amplitude Sensitivity Test (eFAST) method employed here is a global method. It simultaneously explores the entire parameter space and quantifies the contribution of each parameter to the variability of the output variables of interest. In this study, the analysis is applied to a multi-seasonal model of interactions between the papaya tree (*Carica papaya*), the mealybug (*Paracoccus marginatus*), and its natural enemies, distinguishing two periods with contrasting dynamics: the growing season (harvest period, Figure 7) and the inter-season (Figure 8). The results, presented below for the main state variables, reveal fundamental differences in system control depending on the season.

During the growing season, leaf density dynamics (L_1) are primarily governed by parameters related to growth and biotic pressure, with a strong influence from parameters α, K_L, and μ_L, among which the intrinsic growth rate α is the most sensitive (Figure 7(a)). In contrast, during the inter-season, the system switches to the wintering parameter set where α^i, K_L^i, and μ_L^i exhibit exclusive sensitivity (Figure 8(a)). Thus, while the growing season is marked by an active trade-off between plant production and pest attack, the inter-season sees a regime shift toward pure survival and reserve maintenance processes.

Flowering (F) responds strongly during the growing season to a wider cascade of parameters (α, K_L, μ_L, β, K_F, ν_F, and μ_F), with α remaining the primary driver, reflecting direct agro-physiological control linked to overall plant vigor (Figure 7(b)). During the inter-season, a distinct reconfiguration occurs: the sensitivity shifts entirely toward the inter-seasonal counterparts (α^i, K_L^i, μ_L^i, β^i, K_F^i, and ν_F^i) (Figure 8(b)). This indicates that during the inter-season, flowering no longer reflects active reproductive growth but rather an ecophysiological maintenance strategy dependent on internal resource stress.

During the growing season, the dynamics of healthy fruits (S) are highly sensitive to plant vigor (μ_L, α) and infection pressure (γ, K, λ_2) (Figure 7(c)), while infected fruits (I) are explicitly driven by transmission and pest abundance parameters (μ_L, β, D, λ_2) (Figure 7(d)). In stark contrast, during the inter-season, the eFAST analysis yields perfectly uniform, flat sensitivity distributions across all

parameters for both compartments (Figure 8(c),(d)). Rather than indicating active biological regulation, this uniform pattern mathematically reflects a statistical baseline noise. Because fruit production ceases during the inter-season, these compartments become dynamically decoupled from the model's active driving parameters, evolving via simple, unmanaged decay processes over time.

During the growing season, the immature mealybug dynamics (L) are co-governed by crop availability (α, K_L) and regulated by larval/pupal parameters (K_P, μ_P), with the pupal mortality rate μ_P being dominant (Figure 7(e)). This demonstrates that immature mortality is a key controlling factor during vegetative growth. During the inter-season, however, the adult mortality rate μ_A^i becomes overwhelmingly dominant (Figure 8(e)). This transition uncovers a structural shift in the pest's demographic bottleneck, moving from pupal mortality control during the harvest period to adult survival during the adverse season.

Adult female (A) abundance during the harvest period is strongly sensitive to host growth (α) and epidemic parameters (β, D, λ_2) (Figure 7(f)). During the inter-season, their sensitivity landscape is flattened except for a massive spike in the inter-seasonal adult mortality rate μ_A^i (Figure 8(f)). This confirms that while the active season supports a rich, multi-parameter epidemic regime, inter-seasonal adult abundance behaves as a survival-driven system highly vulnerable to winter mortality.

The environmental reservoir (R) compartment is dynamically active exclusively during the inter-season. Its dynamics are multi-factorial, showing high sensitivity to the pest regrowth rate ν_L^i, adult mortality μ_A^i, natural carrying capacity K_R^i, and predation factors (Λ_p). This confirms that the reservoir serves as a critical biological buffer during adverse periods, regulated by environmental capacity and residual natural enemy pressure.

During the growing season, the natural enemy population (Pr) is heavily dominated by its mortality rate μ_{P_r} and the functional response search/attack rate a (Figure 7(g)). This sensitivity pattern provides the empirical foundation for the model's multi-stable behaviors. The high sensitivity to predation parameters (a and μ_{P_r}) at this stage validates that the conjectured bistability is a density-dependent phenomenon driven by the Holling Type II functional response loophole. During the inter-season, the control reconfigures toward the winter mortality $\mu_{P_r}^i$ and the residual search parameter ν^i (Figure 8(g)), indicating that biological control efficiency during low resource periods becomes strictly dependent on overwintering survival and spatial search movements.

The marked seasonal reconfigurations of these global sensitivity indices demonstrate that uniform pest management strategies are fundamentally flawed. The exact same intervention can have radically different efficiencies depending on the temporal window, supporting the implementation of adaptive control calendars. Curative interventions targeting predation loopholes and larval mortality (μ_{P_r}, a) should be concentrated during the growing season. Conversely, proactive tactics must dominate the inter-season, focusing on augmenting adult mealybug winter mortality (μ_A^i) and destroying host reservoirs through sanitary fallows, directly targeting the demographic bottlenecks revealed by the eFAST analysis. Integrating these results into a decision support system would optimize the allocation of public resources, reduce chemical input use, and increase the sustainability of production systems in the face of environmental changes.

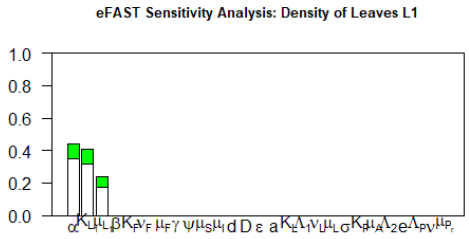

(a)

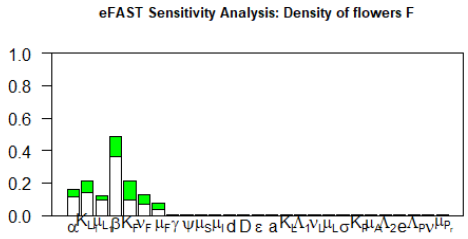

(b)

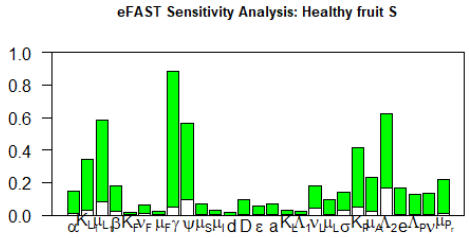

(c)

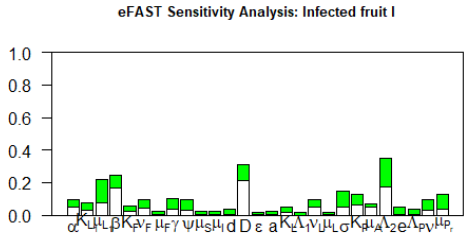

(d)

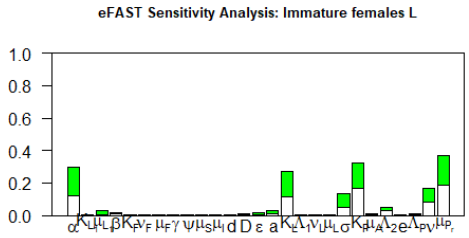

(e)

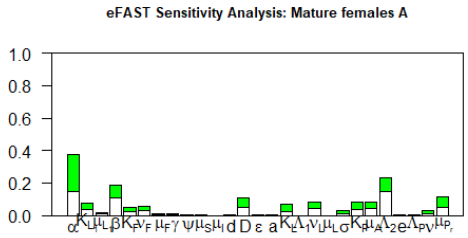

(f)

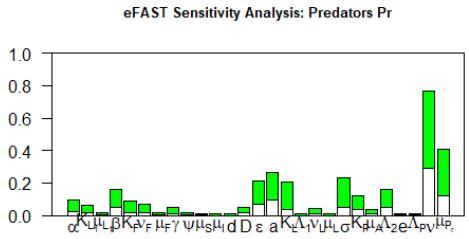

(g)

Figure 7. eFast sensitivity analysis of system (2.9) during the growing season. (a) Density of leaves L_1; (b) Density of flowers F; (c) Healthy fruit S; (d) Infected fruit I; (e) Immature females L; (f) Mature females A; and (g) Predator Pr.

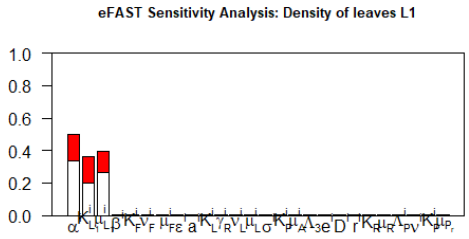

(a)

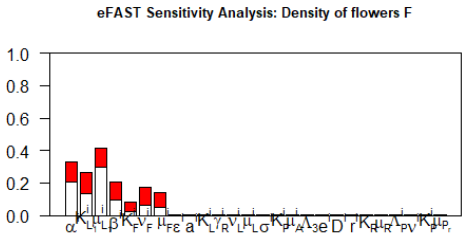

(b)

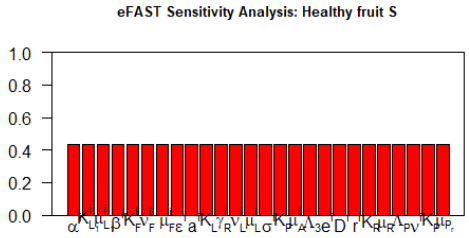

(c)

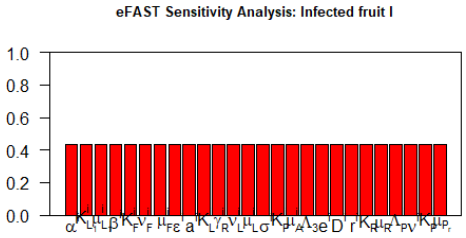

(d)

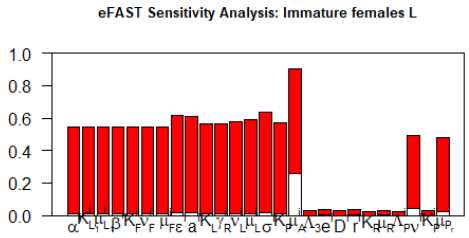

(e)

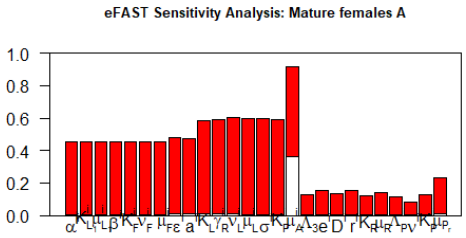

(f)

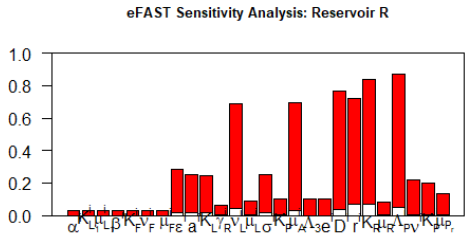

(g)

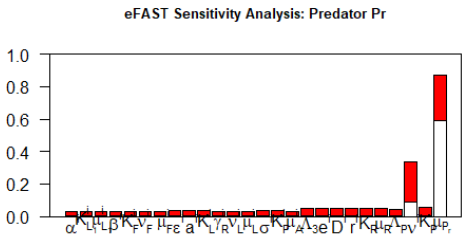

(h)

Figure 8. eFAST global sensitivity analysis of system (2.19) during the inter-season. (a) Density of leaves L_1; (b) Density of flowers F; (c) Healthy fruit S; (d) Infected fruit I; (e) Immature females L; (f) Mature females A; and (g) Parasitoids Pr.

4. Mathematical analysis

In this section, we present the theoretical results of systems (2.9) and (2.19).

4.1. Positivity and boundedness of solutions

To prove that systems (2.9) and (2.19) are biologically feasible, we show that all the variables are non-negative for all time t. Thus, we have the following results.

Lemma 1. *For all $\phi \in C([-\tau; 0]; \mathbb{R}^7_+)$, there is a unique nonnegative and uniformly bounded solution of systems (2.9) and (2.19), satisfying the initials conditions (2.11) and (2.25).*

Proof. The proof is given in Appendix A.2.

Lemma 1 implies that the omega limit sets of systems (2.9) and (2.19) are contained in the following bounded feasible region:

$$\Gamma = \Gamma_1 \times \Gamma_2 \times \Gamma_3, \tag{4.1}$$

where

$$\Gamma_1 = \{(L_1, F, S, I, L, A) \in C^6_+ : L_1 \leq M_0,\ F \leq M_1,\ S \leq M_2,\ I \leq M_2,\ L \leq M_3,\ A \leq M_4\},$$

$$\Gamma_2 = \{R \in C_+; R \leq K_R\} \text{ and } \Gamma_3 = \{P_r \in C_+; P_r \leq M_6\},$$

with

$$M_0 = K_L + K^i_L,\ \ M_1 = K_F + K^i_F,\ \ M_2 = \frac{\nu_{F_{2max}} M_1}{\min\{\mu_{S_{\min}}, \mu_I\}},\ \ M_3 = (1 + (\pi_S + \pi_I))M_2,$$

$$M_4 = K_{L_{\max}} + K^i_{L_{\max}} + \lambda_1 M_3 + \gamma_R K^i_R,\ \ M_5 = \frac{\nu_{L_{\max}} M_3(1 + \lambda_2 M_2)}{\mu_{A_{\min}} - ed(1 + \lambda_2 M_2)} + \frac{\nu^i_{L_{\max}} M_3(1 + \lambda_3 K^i_R)}{\mu^i_{A_{\min}} - e^i d^i(1 + \lambda_3 K_R)}$$

$$\text{and } M_6 = \frac{\Lambda_p}{\mu_p - \nu\sigma} + \frac{\Lambda^i_p}{\mu^i_p - \nu^i\sigma^i}.$$

One can show that the region Γ is positively invariant with respect to systems (2.9) and (2.19), that is, systems (2.9) and (2.19) are well posed.

4.2. The pest-free solution and its stability

Herein, we study the existence and stability of the pest-free solution of systems (2.9) and (2.19).

4.2.1. The pest-free solution

The pest-free solution of systems (2.9) and (2.19) corresponds to the case where $L(t) = A(t) = 0$, for all $t \geq 0$.

The following result, as demonstrated in Appendix A.1, ensures the existence of a unique pest-free solution:

Lemma 2. *Systems (2.9)–(2.11), (2.19), and (2.25) admit a unique non-negative pest-free solution $Y^* = (L^*_1(t), F^*(t), S^*(t), 0, 0, 0, R^*(t), P^*_r(t))$, where $L_1{}^*(t)$, $F^*(t)$, $S^*(t)$, $R^*(t)$ and $P^*_r(t)$ are given in Eqs (A.7), (A.10), (A.12), (A.15), and (A.16) of Appendix A.1.*

4.2.2. Local stability of the pest-free solution

Herein, we study the stability of the pest-free solution of the semi-discrete systems (2.9) and (2.19). Let $x(t) = (L_1(t), F(t), S(t), I(t), L(t), A(t))^\top$ be small perturbations around Y^*.

The linearized system around the pest-free solution during the cropping season corresponding to $t \in (t_n, t_n + \eta]$ is given by :

$$M_1(t) = \begin{pmatrix} -\frac{\alpha(P(t))L_1^*(t)}{K_{L_1}} & 0 & 0 & 0 & 0 & 0 & 0 \\ \beta(T(t))\left(1 - \frac{F^*(t)}{K_F}\right) & -B(t) & 0 & 0 & 0 & 0 & 0 \\ 0 & 0 & -\mu_S(T) & 0 & 0 & 0 & 0 \\ 0 & 0 & 0 & -\mu_I & 0 & 0 & 0 \\ 0 & 0 & 0 & 0 & -\varrho(t) & \varepsilon a & 0 \\ 0 & 0 & 0 & 0 & \nu_L(T(t)) & -\frac{\mu_A(T(t))}{1+\lambda_2 S^*(t)} & 0 \\ 0 & 0 & 0 & 0 & \frac{\sigma P_r^*(t)}{K_P} & 0 & -\mu_{P_r} \end{pmatrix}, \tag{4.2}$$

where

$$B(t) = \frac{\beta(T(t))L_1^*(t)}{K_F} + \nu_F(T(t)) + \mu_F(T(t)), \quad \varrho(t) = \mu_L(T(t)) + \nu_L(T(t)) + \frac{\sigma P_r^*(t)}{K_P}.$$

Additionally, the Linearization matrix around the pest-free solution during the cropping season corresponding to $t \in (t_n + \eta, t_{n+1}]$ is given by :

$$M_2(t) = \begin{pmatrix} -\frac{\alpha^i(P(t))L_1^*(t)}{K_{L_1}^i} & 0 & 0 & 0 & 0 & 0 & 0 & 0 \\ g(t) & -B^i(t) & 0 & 0 & 0 & 0 & 0 & 0 \\ 0 & 0 & 0 & 0 & 0 & 0 & 0 & 0 \\ 0 & 0 & 0 & 0 & 0 & 0 & 0 & 0 \\ 0 & 0 & 0 & 0 & -a_0^i(t) & \varepsilon^i a^i & 0 & 0 \\ 0 & 0 & 0 & 0 & \nu_L^i(T(t)) & -\left(\frac{\mu_A^i(T(t))}{1+\lambda_3 R^*(t)} - \frac{e^i d^i R^*}{D^i + R^*}\right) & 0 & 0 \\ 0 & 0 & 0 & 0 & 0 & -\frac{d^i R^*(t)}{D^i + R^*(t)} & -\frac{r^i}{K_R} R^*(t) & 0 \\ 0 & 0 & 0 & 0 & \frac{\sigma^i P_r^*(t)}{K_P^i} & 0 & 0 & -\mu_{P_r}^i \end{pmatrix}, \tag{4.3}$$

where

$$g(t) = \beta^i(T(t))\left(1 - \frac{F^*(t)}{K_F^i}\right),$$

$$B^i(t) = \beta^i(T(t))\frac{L_1^*(t)}{K_F^i} + \mu_F^i(T(t)) + \nu_F^i(T(t)),$$

$$a_0^i(t) = \mu_L^i(T(t)) + \nu_L^i(T(t)) + \frac{\sigma^i P_r^*(t)}{K_P^i}.$$

Let $\Phi_1(t, s)$ and $\Phi_2(t, s)$ be the fundamental matrix solutions satisfying:

$$\frac{d}{dt}\Phi_1(t, s) = M_1(t)\Phi_1(t, s), \quad \Phi_1(s, s) = I_7, \quad t, s \in [t_n, t_n + \eta), \tag{4.4}$$

$$\frac{d}{dt}\Phi_2(t, s) = M_2(t)\Phi_2(t, s), \quad \Phi_2(s, s) = I_8, \quad t, s \in (t_n + \eta, t_{n+1}]. \tag{4.5}$$

The linearized impulsive conditions are:

$$\begin{aligned} x(t_n^+) &= D_{\phi_0} x(t_n), \\ x((t_n + \eta)^+) &= D_\eta x(t_n + \eta), \\ x(t_{n+1}^+) &= D_\psi x(t_{n+1}), \end{aligned}$$

with diagonal matrices

$$D_{\phi_0} = \mathrm{diag}(1, 1, 1, 1, \phi_0, \phi_0, 1), \tag{4.6}$$

$$D_\eta = \mathrm{diag}(\pi_{L_1}, \pi_F, 0, 0, \phi_h, \phi_h, 1), \tag{4.7}$$

$$D_\psi = \mathrm{diag}(\psi_{L_1}, \psi_F, 0, 0, \psi_L, \psi_A, \psi_R, \psi_P). \tag{4.8}$$

Note that D_{ϕ_0} and D_η are 7×7, while D_ψ is 8×8; the dimensions match because R appears only in Phase 2.

We have the following result:

Proposition 1 (Monodromy operator)**.** *The evolution of small perturbations over one complete cycle* $[t_n^+, t_{n+1}^+]$ *is governed by the discrete map*

$$x(t_{n+1}^+) = \mathcal{L}x(t_n^+),$$

where the monodromy operator $\mathcal{L}$ *is*

$$\mathcal{L} = D_\psi \, \Phi_2(t_{n+1}, t_n + \eta) \, \tilde{D}_\eta \, \Phi_1(t_n + \eta, t_n) \, D_{\phi_0}^{-1},$$

and

$$\tilde{D}_\eta = \mathrm{diag}(D_\eta, 1) \tag{4.9}$$

is the 8×8 *extension of* D_η *adding an entry 1 for the R component (which starts at zero in phase 2).*

Proof. From t_n^+ to $t_n + \eta$, we have

$$x(t_n + \eta) = \Phi_1(t_n + \eta, t_n)x(t_n^+). \tag{4.10}$$

The impulse at $t_n + \eta$ gives

$$x((t_n + \eta)^+) = D_\eta x(t_n + \eta). \tag{4.11}$$

To extend to phase 2, let us define

$$\tilde{x}((t_n + \eta)^+) = (x((t_n + \eta)^+)^\top, 0)^\top \in \mathbb{R}^8, \tag{4.12}$$

where the extra zero corresponds to $R((t_n + \eta)^+) = 0$. This can be written as

$$\tilde{x}((t_n + \eta)^+) = \tilde{D}_\eta \Phi_1(t_n + \eta, t_n) x(t_n^+), \tag{4.13}$$

with $\tilde{D}_\eta$ defined as in Eq (4.9).

For $t \in (t_n + \eta, t_{n+1}]$, one has that

$$\tilde{x}(t) = \Phi_2(t, t_n + \eta)\tilde{x}((t_n + \eta)^+). \tag{4.14}$$

At $t = t_{n+1}$,

$$x(t_{n+1}^+) = D_\psi \tilde{x}(t_{n+1}). \tag{4.15}$$

Combining these expressions (4.10)–(4.15) and using the fact that $x(t_n^+) = D_{\phi_0} x(t_n)$ give the result.

The matrices $M_1(t)$ and $M_2(t)$ exhibit a block structure when considering only the pest compartments (L_1, F, S, I, L, A). Extract the submatrices:

$$\tilde{M}_1(t) = \begin{pmatrix} A_{11}(t) & 0 & 0 \\ A_{21}(t) & A_{22}(t) & 0 \\ 0 & 0 & A_{33}(t) \end{pmatrix}, \quad \tilde{M}_2(t) = \begin{pmatrix} B_{11}(t) & 0 & 0 \\ B_{21}(t) & 0 & 0 \\ 0 & 0 & B_{33}(t) \end{pmatrix}, \tag{4.16}$$

where

$$A_{11}(t) = \begin{pmatrix} -\dfrac{\alpha L_1^*}{K_{L_1}} & 0 \\ \beta\left(1 - \dfrac{F^*}{K_F}\right) & -B(t) \end{pmatrix}, \; A_{22}(t) = \begin{pmatrix} -\mu_S & 0 \\ 0 & -\mu_I \end{pmatrix}, \; A_{33}(t) = \begin{pmatrix} -\varrho(t) & \varepsilon a \\ \nu_L & -\dfrac{\mu_A}{1 + \lambda_2 S^*} \end{pmatrix},$$

$$B_{11}(t) = \begin{pmatrix} -\dfrac{\alpha^i L_1^*}{K_{L_1}^i} & 0 \\ g(t) & -B^i(t) \end{pmatrix}, \; B_{33}(t) = \begin{pmatrix} -a_0^i(t) & \varepsilon^i a^i \\ \nu_L^i & -\left(\dfrac{\mu_A^i}{1 + \lambda_3 R^*} - \dfrac{e^i d^i R^*}{D^i + R^*}\right) \end{pmatrix}.$$

The blocks $A_{22}(t)$ and the corresponding block in $M_2(t)$ for (S, I) are zero in Phase 2 because $\dot{S} = \dot{I} = 0$.

Let $\Phi_1^{LF}, \Phi_1^{SI}, \Phi_1^{LA}$ denote the 2×2 fundamental matrices associated with the diagonal blocks of $\tilde{M}_1(t)$, with analogous definitions for Φ_2 in Phase 2. We have the following result:

Proposition 2. *The monodromy operator $\mathcal{L}$ inherits the block-triangular structure of the underlying continuous-time dynamics. When restricted to the pest compartments, it admits the representation:*

$$\mathcal{L} = \begin{pmatrix} \mathcal{L}^{LF} & 0 & 0 \\ * & 0 & 0 \\ * & 0 & \mathcal{L}^{LA} \end{pmatrix}, \tag{4.17}$$

where the reduced operators for the (L_1, F) and (L, A) subsystems are given by:

$$\begin{aligned} \mathcal{L}^{LF} &= \operatorname{diag}(\psi_{L_1}, \psi_F)\, \Phi_2^{LF}(t_{n+1}, t_n + \eta)\, \operatorname{diag}(\pi_{L_1}, \pi_F)\, \Phi_1^{LF}(t_n + \eta, t_n), \\ \mathcal{L}^{LA} &= \operatorname{diag}(\psi_L, \psi_A)\, \Phi_2^{LA}(t_{n+1}, t_n + \eta)\, \phi_h\, \Phi_1^{LA}(t_n + \eta, t_n)\, \phi_0. \end{aligned} \tag{4.18}$$

Proof. The block-triangular form of the infinitesimal generators $\tilde{M}_k(t)$ ensures that the resulting fundamental matrices preserve this structure. Since the impulsive matrices are diagonal, the global operator $\mathcal{L}$ remains block-triangular. The annihilation of the (S, I) block stems from the zero-entries in D_η and the trivial dynamics of these variables in Phase 2. Extracting the principal diagonal blocks yields the expressions in (4.18).

To characterize the stability of the pest-free equilibrium, we introduce the spectral thresholds associated with the decoupled subsystems.

Let the threshold parameters be defined as:

$$\mathcal{N}_0^{LF} = \rho(\mathcal{L}^{LF}) \quad \text{and} \quad \mathcal{N}_0^{LA} = \rho(\mathcal{L}^{LA}), \tag{4.19}$$

where $\rho(\cdot)$ denotes the spectral radius. The global threshold parameter for the system is then given by:

$$\mathcal{N}_0 = \max(\mathcal{N}_0^{LF}, \mathcal{N}_0^{LA}). \tag{4.20}$$

The following theorem establishes the local asymptotic stability (LAS) of the pest-free solution $Y^*(t)$ based on the magnitude of $\mathcal{N}_0$.

Theorem 1. *The pest-free solution $Y^*(t)$ is locally asymptotically stable if $\mathcal{N}_0 < 1$, and unstable if $\mathcal{N}_0 > 1$.*

Proof. The stability of solution $Y^*(t)$ is determined by the Floquet multipliers of the linearized impulsive system, which correspond to the eigenvalues of the monodromy operator $\mathcal{L}$ [34].

As established in Proposition 2, the operator $\mathcal{L}$ admits a block-triangular structure. Consequently, the spectrum of $\mathcal{L}$, denoted by $\sigma(\mathcal{L})$, is the union of the spectra of its diagonal blocks:

$$\sigma(\mathcal{L}) = \sigma(\mathcal{L}^{LF}) \cup \sigma(\mathcal{L}^{LA}) \cup \{0\}. \tag{4.21}$$

The zero eigenvalue arises from the (S, I)-subsystem, which is periodically reset at each transition $t_n + \eta$, effectively annihilating its contribution to the long-term spectral growth. Thus, the spectral radius of the full operator is exactly:

$$\rho(\mathcal{L}) = \max\left(\rho(\mathcal{L}^{LF}), \rho(\mathcal{L}^{LA})\right) = \mathcal{N}_0. \tag{4.22}$$

If $\mathcal{N}_0 < 1$, all Floquet multipliers lie strictly within the unit circle in the complex plane ($|\mu| < 1$). According to Floquet theory for impulsive differential equations, this condition implies that the trivial solution of the linearized system is exponentially stable. By the principle of linearized stability, the nonlinear pest-free solution $Y^*(t)$ is locally asymptotically stable.

Conversely, if $\mathcal{N}_0 > 1$, at least one Floquet multiplier lies outside the unit circle ($|\mu| > 1$), which is a sufficient condition for the instability of the periodic solution $Y^*(t)$.

Remark 1. *The biological interpretation of $\mathcal{N}_0$ is the average number of female offspring produced by a single adult female throughout its life cycle.*

Biologically, Theorem 1 implies that a pest population may naturally go extinct even in the absence of external control strategies, provided the initial population is within the basin of attraction of the pest-free solution.

However, for effective pest management in a papaya field, local stability is often insufficient. Establishing global asymptotic stability is crucial as it ensures that the pest-free solution $Y^*(t)$ attracts all trajectories within the feasible region Γ, regardless of the initial infestation level. Demonstrating this global property for this model remains a significant challenge, requiring advanced mathematical techniques for impulsive differential systems.

4.2.3. Global stability of the pest-free solution

Herein we prove the global stability of the est-free solution $Y^*(t)$.

Let $X(t) = (L(t), A(t))^T$ be the vector representing the pest populations. We analyze the evolution of $X(t)$ over the cropping interval $t \in (t_n, t_n+\eta]$. By observing that $1-\dfrac{L}{K_L + \lambda_1(S+I)} \leq 1$, $\dfrac{\sigma P_r(t)}{K_P} \geq 0$, and $\dfrac{edI(t)}{D+I(t)} \leq ed$, the nonlinear dynamics can be upper-bounded by the following linear impulsive system:

$$\dot{X}(t) \leq \mathcal{M}_1 X(t), \tag{4.23}$$

where the constant matrix $\mathcal{M}_1$ is defined as:

$$\mathcal{M}_1 = \begin{pmatrix} -(\nu_{L_{\min}} + \mu_{L_{\min}}) & \epsilon a \\ \nu_{L_{\max}} & -\left(\dfrac{\mu_{A_{\min}}}{1+\lambda_2 M_2} - ed\right) \end{pmatrix}.$$

Since the off-diagonal elements of $\mathcal{M}_1$ are non-negative, the system is cooperative. Consequently, by the comparison principle (Theorem B.1 [35]), the solution $X(t)$ is dominated by the solution $Y(t)$ of the associated linear system. Integrating (4.23) over the interval $t \in (t_n, t_n + \eta]$ yields:

$$Y(t) = \exp\left(\mathcal{M}_1(t - t_n)\right) Y(t_n^+), \tag{4.24}$$

where $Y(t)$ serves as a supersolution for the pest compartments.

In a similar manner, over the intercropping interval $t \in (t_n+\eta, t_{n+1}]$, the comparison system satisfies:

$$Y(t) = \exp\left(\mathcal{M}_2(t - (t_n + \eta))\right) Y((t_n + \eta)^+), \tag{4.25}$$

where the matrix $\mathcal{M}_2$, representing the dynamics during the fallow period, is given by:

$$\mathcal{M}_2 = \begin{pmatrix} -(\nu^i_{L_{\min}} + \mu^i_{L_{\min}}) & \epsilon^i a^i \\ \nu^i_{L_{\max}} & -\left(\dfrac{\mu^i_{A_{\min}}}{1+\lambda_3 K_R} - e^i d^i\right) \end{pmatrix}.$$

This matrix, $\mathcal{M}_2$, is also cooperative, ensuring that the comparison principle remains valid throughout the intercropping phase.

By combining the jump conditions defined in Eqs (2.11) and (2.22) with the transition dynamics established in (4.24) and (4.25), the evolution of the supersolution over one full period $\mathcal{T}$ can be expressed as:

$$Y(t_{n+1}^+) = \mathcal{L}^{\max}_{L,A} Y(t_n^+), \tag{4.26}$$

where $\mathcal{L}_{L,A}^{\max}$ denotes the maximal monodromy operator for the pest compartments, defined by the following product of transition and impulse matrices:

$$\mathcal{L}_{L,A}^{\max} = \begin{pmatrix} \psi_L & 0 \\ 0 & \psi_A \end{pmatrix} \exp\left((\mathcal{T}-\eta)\mathcal{M}_2\right) \begin{pmatrix} \phi_h & 0 \\ 0 & \phi_h \end{pmatrix} \exp\left(\eta\mathcal{M}_1\right).$$

According to Floquet theory for impulsive differential systems [36], the stability of the pest- free solution is determined by the spectral radius of the monodromy operator $\mathcal{L}_{L,A}^{\max}$. Let $\rho(\mathcal{L}_{L,A}^{\max})$ denote this spectral radius. By recursive application of (4.26) over n periods, we obtain:

$$Y(t_{n+1}^+) = \left(\mathcal{L}_{L,A}^{\max}\right)^n Y(t_1^+). \tag{4.27}$$

If the stability condition $\rho(\mathcal{L}_{L,A}^{\max}) < 1$ is satisfied, then:

$$\lim_{n\to\infty} Y(t_n^+) = \Big(0,0\Big).$$

Since $0 \le X(t) \le Y(t)$ for all $t \ge t_1$ by the comparison principle (Theorem B.1 [35]), it follows that the pest populations $(L(t), A(t))$ converge to zero as $t \to \infty$.

Once the extinction of the larval and adult pest populations $(L, A) \to (0, 0)$ is established, the dynamics of the infected population $I(t)$ become asymptotically autonomous. According to the system structure, the evolution of $I(t)$ over one full period $[t_n, t_{n+1}]$ is governed by:

$$\begin{cases} \dot{I}(t) = -\mu_I(T(t))I(t), & t \in (t_n, t_n+\eta], \\ \dot{I}(t) = 0, & t \in (t_n+\eta, t_{n+1}]. \end{cases} \tag{4.28}$$

Integrating (4.28) over the cropping interval $(t_n, t_n + \eta]$ yields:

$$I(t_n+\eta) = I(t_n^+)\exp\left(-\int_{t_n}^{t_n+\eta} \mu_I(T(s))ds\right).$$

During the intercropping phase $t \in (t_n + \eta, t_{n+1}]$, since $\dot{I}(t) = 0$, the population remains constant: $I(t_{n+1}) = I(t_n + \eta)$. By applying the impulsive jump condition at t_{n+1} (with survival coefficient $\theta_I \in (0, 1]$), we obtain the following recurrence relation for the sequence of densities at the impulse points:

$$I(t_{n+1}^+) = \theta_I \cdot I(t_n^+)\exp\left(-\int_{t_n}^{t_n+\eta} \mu_I(T(s))ds\right). \tag{4.29}$$

Let $\lambda_I = \theta_I \exp\left(-\int_0^{\eta} \mu_I(T(s))ds\right)$ be the multiplicative factor over one period. Given that $\mu_I(T(t)) > 0$ and $\theta_I \le 1$, it follows that $0 < \lambda_I < 1$. Thus, the sequence $\{I(t_n^+)\}_{n\in\mathbb{N}}$ is a strictly decreasing geometric sequence converging to zero. Consequently, $\lim_{t\to\infty} I(t) = 0$.

With $I(t) \to 0$, the remaining state variables (L_1, F, S, R, P_r) are no longer subject to pest-induced pressure or infection terms. The system reduces to the pest-free impulsive subsystem. Under the assumption of existence and uniqueness of the pest-free periodic solution $Y^*(t)$, and as demonstrated in Appendix A.4, the trajectories of these variables are attracted to their respective unique periodic orbits:

$$(L_1(t), F(t), S(t), R(t), P_r(t)) \longrightarrow (L_1^*(t), F^*(t), S^*(t), R^*(t), P_r^*(t)) \quad \text{as } t \to \infty.$$

We have established the following result :

Theorem 2. *If $\mathcal{N}_g < 1$ and $\mathcal{N}_g \leq \mathcal{N}_0$, the pest-free periodic solution $Y^*(t)$ of the system is globally asymptotically stable (GAS) in Γ. Under these combined conditions, pest eradication is guaranteed regardless of the initial infestation level in the field.*

Remark 2. *Due to the non-autonomous nature of the model, where parameters explicitly depend on complex climatic driving forces (temperature and precipitation profiles) and multi-seasonal transitions, isolating a single analytical bifurcation parameter is mathematically intractable. Moreover, a strict analytical ordering between the local threshold $\mathcal{N}_0$ and the global threshold $\mathcal{N}_g$ cannot be generic. However, by cross-examining the relative values of $\mathcal{N}_0$ and $\mathcal{N}_g$ against the critical threshold of* 1*, we can conjecture six ecologically plausible scenarios that characterize the pest management dynamics:*

(1) (Absolute Eradication: ($\mathcal{N}_0 \leq \mathcal{N}_g < 1$): The pest-free solution is robustly stable globally. Eradication is guaranteed, and the control strategy is independent of the initial field state.

(2) (Bistability Conjecture: ($\mathcal{N}_g < \mathcal{N}_0 < 1$): Since $\mathcal{N}_g < \mathcal{N}_0$, the global stability guaranteed by Theorem 2 no longer applies. Although the pest-free state remains locally stable, a bistability phenomenon is numerically suspected. In this zone, a stable positive solution may coexist with the pest-free state, meaning that eradication depends strictly on the initial pest density; if the initial infestation exceeds a critical threshold, the pest population will persist.

(3) (Standard Outbreak: ($1 \leq \mathcal{N}_0 \leq \mathcal{N}_g$): The pest-free solution is unstable. The system tends toward a stable positive solution, leading to a permanent establishment of the pest throughout the crop.

(4) Extreme Infestation: ($\mathcal{N}_0 \geq \mathcal{N}_g > 1$): The pest-free solution is unstable, and environmental conditions are exceptionally favorable to the pest, rendering current control measures insufficient to suppress the population.

Now, we conduct numerical simulations to demonstrate the outcomes of pest extinction in the plantation. The initial conditions are set as $(L_1(0), F(0), S(0), I(0), L(0), A(0), R(0)) = (100.5, 107.5, 100, 0, 100, 10, 5)$. We choose $\mu_I = 0.00000005$, $\epsilon = 0.0015$, and $\epsilon^i = 0.0025$, (so that $\mathcal{N}_0 = 0.83$). All other parameter values are given in Tables A.2 and A.3.

Figure 9 shows the pest's extinction, supporting Theorem 2. These curves also demonstrate that in the absence of pests, the density of healthy leaves, flowers, and fruits evolve due to seasonal temperature variations, affecting their development rates. During favorable temperatures, papaya plants thrive, producing abundant leaves, flowers, and fruits. Leaves grow plentifully, setting the stage for future flowering. Flowers develop quickly, leading to a high fruit set and a bountiful harvest of healthy fruits. However, when temperatures deviate from the optimum, these processes slow down, causing fluctuations in leaf, flower, and fruit populations. Moreover, the populations of infected fruits and mealybugs drop to zero during this period. Unfavorable thermal conditions hinder mealybug development and survival, preventing their proliferation. Infected fruits cannot form under these conditions. During the inter-cropping season, when the field is not conducive to plant growth, the mealybug reservoir population does not drop to zero. Mealybugs can enter diapause or migrate to other hosts to survive during unfavorable periods. This persistence enables them to reinvest papaya plants in the next growing season.

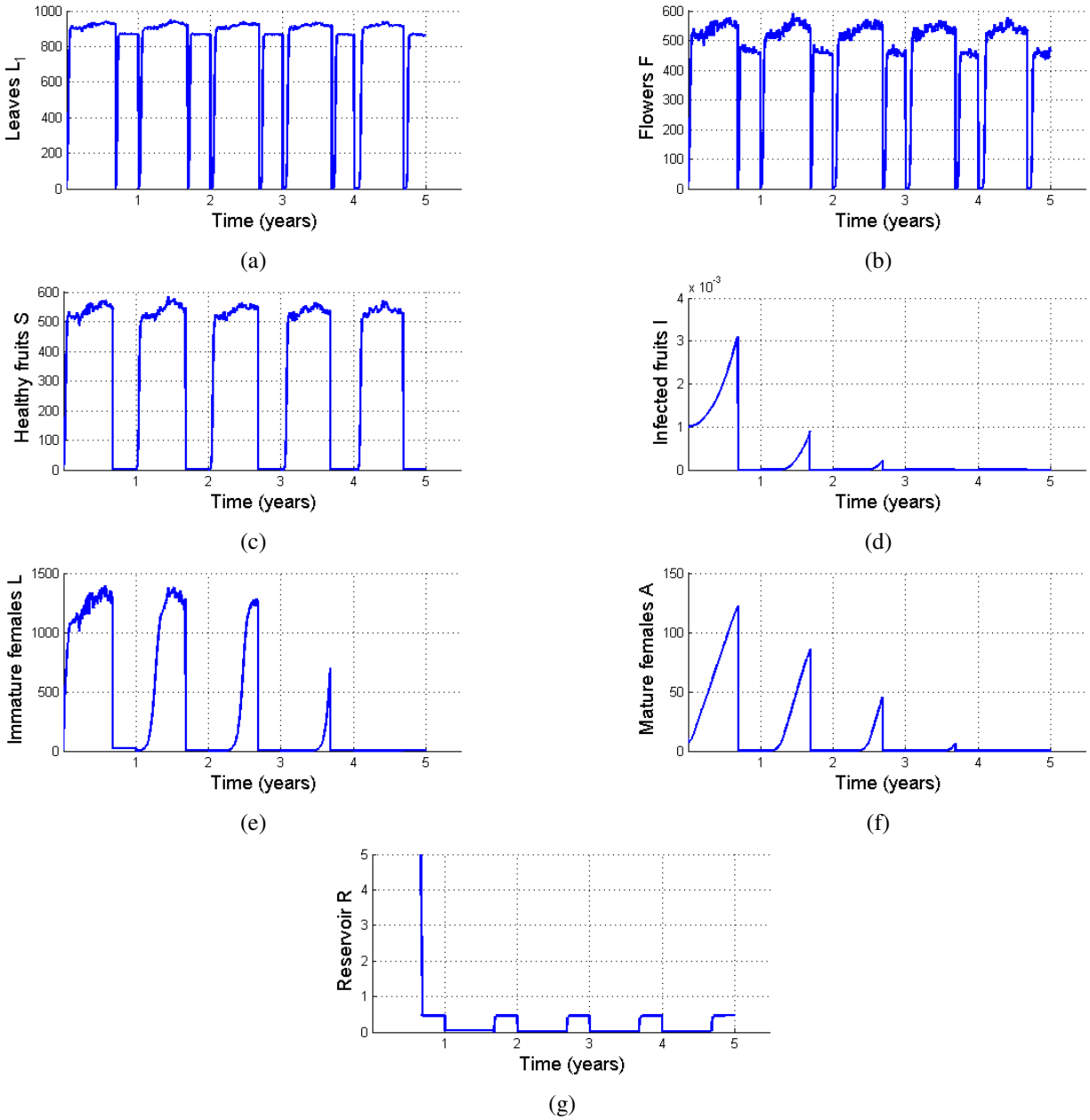

Figure 9. Numerical simulation of systems (2.9) and (2.19) for several initial conditions, such that $\mathcal{N}_0 = 0.83 < 1$. All other parameter values are given in Tables A.2 and A.3. (a) Leaves L_1; (b) Flowers F; (c) Healthy fruits S; (d) Infected fruits I; (e) Immature females L; (f) Mature females A; and (g) Reservoir R.

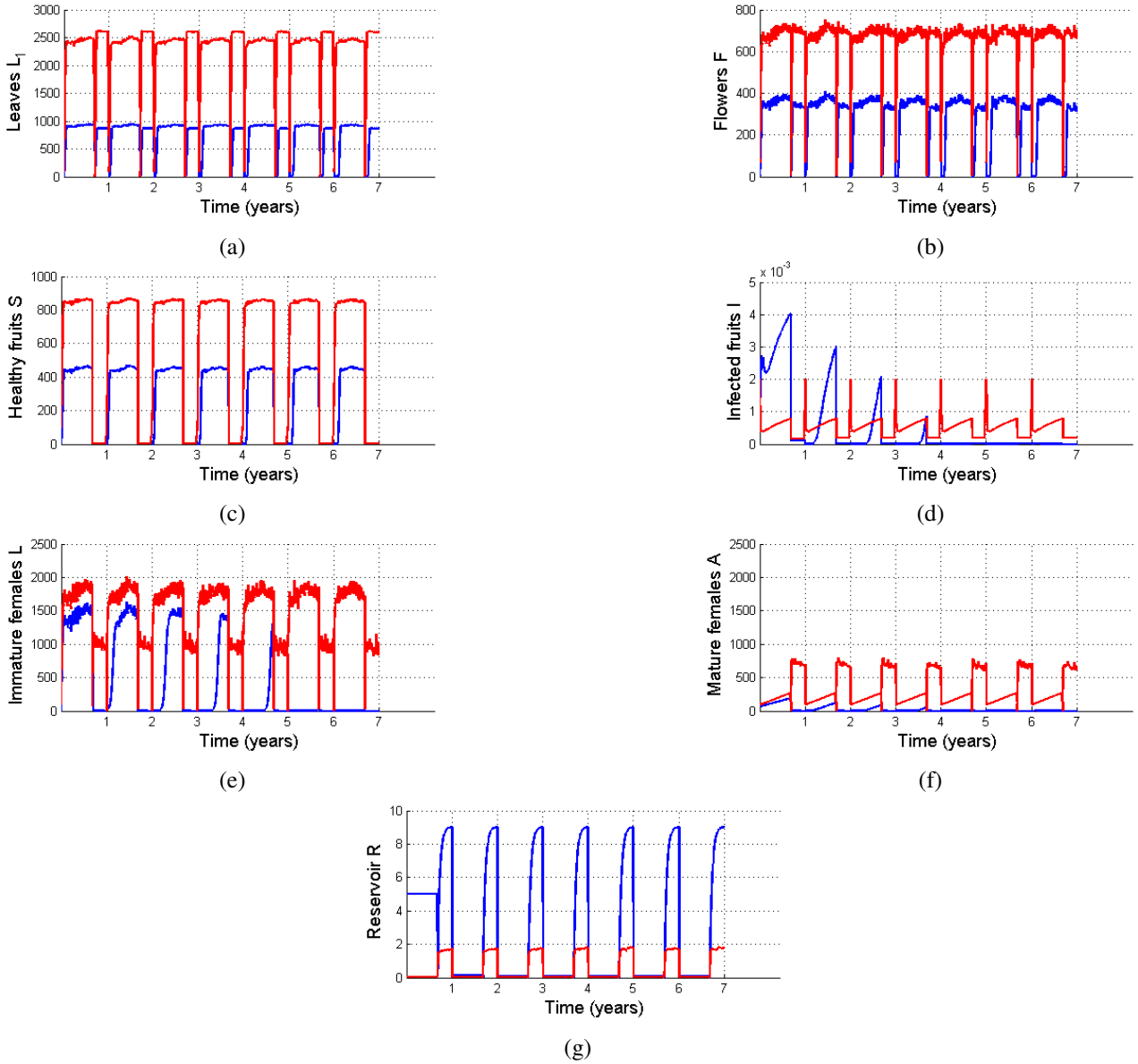

Figure 10. Numerical illustration of the bistability conjecture exhibited by systems (2.9) and (2.19) for several initial conditions, where $\mathcal{N}_g = 0.816$, $\mathcal{N}_0 = 0.96$, and $\mathcal{N}_g < \mathcal{N}_0 < 1$. All other parameter values are given in Tables A.2 and A.3. The trajectories demonstrate that pest eradication or persistence strictly depends on the initial infestation levels: (a) Leaves L_1; (b) Flowers F; (c) Healthy fruits S; (d) Infected fruits I; (e) Immature females L; (f) Mature females A; and (g) Reservoir R.

Figure 10 illustrates the bistability behavior conjectured for systems (2.9) and (2.19). The initial conditions are set to be $(L_1(0), F(0), S(0), I(0), L(0), A(0), R(0)) = (100, 100, 100, 0.002, 100, 100, 0.01)$. We choose $\gamma = 0.002$, $\epsilon = 0.25$, $\psi = 0.001$, $\mu_A = 0.6$, $\mu_A^i = 0.7$, $\mu_I = 0.05$, $K_L = 4000$, $\epsilon^i = 0.61$ and $K_L^i = 3000$ so that $\mathcal{N}_g = 0.816$, $\mathcal{N}_0 = 0.96$ and $\mathcal{N}_g < \mathcal{N}_0 < 1$. All other parameters are listed in Tables A.2 and A.3. The simulations highlight the bistable behavior of the system. These

figures reveal the coexistence of two distinct dynamical regimes under identical parameter values. For low initial infestation levels, all infected compartments decline over time, and the system converges toward the pest-free periodic solution. This indicates that natural mortality, environmental constraints, and control measures are sufficient to eliminate the pest. In contrast, when the initial pest density is sufficiently high, the system evolves toward a persistent periodic infestation state. The infected population remains strictly positive and oscillatory, showing that the pest can persist despite $\mathcal{N}_0 < 1$. From a practical viewpoint, these results highlight the importance of early and sufficiently strong intervention. Even when $\mathcal{N}_0 < 1$, delayed control may drive the system into the basin of attraction of the endemic periodic solution, making eradication difficult or impossible.

Now, we assess the capacity of the pest population to endure multiple seasons.

4.2.4. Pest persistence when $\mathcal{N}_0 > 1$

When the basic reproduction number exceeds unity, the pest population persists in the long term. We establish this result using persistence theory for impulsive semi-dynamical systems.

Theorem 3. *Assume that $\mathcal{N}_0 > 1$, where $\mathcal{N}_0$ is defined in (4.20). Then there exists $\epsilon > 0$ such that for any initial condition with $L(0) > 0$ or $A(0) > 0$, the solution of systems (2.9), (2.11), (2.19), and (2.25) satisfies*

$$\liminf_{t\to\infty} (L(t) + A(t)) \geq \epsilon.$$

Moreover, the system admits at least one positive solution.

Proof. We prove the theorem through several steps, focusing on the pest compartments (L, A).

From systems (2.9) and (2.19), the pest dynamics satisfy:

For $t \in [t_n, t_n + \eta)$:

$$\begin{aligned}
\dot{L} &= \varepsilon a A \left(1 - \frac{L}{K_L + \lambda_1(S + I)}\right) - (\nu_L + \mu_L)L - \frac{\sigma L P_r}{L + K_P},\\
\dot{A} &= \nu_L L - \left(\frac{\mu_A}{1 + \lambda_2(S + I)} - \frac{edI}{D + I}\right)A.
\end{aligned}$$

For $t \in (t_n + \eta, t_{n+1}]$:

$$\begin{aligned}
\dot{L} &= \varepsilon^i a^i A \left(1 - \frac{L}{K_L^i + \gamma_R^i R}\right) - (\nu_L^i + \mu_L^i)L - \frac{\sigma^i L P_r}{L + K_P^i},\\
\dot{A} &= \nu_L^i L - \left(\frac{\mu_A^i}{1 + \lambda_3 R} - \frac{e^i d^i R}{D^i + R}\right)A.
\end{aligned}$$

The impulsive conditions are:

$$\begin{aligned}
&L(t_n^+) = \phi_0 L(t_n), \quad A(t_n^+) = \phi_0 A(t_n),\\
&L((t_n + \eta)^+) = \phi_h L(t_n + \eta), \quad A((t_n + \eta)^+) = \phi_h A(t_n + \eta),\\
&L(t_{n+1}^+) = \psi_L L(t_{n+1}), \quad A(t_{n+1}^+) = \psi_A A(t_{n+1}).
\end{aligned}$$

When L and A are sufficiently small, the higher-order terms become negligible. The linearized dynamics during interval $[t_n, t_n + \eta)$ are:

$$\frac{d}{dt}\begin{pmatrix} L \\ A \end{pmatrix} \approx \mathcal{A}(t)\begin{pmatrix} L \\ A \end{pmatrix},$$

with

$$\mathcal{A}(t) = \begin{pmatrix} -(\nu_L + \mu_L + \sigma P_r^*(t)/K_P) & \varepsilon a \\ \nu_L & -\mu_A/(1 + \lambda_2 S^*(t)) \end{pmatrix}.$$

During Interval time $(t_n + \eta, t_{n+1}]$, one has that :

$$\frac{d}{dt}\begin{pmatrix} L \\ A \end{pmatrix} \approx \mathcal{A}^i(t)\begin{pmatrix} L \\ A \end{pmatrix},$$

with

$$\mathcal{A}^i(t) = \begin{pmatrix} -(\nu_L^i + \mu_L^i + \sigma^i P_r^*(t)/K_P^i) & \varepsilon^i a^i \\ \nu_L^i & -(\mu_A^i/(1 + \lambda_3 R^*(t)) - e^i d^i R^*(t)/(D^i + R^*(t))) \end{pmatrix}.$$

Let $\Phi_1(\eta)$ and $\Phi_2(\mathcal{T} - \eta)$ be the state transition matrices corresponding to these linear systems over intervals of length η and $\mathcal{T} - \eta$, respectively.

The discrete-time dynamics over one complete cycle are approximately:

$$\begin{pmatrix} L(t_{n+1}^+) \\ A(t_{n+1}^+) \end{pmatrix} \approx \mathcal{M}\begin{pmatrix} L(t_n^+) \\ A(t_n^+) \end{pmatrix},$$

where

$$\mathcal{M} = \begin{pmatrix} \psi_L & 0 \\ 0 & \psi_A \end{pmatrix}\Phi_2(\mathcal{T} - \eta)\begin{pmatrix} \phi_h & 0 \\ 0 & \phi_h \end{pmatrix}\Phi_1(\eta)\begin{pmatrix} \phi_0 & 0 \\ 0 & \phi_0 \end{pmatrix}.$$

The condition $\mathcal{N}_0 > 1$ is equivalent to $\rho(\mathcal{M}) > 1$, where ρ denotes the spectral radius. This follows from the definition (4.20), since $\mathcal{N}_0^{LA} = \rho(\mathcal{M})$ when considering only the (L, A) pathway.

Let $\lambda > 1$ be the dominant eigenvalue of $\mathcal{M}$ with corresponding positive eigenvector $\mathbf{v} = (v_L, v_A)^\top > 0$ (by the Perron-Frobenius theorem for nonnegative matrices).

Define $V_n = v_L L(t_n^+) + v_A A(t_n^+)$. For the linearized system:

$$V_{n+1} = \lambda V_n.$$

For the nonlinear system, when (L, A) are small, we have:

$$V_{n+1} \geq (\lambda - \delta(V_n))V_n,$$

where $\delta(V_n) \to 0$ as $V_n \to 0$, due to the continuity of the nonlinear terms.

Since $\lambda > 1$, there exists $\eta > 0$ and $\epsilon_0 > 0$ such that for all $V_n < \epsilon_0$:

$$V_{n+1} \geq (1 + \eta)V_n.$$

Suppose, for contradiction, that $\liminf_{t\to\infty}(L(t) + A(t)) = 0$. Then there exists a subsequence $\{t_{n_k}^+\}$ such that $V_{n_k} \to 0$. Choose k large enough so that $V_{n_k} < \epsilon_0$. Then, by the inequality above:

$$V_{n_k+1} \geq (1 + \eta)V_{n_k}, \quad V_{n_k+2} \geq (1 + \eta)^2 V_{n_k}, \quad \ldots$$

This implies $V_{n_k+m} \to \infty$ as $m \to \infty$, contradicting the boundedness of solutions (all state variables are bounded due to carrying capacities and bounded parameters). Therefore:

$$\liminf_{n\to\infty} V_n \geq \epsilon_0.$$

Since the continuous dynamics between impulses are governed by cooperative differential equations (the off-diagonal terms εa, ν_L, etc., are nonnegative), there exists a constant $\kappa > 0$ such that for all $t \in [t_n, t_{n+1}]$:

$$L(t) + A(t) \geq \kappa \left(L(t_n^+) + A(t_n^+)\right).$$

This follows from the comparison principle applied to the linearized cooperative system. Therefore,

$$\liminf_{t\to\infty} (L(t) + A(t)) \geq \kappa\epsilon_0 =: \epsilon > 0.$$

Now, we proove the existence of a positive solution.

Consider the Poincaré map $\mathcal{P} : \mathbb{R}^2_+ \to \mathbb{R}^2_+$ defined by:

$$\mathcal{P}(L_0, A_0) = \left(L(\mathcal{T}^+), A(\mathcal{T}^+)\right),$$

where $(L(t), A(t))$ is the solution with initial condition $(L(0^+), A(0^+)) = (L_0, A_0)$. The map $\mathcal{P}$ is continuous and compact. The persistence result implies that $\mathcal{P}$ is uniformly persistent with respect to the origin. By the theory of topological dynamics for monotone maps [37], there exists a positive fixed point of $\mathcal{P}$, which corresponds to a positive solution of the original impulsive system.

Herein, we present numerical simulation results on pest persistence, elucidating the critical threshold parameters influencing population maintenance. The initial conditions are set as $(L_1(0), F(0), S(0), I(0), L(0), A(0), R(0)) = (100.5, 107.5, 100, 0, 100, 10, 5)$. We choose $\mu_I = 0.00000005$, $\epsilon = 0.0015$, $\epsilon^i = 0.0025$, $\gamma = 0.00045$, and $\psi = 0.00035$ (so that $\mathcal{N}_0 = 12.3$, $\mathcal{N}_g = 42.31$ and $1 < \mathcal{N}_0 < \mathcal{N}_g$). All other parameter values are given in Tables A.2 and A.3.

Figure 11 shows the dynamics of leaves (L_1), flowers (F), healthy fruits (S), and infected fruits (I) over time, as well as the dynamics of immature (L) and mature (A) females about the reservoir (R). It is observed that during periods of optimal conditions, the available resources (leaves, flowers, and healthy fruits) promote mealybug reproduction, enabling their population to be maintained. However, when temperatures become unfavorable, the growth of these resources slows down, leading to a decrease in the populations of leaves and flowers. Nevertheless, the mealybug reservoir population continues to persist through several mechanisms. On one hand, they can enter diapause to survive harsh periods. On the other hand, they are capable of migrating to other host plants where conditions are more favorable. This resilience enables part of the population to survive and quickly recolonize papaya plantations when temperatures become optimal again. Regarding panel (d) in Figure 11, the reservoir (R) decreases rapidly and then stabilizes at a low level, while immature (L) and mature (A) females remain at higher, stable densities. This difference arises because the reservoir represents mealybugs on alternative host plants outside the plantation, whose dynamics are driven primarily by migration rather than local reproduction. When unfavorable conditions set in, migration from the plantation to the reservoir ceases, and reservoir individuals experience natural mortality without being

replenished, causing the reservoir to decline. Once the reservoir reaches a low density, the population stabilizes because a small number of mealybugs still survive locally on alternative hosts, but without sustained migration, it cannot recover to its initial level. In contrast, immature and mature females inside the plantation maintain their densities through direct access to residual resources (leaves, flowers, fruits) and through adaptive mechanisms such as diapause and reduced metabolic activity, which enable them to persist despite environmental fluctuations.

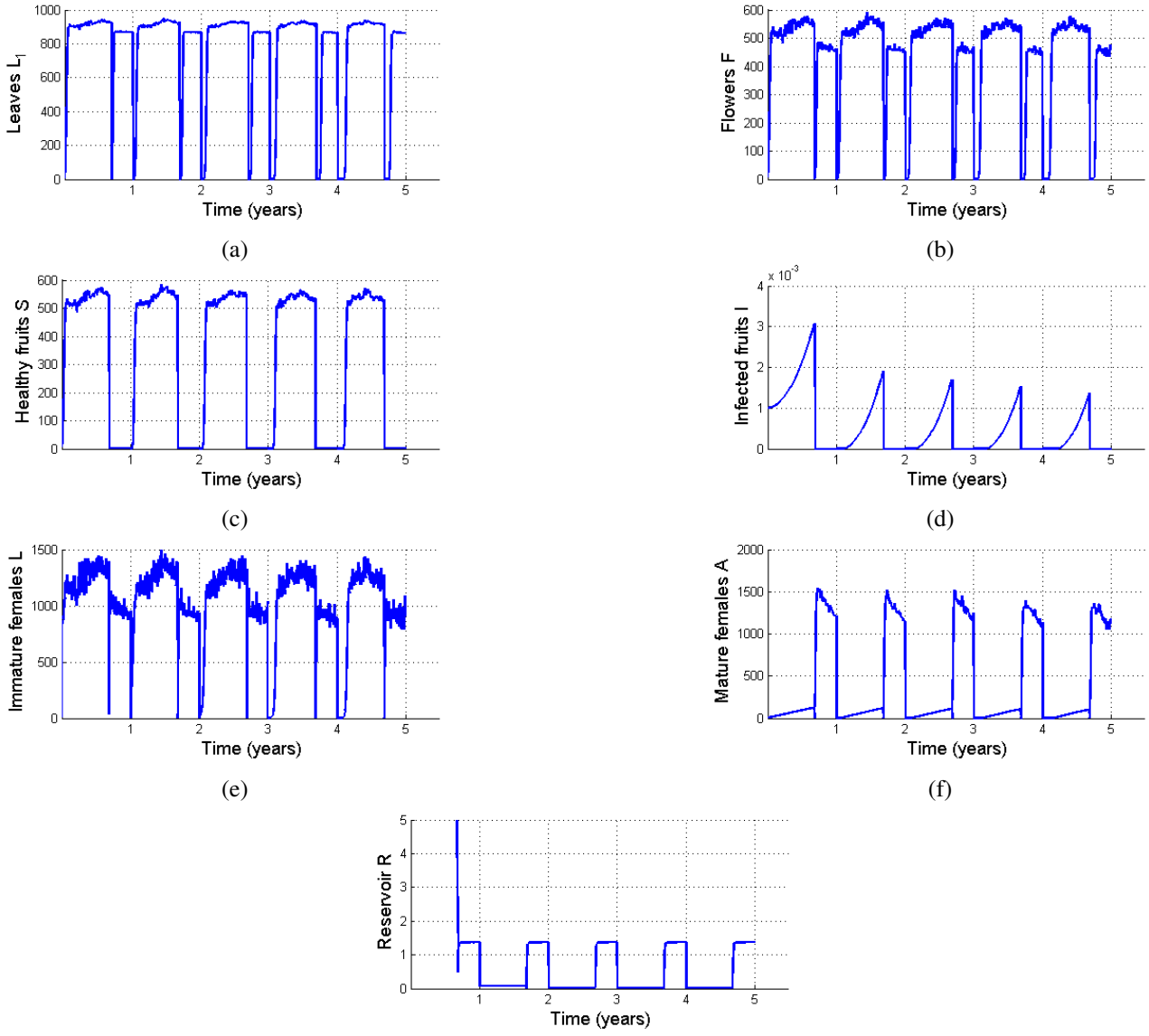

Figure 11. Numerical simulation of systems (2.9) and (2.19) when $\mu_I = 0.00000005$, $\epsilon = 0.0015$, $\epsilon^i = 0.0025$, $\gamma = 0.00045$, and $\psi = 0.00035$ (such that $\mathcal{N}_0 = 12.31$, $\mathcal{N}_g = 42.31$, and $1 < \mathcal{N}_0 < \mathcal{N}_g$). The other parameter values are given in Table A.2. (a) Leaves L; (b) Flowers F; (c) Healthy fruits S; (d) Infected fruits I; (e) Immature females L; (f) Mature females A; and (g) Reservoir R.

4.3. *Impact of reservoirs on the population dynamics of P. marginatus*

Herein, we examine the impact of the reservoir on the population dynamics of *P. marginatus*.

Figure 12 presents the evolution of the mealybug population in the presence and absence of the reservoir. From this figure, one can observe that without a reservoir, the dynamics of the mealybug population are completely dependent on the seasonal temperature variations in the plantation. During favorable periods, the population can increase rapidly, but it also collapses just as abruptly when conditions become unfavorable. This cycle of peaks and crashes prevents the mealybug population from reaching high and stable levels over time. Each return of favorable conditions sees the starting point from zero or close to it, preventing it from establishing itself durably. Conversely, in the presence of an external reservoir, the mealybugs can regularly reinfest the papayas, even when the population drops during unfavorable periods. This reservoir acts as a guarantee, enabling the continuous maintenance of the population, at varying levels, but always higher than those observed without a reservoir. Thus, the mealybug reservoir plays a decisive role in maintaining a higher and more regular pest pressure on the papaya crop, compared to a situation without a reservoir, where the population remains constantly lower.

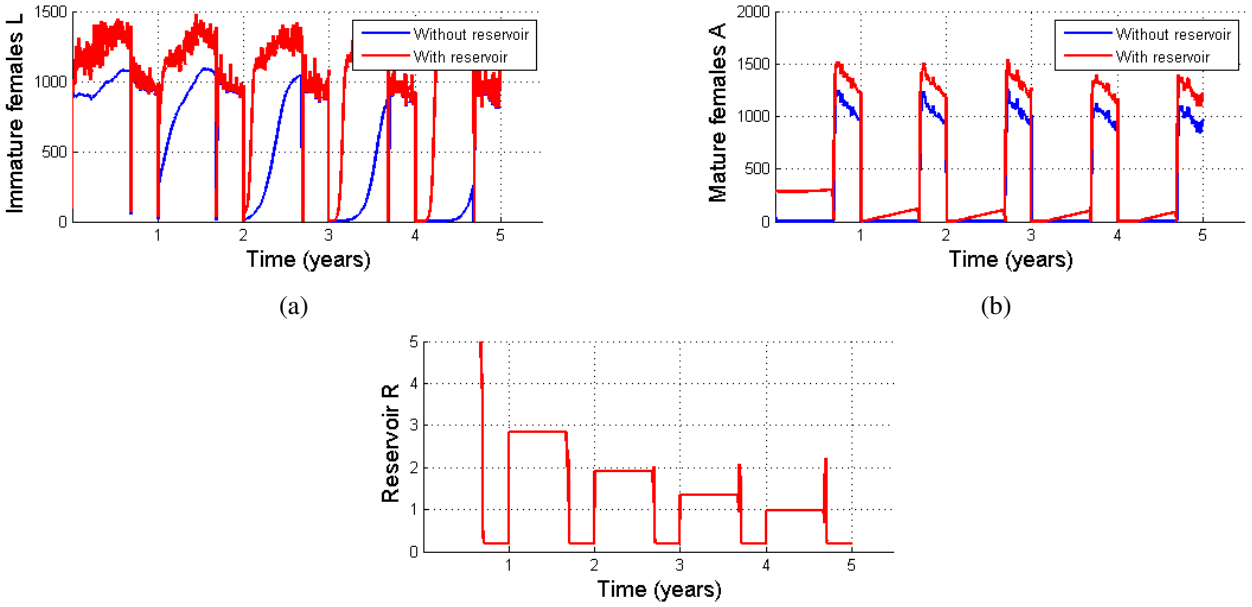

Figure 12. Impact of the reservoir on the population dynamics of *Paracoccus marginatus*, with parameters set to $\mu_I = 0.00000005$, $\epsilon = 0.0015$, $\epsilon^i = 0.0025$, $\gamma = 0.00045$, $\eta = 250$, and $\psi = 0.00035$ (such that $\mathcal{N}_0 = 12.31$, $\mathcal{N}_g = 42.31$, and $1 < \mathcal{N}_0 < \mathcal{N}_g$). All other parameter values are given in Table A.2. (a) Immature females L; (b) Mature females A; and (c) Reservoir R.

Table 1 highlights the significant impact of the presence of a *P. marginatus* (papaya mealybug) reservoir on the populations of immature and mature females of this pest. The results show that the presence of the reservoir leads to a 25.13% increase in the number of immature females and an 18.08% increase in the number of mature females, compared to a situation without the reservoir.

This difference underscores the importance of the reservoir in the maintenance and spread of papaya mealybug populations, even outside the growing season. The survival and reproduction within the reservoir enable more significant and recurrent re-infestation of papaya plantations.

Table 1. Cumulative number of immature and mature females.

	Immature females	Mature females
Without reservoir	1081	1246
With reservoir	1444	1521
Percentage	25.13%	18.08%

5. Implementation of some targeted intervention strategy

Herein, we investigate the impact of two control strategies based on the releases of parasitoïds and the use of biopesticides on the population dynamics of *P. marginatus*.

5.1. Impact of impulsive release of parasitoids

Herein, we present the impact of the yearly release frequency of parasitoids on the *P. marginatus* control. This is done using numerical simulations of the model with multiple releases to show the stability of the pest-free equilibrium $Y^*(t)$ for different values of the release of the parasitoid *Acerophagus papayae*. We present numerical simulations of the asymptotic behavior of systems (2.9) and (2.11). We consider multiple impulsive releases of parasitoids, where the initial condition for parasitoids depends on the number of releases, and we assume $Pr(0^+) = \frac{\Lambda_P}{m}$, where m is the number of parasitoid releases. The new initial condition in the case of multiple releases is:

$$(L_1(0^+), F(0^+), S(0^+), I(0^+), L(0^+), A(0^+), R(0^+), P_r(0^+)) = \left(100.5, 107.5, 100, 100, 100, 100, 100, \frac{\Lambda_P}{m}\right).$$

We choose $\mu_I = 0.00000005$, $\epsilon = 0.0015$, $\epsilon^i = 0.0025$, $\gamma = 0.00045$, and $\psi = 0.00035$ (so that $\mathcal{N}_0 = 12.31$, $\mathcal{N}_g = 42.31$ and $1 < \mathcal{N}_0 < \mathcal{N}_g$). All other parameter values are given in Tables A.2 and A.3. In Figure 13, the repeated releases of parasitoids targeting young female scale insects are applied on days 1, 3, 5, 8, and 10 of each cropping season, and this pattern is repeated annually throughout the simulation period. One can observe that these impulsive interventions maintain a high predation pressure on the scale insect population. With each release, the pest population decreases significantly, especially during favorable periods when reproduction is active. During unfavorable periods (less favorable temperatures), the natural decline in the pest population further enhances the effectiveness of biological control.

As a result, the scale insect population is maintained at very low levels, preventing uncontrolled proliferation. This leads to an increase in healthy fruits and a decrease in infected fruits, thereby improving crop quality. However, as the pest population declines, food resources for parasitoids become scarcer, leading to a gradual decrease in their population. Similarly, the external reservoir is no longer able to sustain or renew the pest population, resulting in its decline. Thus, impulsive biological control proves particularly effective when combined with seasonal temperature variations affecting the dynamics of *P. marginatus*.

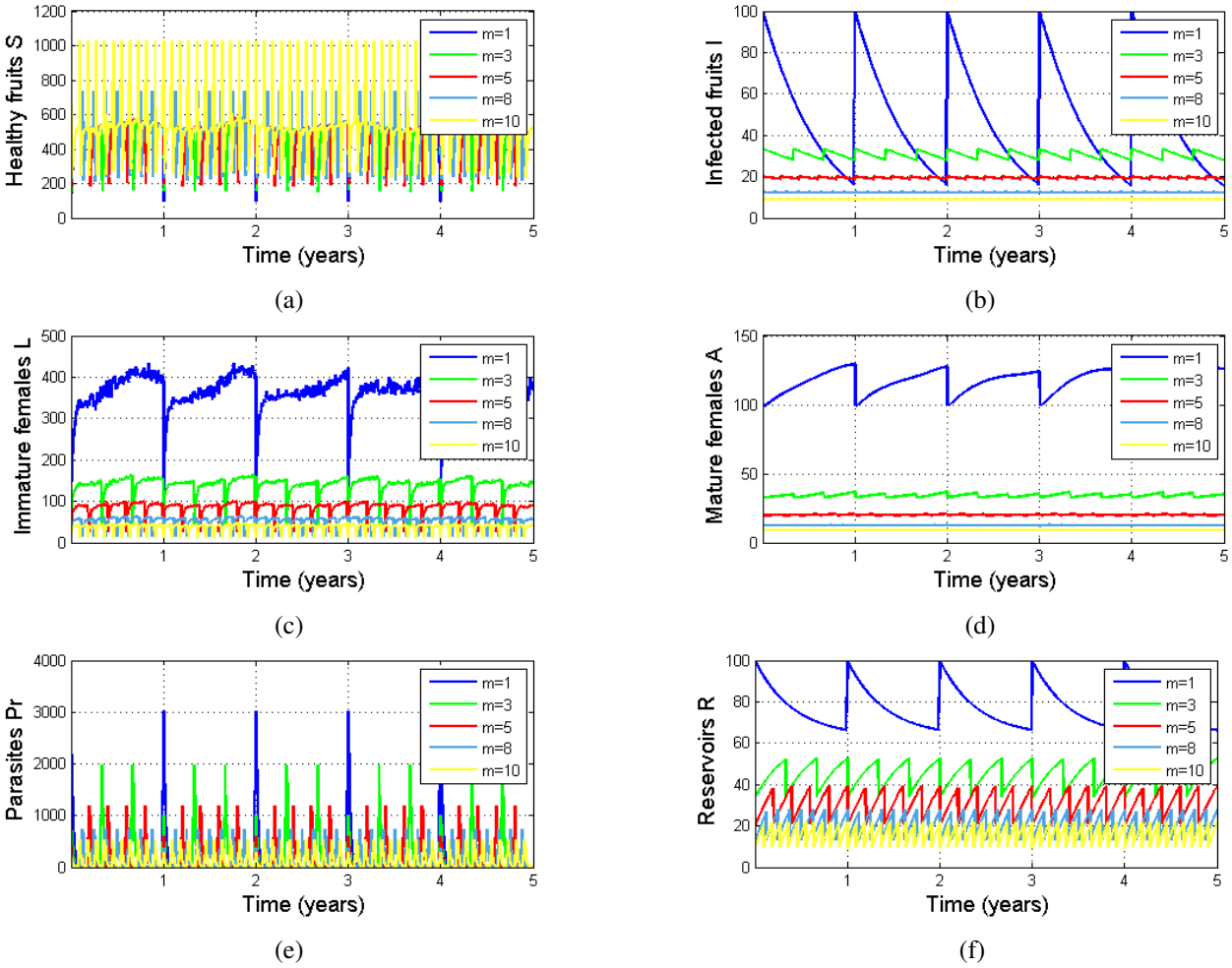

Figure 13. Impact of the impulsive release of parasites on the population dynamics of *P. marginatus*, when $\mu_I = 0.00000005$, $\epsilon = 0.0015$, $\epsilon^i = 0.0025$, $\gamma = 0.00045$, $\eta = 250$, and $\psi = 0.00035$ (such that $\mathcal{N}_0 = 12.31$, $\mathcal{N}_g = 42.31$, and $1 < \mathcal{N}_0 < \mathcal{N}_g$). All other parameter values are given in Table A.2. (a) Leaves L; (b) Flowers F; (c) Healthy fruits S; (d) Infected fruits I; (e) Immature females L; (f) Mature females A; and (g) Reservoir R.

Table 2 illustrates the positive impact of increasing the number of parasite releases (m) on the population dynamics of *P. marginatus* and the production of healthy fruits. We observe a significant increase in the cumulative number of healthy fruits, from 245.6 for 1 release ($m = 1$) to 1020 fruits (75.92% increase) with 10 releases (m = 10). Furthermore, the number of infected fruits drops drastically, from 100 to only 9.01 (90.99% reduction). Similarly, the populations of immature and mature female mealybugs decrease significantly, with 89.35% and 93.04% reduction, respectively, for 10 releases. These results highlight the effectiveness of introducing natural parasites as a biological control strategy for the sustainable management of this pest in papaya plantations.

Table 2. Cumulative number of healthy fruits, infected fruits, immature females, and mature females.

Releases	Healthy fruits	Infected fruits	Immature females	Mature females
m = 1	245.6	100	433.9	129.4
m = 3	312	33.3	164	36.9
m = 5	523.1	20	100.9	21
m = 8	738.57	12.49	63.51	12.82
m = 10	1020 (75.92%)	9.01 (90.99%)	46.2 (89.35%)	9 (93.04%)

5.2. Effect of the combination of two control strategies on the population dynamic of P. marginatus

To effectively manage the pest *P. marginatus*, it is important to adjust various control measures. One strategy is to apply repellents, such as neem-based products, to prevent adult pests from reaching the crops and reproducing. Additionally, using insecticides is recommended to target the larvae, particularly during their early developmental stages. Finally, it is essential to remove crop residues after the harvest to minimize the risk of infestation from emerging adults and to disrupt their reproductive cycle in new crops. The control measures are designed to increase the values of μ_A and μ_L while decreasing the values of a and ν_L. We incorporate control actions using impulsive differential equations, as studied in [38]. The temporal dynamics of ξ, which may correspond to μ_A, a, or ν_L, are governed by two principal parameters: The empirical target value ξ^* and the rate of adjustment ρ.

Several forms of empirical modeling may be considered; however, we opt for the simplest ordinary differential formulation:

$$\begin{cases} \dfrac{d\xi}{dt} &= \rho(\xi^* - \xi), \\ \xi(0) &= \xi_0. \end{cases} \tag{5.1}$$

Assuming $\rho > 0$, the closed-form solution to Eq (5.1) is given by:

$$\xi(t) = \xi^* - (\xi^* - \xi_0)e^{-\rho t}. \tag{5.2}$$

Hence, $\xi(t)$ asymptotically approaches the empirical target ξ^*, with the rate of convergence contingent upon the magnitude of ρ.

Let η denote the proportion of farms implementing control strategies against *P. marginatus*. Such interventions lead to a more substantial suppression of both ν_L and a, as well as elevated mortality rates. We posit that the effectiveness of control is positively correlated with η, an important consideration given the diversity of control practices adopted across farming systems. Furthermore, we assume that the implementation of control measures occurs instantaneously, yielding:

$$\Delta\xi(t_i) = -\psi(\eta)\,\xi(t_i),$$

where $\Delta\xi(t_i) = \xi(t_i^+) - \xi(t_i^-)$, and $\xi(t_i^+)$ represents the right-hand limit of ξ at time t_i.

The function $\psi : [0, 1] \to [0, 1]$, modeling the control impact, is strictly increasing with $\psi(0) = 0$ and $\psi(1) < 1$, thereby reflecting the fact that no control strategy is perfectly efficacious. We consider two functional forms for ψ:

- A linear profile, $\psi(x) = bx$, with $b \in (0, 1)$;
- A saturating nonlinear form, $\psi(x) = \frac{bx}{1+bx}$, where $b > 0$.

Here, the parameter b encapsulates the baseline efficiency of the implemented control interventions.

Assuming control actions are initiated at time t_0 and subsequently repeated at regular intervals of duration τ, we obtain the following impulsive differential model:

$$\begin{cases} \dfrac{d\xi}{dt} & = & \rho(\xi^* - \xi), \\ \Delta\xi(t_0 + n\tau) & = & -\psi(\eta)\,\xi(t_0 + n\tau), \quad n \in \{0, 1, 2, \dots\}, \\ \xi(0) & = & \xi_0. \end{cases} \tag{5.3}$$

According to the theory of impulsive differential equations, the system in Eq (5.3) is well-posed and admits a unique, globally positive solution. When the control intensity remains constant, i.e., $\eta(t) = \eta_0$, the solution may be expressed as follows:

Proposition 3. *The periodic function $\xi^c(t)$ defined by:*

$$\xi^c(t) = \begin{cases} \xi^* - (\xi^* - \xi_0)e^{-\rho t}, & t \in [0, t_0], \\ \xi^* - [\xi^* - (1 - \psi(\eta))\xi^c((n-1)\tau + t_0)]\, e^{-\rho(t-(n-1)\tau-t_0)}, & t \in ((n-1)\tau + t_0,\, n\tau + t_0], \quad n \geq 1, \end{cases} \tag{5.4}$$

is the unique solution of the impulsive system in Eq (5.3)*.*

Proof. To verify Proposition 3, it suffices to show that both expressions defining $\xi^c(t)$ satisfy the impulsive initial value problem stated in Eq (5.3). Differentiation of the analytical expressions and substitution into the differential equation confirms the required identity. Thus, the proposition is proven.

Thus, the model is described by the following differential equations.

For $t \in (t_n, t_{n+\eta}]$,

$$\begin{cases} \dot{L}_1(t) & = & \alpha(P)L_1(t)\left(1 - \dfrac{L_1(t)}{K_{L_1}}\right) - \mu_{L_1}(T)L_1(t), \\ \dot{F}(t) & = & \beta(T)L_1(t)\left(1 - \dfrac{F(t)}{K_F}\right) - (\nu_F(T) + \mu_F(T))F(t), \\ \dot{S}(t) & = & \nu_F(T)F(t) - \dfrac{\gamma\psi A(t-\tau)S(t-\tau)}{N(t-\tau)} - \mu_S(T)S, \\ \dot{I}(t) & = & \dfrac{\gamma\psi A(t-\tau)S(t-\tau)}{N(t-\tau)} - \left(\mu_I + \dfrac{dA(t)}{D + I(t)}\right)I(t), \\ \dot{L}(t) & = & \varepsilon a^c A(t)\left(1 - \dfrac{L(t)}{K_L(T) + \lambda_1(S(t) + I(t))}\right) - (\nu_L^c(T) + \mu_L(T))L(t) - \dfrac{\sigma L(t)P_r(t)}{L(t) + K_P}, \\ \dot{A}(t) & = & \nu_L^c(T)L(t) - \left(\dfrac{\mu_A^c(T)}{1 + \lambda_2(S(t) + I(t))} - \dfrac{edI(t)}{D + I(t)}\right)A(t), \\ \dot{P}_r(t) & = & \Lambda_p + \dfrac{\nu\sigma L(t)P_r(t)}{L(t) + K_P} - \mu_{P_r}P_r(t), \end{cases} \tag{5.5}$$

for $t \in (t_{n+\eta}, t_{n+1}]$ and

$$\begin{cases} \dot{L}_1(t) &= \alpha_1^i(P)L_1(t)\left(1-\dfrac{L_1(t)}{K_{L_1}^i}\right) - \mu_{L_1}^i(T)L_1(t), \\ \dot{F}(t) &= \beta^i(T)L_1(t)\left(1-\dfrac{F(t)}{K_F^i}\right) - (\mu_F^i(T)+\nu_F^i(T))F(t), \\ \dot{S}(t) &= 0, \\ \dot{I}(t) &= 0, \\ \dot{L}(t) &= \varepsilon^i a^{ic} A(t)\left(1-\dfrac{L(t)}{K_L^i(T)+\gamma_R^i R(t)}\right) - (\nu_L^{i\,c}(T)+\mu_L^i(T))L(t) - \dfrac{\sigma^i L(t)P_r(t)}{L(t)+K_P^i}, \\ \dot{A}(t) &= \nu_L^{i\,c}(T)(T)L(t) - \left(\dfrac{\mu_A^{i\,c}(T)}{1+\lambda_3 R(t)} - \dfrac{e^i d^i R(t)}{D^i+R(t)}\right)A(t), \\ \dot{R}(t) &= r^i R(t)\left(1-\dfrac{R(t)}{K_R}\right) - \left(\mu_R + \dfrac{d^i A(t)}{D^i+R(t)}\right)R(t), \\ \dot{P}_r(t) &= \Lambda_p^i + \dfrac{\nu^i\sigma^i L(t)P_r(t)}{L(t)+K_P^i} - \mu_{P_r}^i P_r(t). \end{cases} \tag{5.6}$$

Systems (5.5) and (5.6) share the same characteristics regarding existence, uniqueness, non-negativity, and boundedness of solutions as systems (2.9) and (2.19).

Next, we numerically assess the combined impact of the use of biopesticides and the releases of parasitoids on the population dynamics of *P. marginatus*.

Figure 14 illustrates the changes in the populations of flowers, healthy and infected fruits, mature and immature females, as well as the reservoir under the implementation of control strategies. The initial conditions are set as $(F(0), S(0), I(0), L(0), A(0), R(0)) = (107.5, 100, 0.001, 100, 100, 5)$. We choose $\mu_I = 0.00000005$, $\epsilon = 0.0015$, $\epsilon^i = 0.0025$, $\gamma = 0.00045$, and $\psi = 0.00035$ (so that $\mathcal{N}_0 = 12.31$, $\mathcal{N}_g = 42.31$ and $1 < \mathcal{N}_0 < \mathcal{N}_g$). All other parameter values are given in Table A.2. The results show that the population of flowers decreases over the cultivation period due to their transformation into fruits, a key process in plant development that reflects reproductive success. In parallel, the population of healthy fruits increases, while infected fruits progressively decline, tending toward zero after the second year. This indicates that the implemented control strategies are effective in reducing pest pressure. Similarly, both mature and immature female populations decrease gradually during the intercropping season, mainly due to reduced food availability and the combined effect of parasitoid releases and biopesticide applications, which limit survival and reproduction. However, as shown in Figure 14 (panels (c), (e), and (f)), an unexpected transient increase in infected fruits and mature females is observed during the first year compared to the no-control scenario, while the reservoir remains largely unaffected. This counterintuitive behavior can be explained by several mechanisms inherent to the system. First, control measures do not produce immediate effects, as there is a time lag for parasitoids to establish and exert effective suppression, enabling a temporary pest resurgence. Second, infected fruits act as protected niches where immature females continue to develop despite control pressure, contributing to short-term infection persistence. Third, the increase in mature females results from the continued development of individuals emerging from these infected fruits. Regarding the reservoir, its slower dynamics reflect its role as an alternative host or refuge, with gradual migration of mealybugs during intercropping seasons and limited immediate exposure to control actions. Importantly, this transient increase is short-lived. After the second year,

infected fruits decline toward zero, and mature female populations decrease steadily, confirming the long-term effectiveness of the control strategies. Thus, the initial rise should not be interpreted as a failure of control, but rather as a nonlinear transient dynamic preceding the stabilization of the system at a lower equilibrium.

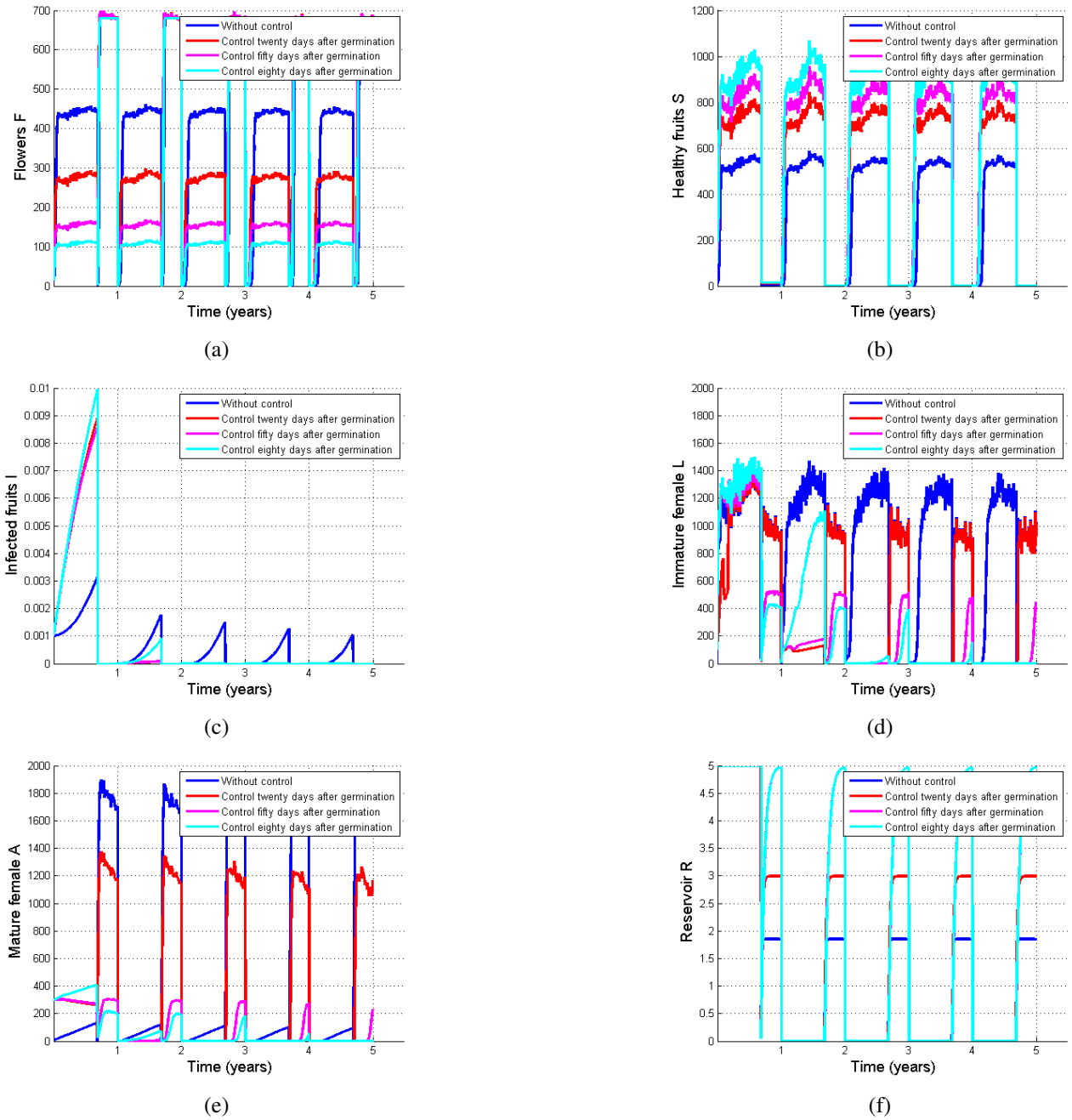

Figure 14. Effect of the combination of two control strategies on the population dynamics of *P. marginatus*, when $\mu_I = 0.00000005$, $\epsilon = 0.0015$, $\epsilon^i = 0.0025$, $\gamma = 0.00045$, $\eta = 250$, and $\psi = 0.00035$ (such that $\mathcal{N}_0 = 12.31$, $\mathcal{N}_g = 42.31$, and $1 < \mathcal{N}_0 < \mathcal{N}_g$). The other parameter values are given in Table A.2. (a) Leaves L; (b) Flowers F; (c) Healthy fruits S; (d) Infected fruits I; (e) Immature females L; (f) Mature females A; and (g) Reservoir R.

Table 3 illustrates the variations in the populations of flowers, healthy fruit, immature and mature females, and the reservoir when the use of biopesticides and the releases of parasitoids are applied.

First, there is a significant reduction in the number of flowers, which decreases by 74.62%. This reduction is primarily due to the transformation of flowers into fruit, indicating successful pollination and fruit development. Concurrently, the table shows a notable increase in the healthy fruit population, which rises by 44.92%. This increase highlights the effectiveness of the implemented control strategies, contributing to improved harvest quality. Additionally, the population of mature and immature female mealybugs is significantly reduced by 99.70% and 99.90%, respectively, testifying to the remarkable effectiveness of the combined action of parasites and biopesticides on these pests. This drastic reduction indicates not only successful control of the mealybug population but also a positive dynamic in the regulation of infestations within the ecosystem. These results underline the importance of parasites and biopesticides as biocontrol agents, contributing to the health and productivity of affected crops.

Finally, it is important to note that the reservoir population remains stable during the off-season, maintaining a level of 68%. This stability suggests that environmental conditions, coupled with the control strategies, help sustain a sufficient reservoir population, which is essential for the proper functioning of the ecosystem.

Table 3. Cumulative number of flowers, healthy fruit, and reservoirs.

	Without control	Control twenty days after germination	Control fifty days after germination	Control eighty days after germination	Percentage
Flowers	456.5	293.016	166	115.82	74.62%
Healthy fruit	588.6	842.56	956.83	1069.05	44.92%
Immature female	1468	1095	445.5	4.3	99.70%
Mature female	1896.2	1377.5	230	1.42	99.90%
Reservoir	1.8	3	4.96	5	68%

6. Conclusions

Motivated by the damages caused by a *P. marginatus* population within a papaya field, we focused on the study of the population dynamics of *P. marginatus* under several cropping seasons under the effect of climatic factors and the natural reservoir. Our findings on the long-term dynamics of the system can be summarized as follows:

(1) A qualitative analysis of the model was conducted to investigate the multi-seasonal population dynamics of *P. marginatus* in papaya fields, integrating the effects of climatic factors, natural reservoirs, and control strategies. A global sensitivity analysis via the eFAST method was performed, successfully identifying the most influential parameters across seasons and revealing how their structural reconfigurations govern the system's multistability. We first established that the problem was well-posed, ensuring that the model was mathematically and epidemiologically viable, and derived the pest-free periodic solution (PFPS) $Y^*(t)$. The basic offspring number $\mathcal{N}_0$ and the global threshold $\mathcal{N}_g$ were identified as key indicators governing the long-term evolution of the pest population. Mathematically, we proved that when $\mathcal{N}_g < 1$, the PFPS is globally asymptotically stable, indicating guaranteed pest eradication regardless of the initial field state.

Furthermore, our theoretical and numerical discussions suggest additional operational regimes based on the interaction of these thresholds. Notably, within the range $\mathcal{N}_g < \mathcal{N}_0 < 1$, a regime of bistability is conjectured, where the long-term outcome depends strictly on the initial infestation level. Conversely, when $\mathcal{N}_0 > 1$, the PFPS becomes unstable, leading to the chronic establishment of the pest population. These theoretical thresholds are not merely mathematical abstractions; they provide biologically interpretable criteria that can guide decision-making in real-world pest management. For instance, estimating $\mathcal{N}_0$ from field data would allow practitioners to predict whether a given infestation is likely to die out or become established, and to allocate control resources accordingly.

(2) Numerous numerical simulations were also used to illustrate the role of climate change and the reservoir on the growth of papaya in the presence of *P. marginatus*. We found that

   (a) The presence of the reservoir significantly enhances mealybug populations, leading to a 25.13% increase in immature females and an 18.08% increase in mature females compared to conditions without the reservoir. This means that the reservoir plays a crucial role during the non-production phase of the papaya crop, enabling the mealybug population to survive and maintain itself until the crop returns. This ensures the continuity of infestation from one season to the next, facilitating the re-infestation of new papaya plantations. These findings align with the work of Othim et al. [39], who demonstrated that weeds and crop residues are essential for pest persistence during fallow periods. Thus, managing this alternative reservoir is a key strategy for the integrated management of the mealybug. From a reference perspective, our quantification of the reservoir's impact provides numerical benchmarks that future studies can use to compare the relative importance of alternative host plants across regions or pest species.

   (b) Concerning the role of climate change, we found that *P. marginatus* proliferates rapidly during the first 250 days, which corresponds to the full papaya cultivation period, spanning planting to harvest. This phase overlaps with the dry and transitional climatic periods in Douala (September to early May), when favorable environmental conditions, including high temperatures and low rainfall, promote pest development. Beyond this period, a marked population decline is observed, coinciding with the onset of the long rainy season. These findings suggest that control strategies should be prioritized during the active crop growth phase and adjusted during the off-season, when natural climatic conditions help suppress pest populations. This season-specific insight provides a practical reference for timing interventions, enabling farmers to synchronize parasitoid releases or biopesticide applications with periods of peak pest vulnerability, thereby maximizing efficacy while minimizing costs.

(3) We incorporated two control actions into our model, the impulsive releases of parasitoids, and the combination of biopesticides and natural parasitoids.

   (i) The simulation of the model with the control strategy based on the impulsive releases of parasitoids showed that the introduction of parasitoids significantly boosts healthy fruit production, with cumulative healthy fruits increasing from 245.6 to 1020, a remarkable 75.92% rise. The number of infected fruits drops sharply from 100 to just 9.01. These changes are accompanied by dramatic reductions in mealybug populations, with

immature females decreasing by 89.35% and mature females by 93.04% after ten releases. Parasites as biological control agents have shown significant promise in regulating mealybug populations, promoting the proliferation of healthy fruits, and reducing the number of infected fruits as well as mealybugs in the reservoir. These results support the findings of Franco et. al. [13], which indicate that the targeted introduction of natural parasitoids of papaya mealybugs effectively manages pest populations in infested plantations. This integrated biological control approach represents a sustainable and ecological alternative for managing papaya mealybug infestations, and its large-scale deployment should be encouraged to foster more environmentally friendly agricultural practices. The quantitative performance metrics reported can serve as reference targets for field evaluations of biological control programs. Researchers can compare their results against these benchmarks to assess the relative success of different parasitoid species or release schedules.

(ii) The integration of the use of biopesticides and natural parasitoids has proven to be an effective method for controlling the papaya mealybug (*Paracoccus marginatus*). The combined use of these two approaches has demonstrated synergy, optimizing pest control efficiency. As a result, there is a 44.92% increase in productivity and complete disappearance of mealybugs in the field. This can significantly reduce the number of infected fruits by the second year of implementation. These findings are consistent with the work of Srinivasan [40], who showed that the application of biopesticides derived from *Bacillus thuringiensis* significantly decreased mealybug populations. The effectiveness of pest control was further enhanced, leading to a substantial decline in both the immature and mature stages of the mealybug. The synergy quantified provides a reference for evaluating the added value of integrating biopesticides with biological control, compared to either strategy used alone. This integrated approach achieves what neither method can accomplish independently: Complete field elimination of the pest. However, the effectiveness of this strategy may be undermined by certain agronomic practices, such as excessive plantation cleaning. While intended to maintain hygiene, cleaning can inadvertently remove beneficial organisms such as natural parasitoids and parasitoids that play a crucial role in regulating pest populations. Their elimination may disrupt ecological balance and create conditions favorable to pest resurgence, thereby limiting the success of biologically based management strategies.

(iii) For the successful implementation of effective control strategies, it is imperative to thoroughly understand the parameters at play. A lack of adequate knowledge regarding these parameters can result in biased decisions and diminish the efficacy of control measures. As indicated by the data in Tables A.2 and A.3, numerous parameters remain inadequately understood. This lack of clarity raises doubts about the dependability of the optimization methods discussed earlier. To address these uncertainties, parameter estimation techniques can be employed. These methods could help clarify unknown parameters and analyze the impact of their fluctuations on control outcomes. Additionally, when real-time data is accessible, we can adopt a dynamic control approach that enables us to decide whether to act immediately based on the available information or to defer actions for further data gathering. This flexible strategy ensures that control decisions are grounded in the latest data, significantly improving their effectiveness. From a methodological reference perspective, the parameter estimation framework proposed here can be adapted to other pest models where

key biological rates are uncertain. This provides future researchers with a template for grounding mathematical models in field data, thereby enhancing the practical applicability of theoretical studies.

Use of AI tools declaration

The authors declare they have not used Artificial Intelligence (AI) tools in the creation of this article.

Conflict of interest

The authors declare there are no conflicts of interest.

References

1. C. L. Chia, M. S. Nishina, D. O. Evans, *Papaya*, Commodity Fact Sheet PA-3(A), College of Tropical Agriculture and Human Resources, University of Hawaï, Honolulu, USA, 1989. Available from: http://hdl.handle.net/10125/15083.
2. A. F. Maffo, E. L. M. Ngonkeu, C. Chaintreuil, C. N. Temegne, G. N. Ntsefong, F. Fall, et al., Morphological and molecular diversity of arbuscular mycorrhizal fungi associated to Carica papaya L. rhizosphere in two agro-ecological zones in Cameroon, *Afr. J. Agric. Res.*, **18** (2022), 632–646. https://doi.org/10.5897/AJAR2022.16072
3. P. L. Saran, I. S. Solanki, R. Choudhary, *Papaya: Biology, Cultivation, Production and Uses*, CRC Press/Taylor & Francis, 2016. https://doi.org/10.1201/b18955
4. D. Gonsalves, Control of papaya ringspot virus in papaya: A case study, *Annu. Rev. Phytopathol.*, **36** (1998), 415–437. https://doi.org/10.1146/annurev.phyto.36.1.415
5. R. K. Tanwar, P. Jeyakumar, D. Monga, *Mealybugs and Their Management*, National Centre for Integrated Pest Management, New Delhi, India, 2007. Available from: https://nriipm.res.in/NCIPMPDFs/Publication/BulletinMealybugsEnglish_.pdf.
6. IPPC, Outbreak and Control of Papaya Mealy Bug (*Paracoccus marginatus*), Official Pest Report, 2024. Available from: https://www.ippc.int/fr/countries/india/pestreports/2024/07/outbreak-and-control-of-papaya-mealy-bug-paracoccus-marginatus--1/.
7. K. G. Amarasekare, C. M. Mannion, L. S. Osborne, N. D. Epsky, Life history of *Paracoccus marginatus* (Hemiptera: Pseudococcidae) on four host plant species under laboratory conditions, *Environ. Entomol.*, **37** (2008), 630–635. https://doi.org/10.1603/0046-225X(2008)37[630:LHOPMH]2.0.CO;2
8. R. A. Larson, *Introduction to Floriculture*, 2nd edition, Academic Press, San Diego, USA, 1992. Available from: https://www.sciencedirect.com/book/edited-volume/9780124376519/introduction-to-floriculture.
9. R. Muniappan, B. M. Shepard, G. W. Watson, G. R. Carner, A. Rauf, D. Sartiami, et al., New records of invasive insects (Hemiptera: Sternorrhyncha) in Southeast Asia and West Africa, *J. Agric. Urban Entomol.*, **26** (2009), 167–174. https://doi.org/10.3954/1523-5475-26.4.167

10. R. W. Mwanauta, P. A. Ndakidemi, P. B. Venkataramana, Biopesticide efficacy of four plant essential oils against papaya mealybug, *Paracoccus marginatus* Williams and Granara de Willink (Hemiptera: Pseudococcidae), *Heliyon*, **9** (2023), e14162. https://doi.org/10.1016/j.heliyon.2023.e14162

11. A. Piragalathan, K. Pakeerathan, G. Thirukkumaran, G. Mikunthan, Efficacy of different insecticides and bio-rationals against papaya mealybug, *Paracoccus marginatus* (Hemiptera: Pseudococcidae) infestation in home gardens, *Middle East J. Sci. Res.*, **21** (2014), 1689–1693. Available from: http://repo.lib.jfn.ac.lk/ujrr/handle/123456789/932.

12. D. E. Meyerdirk, R. Muniappan, R. Warkentin, J. Bamba, G. V. P. Reddy, Biological control of the papaya mealybug, *Paracoccus marginatus* (Hemiptera: Pseudococcidae) in Guam, *Plant Prot. Q.*, **19** (2004), 110–114. Available from: https://caws.org.nz/PPQ1819/PPQ%2019-3%20pp110-114%20Meyerdirk.pdf.

13. J. C. Franco, P. Suma, E. B. da Silva, D. Blumberg, Z. Mendel, Management of mealybugs pests of citrus in mediterranean countries, *Phytoparasitica*, **32** (2004), 507–522. https://doi.org/10.1007/BF02980445

14. K. G. Amarasekare, J. H. Chong, N. D. Epsky, C. M. Mannion, Effect of temperature on the life history of the mealybug *Paracoccus marginatus* (Hemiptera: Pseudococcidae), *J. Econ. Entomol.*, **101** (2008), 1798–1804. https://doi.org/10.1603/0022-0493-101.6.1798

15. P. Auger, C. Lett, J. C. Poggiale, *Modélisation Mathématique en Écologie: Cours et Exercices Corrigés*, 2nd ed, Paris: Dunod, 2015. Available from: https://www.dunod.com/sciences-techniques/modelisation-mathematique-en-ecologie-cours-et-exercices-corriges.

16. I. Tankam, S. Touzeau, L. Mailleret, J. Tewa, F. Grognard, Modelling and control of a banana soil-borne pest in a multi-seasonal framework, *Math. Biosci.*, **322** (2020), 108324. https://doi.org/10.1016/j.mbs.2020.108324

17. M. Dountio, A. N. Yankam, S. Bowong, Theoretical assessment of the impact on the population dynamics of *Paracoccus marginatus*, *Bol. Soc. Mat. Mex.*, **30** (2024), 5. https://doi.org/10.1007/s40590-023-00566-4

18. M. Dountio, A. N. Yankam, S. Bowong, Exploring the impact of biocontrol and temperature variations on the population dynamics of *Paracoccus marginatus*, *Appl. Math. Model.*, **130** (2024), 346–377. https://doi.org/10.1016/j.apm.2024.02.035

19. L. F. M. Marcelis, E. Heuvelink, J. Goudriaan, Modelling biomass production and yield of horticultural crops: A review, *Sci. Hortic.*, **74** (1998), 83–111. https://doi.org/10.1016/S0304-4238(98)00083-1

20. E. Heuvelink, M. Dorais, Growth and yield, in *Tomatoes*, CABI Publishing, (2005), 85–144. https://doi.org/10.1079/9780851993966.0085

21. V. M. Jimenez, E. Mora-Newcomer, M. V. Gutiérrez-Soto, Biology of the papaya plant, in *Genetics and Genomics of Papaya*, Springer, (2014), 17–33. https://doi.org/10.1007/978-1-4614-8087-7_2

22. P. Allan, Phenology and production of *Carica papaya* Honey Gold under cool subtropical conditions, *Acta Hortic.*, **740** (2007), 217–223. https://doi.org/10.17660/ActaHortic.2007.740.26

23. L. Zhou, M. Q. R. Eloisa, E. P. Robert, Papaya (*Carica papaya* L) leaf area estimation and single-leaf net photosynthetic CO^2 assimilation rate following leaf defoliation and fruit thinning, *HortScience*, **55** (2020), 1861–1864. https://doi.org/10.21273/HORTSCI15345-20

24. S. Mitra, *The Papaya: Botany, Production and Uses*, CABI, Wallingford, Oxfordshire, UK, 2020. Available from: https://www.cabidigitallibrary.org/doi/book/10.1079/9781789241907.0000.

25. A. Lacointe, Carbon allocation among tree organs: A review of basic processes and representation in functional-structural tree models, *Ann. For. Sci.*, **57** (2000), 521–533. https://doi.org/10.1051/forest:2000139

26. W. Montas, P. A. Moon, J. H. Crane, J. Colee, Effect of ratooning X17-2 × T5 papaya plants on crop yield and survival, *Proc. Fla. State Hort. Soc.*, **130** (2017), 32–34. Available from: https://www.cabidigitallibrary.org/doi/full/10.5555/20193451510.

27. E. Campostrini, D. M. Glenn, Ecophysiology of papaya: A review, *Braz. J. Plant Physiol.*, **19** (2007), 413–424. https://doi.org/10.1590/S1677-04202007000400010

28. A. Seni, A. K. Sahoo, Weather factors influencing population of papaya mealybug, *Paracoccus marginatus* (Hemiptera: Pseudococcidae), *J. Plant Pest Sci.*, **2** (2015), 41–47. Available from: https://www.researchgate.net/publication/309735722_Weather_factors_influencing_population_of_papaya_mealybug_Paracoccus_marginatus_Hemiptera_Pseudococcidae.

29. M. Mani, C. Shivaraju, A. N. Shylesha, *Paracoccus marginatus*, an invasive mealybug of papaya and its biological control, an overview, *J. Biol. Control.*, **26** (2012), 201–216. Available from: https://www.informaticsjournals.co.in/index.php/jbc/article/view/3491.

30. P. Shi, F. Ge, A comparison of different thermal performance functions describing temperature-dependent development rates, *J. Therm. Biol.*, **35** (2010), 225–231. https://doi.org/10.1016/j.jtherbio.2010.05.005

31. M. Li, R. Guo, W. Ding, J. Ma, Temperature dependent developmental time for the larva stage of *Aedes aegypti*, *Math. Biosci. Eng.*, **19** (2022), 4396–4406. https://doi.org/10.3934/mbe.2022203

32. L. M. Carvalho, C. J. Struchiner, L. S. Bastos, Bayesian inference of deterministic population growth models, in *Interdisciplinary Bayesian Statistics*, Springer, (2015), 217–228. https://doi.org/10.1007/978-3-319-12454-4_18

33. I. Rodriguez-Iturbe, A. Porporato, *Ecohydrology of Water-Controlled Ecosystems: Soil Moisture and Plant Dynamics*, Cambridge University Press, Cambridge, 2005. https://doi.org/10.1017/CBO9780511535727

34. G. Floquet, Sur les équations différentielles linéaires à coefficients périodiques, *Ann. Sci. Éc. Norm. Supér.*, **12** (1883), 47–88. https://doi.org/10.24033/asens.220

35. J. P. Tian, J. Wang, Some results in Floquet theory, with application to periodic epidemic models, *Appl. Anal.*, **94** (2015), 1128–1152. https://doi.org/10.1080/00036811.2014.918606

36. H. L. Smith, *Monotone Dynamical Systems: An Introduction to the Theory of Competitive and Cooperative Systems*, American Mathematical Society, 1995. Available from: https://pubs.ams.org/ebooks/surv/041/.

37. A. Daghar, H. Marzougui, Dynamics of monotone maps on regular curves, *Topol. Appl.*, **324** (2023), 108352. https://doi.org/10.1016/j.topol.2022.108352

38. Y. Dumont, J. Thuilliez, Human behaviors: A threat to mosquito control?, *Math. Biosci.*, **281** (2016), 9–23. https://doi.org/10.1016/j.mbs.2016.08.011

39. S. T. O. Othim, S. Opisa, I. Rwomushana, B. Luke, Unleashing nature's defenders: Farmer-managed natural enemies field reservoirs (NEFRs) enhance management of the invasive papaya mealybug (*Paracoccus marginatus*) in coastal Kenya, *Biol. Control*, **193** (2024), 105528. https://doi.org/10.1016/j.biocontrol.2024.105528

40. R. Srinivasan, Integrating biopesticides in pest management strategies for tropical vegetable production, *J. Biopestic.*, **5** (2012), 36–45. https://doi.org/10.57182/jbiopestic.5.0.36-45

41. P. Magal, X. Q. Zhao, Global attractors and steady states for uniformly persistent dynamical systems, *SIAM J. Math. Anal.*, **37** (2005), 251–275. https://doi.org/10.1137/S0036141003439173

42. C. L. Encina, M. L. Granero, J. J. Regalado, In vitro long-term cultures of papaya (Carica papaya L. cv. Solo), *Horticulturae*, **9** (2023), 671. https://doi.org/10.3390/horticulturae9060671

Appendix

A.1. Proof of Lemma 2

Herein, we give the proof of Lemma 2.

A solution of systems (2.9) and (2.19) is called pest-free solution if $E(t) = A(t) = 0$, $\forall t > 0$.

Setting $A(t)$ and $E(t)$ equal to zero into systems (2.9) and (2.19), gives the following systems:

$$\begin{cases} \dot{L}_1(t) &= C(t)L_1 - \dfrac{\alpha(P(t))}{K_{L_1}}L_1^2(t), \\ \dot{F}(t) &= \beta(T)L_1 - B(t)F, \qquad \text{if } t \in (t_n, t_n+\eta], \\ \dot{S}(t) &= \nu_F(T(t))F - \mu_S(T(t))S, \\ \dot{P}_r(t) &= \Lambda_p - \mu_{P_r}P_r, \end{cases} \tag{A.1}$$

and

$$\begin{cases} \dot{L}_1(t) &= C^i(t)L_1 - \dfrac{\alpha^i(P(t))}{K_{L_1}}L_1^2(t), \\ \dot{F}(t) &= \beta(T(t))L_1 - B^i(t)F, \\ \dot{S}(t) &= 0, \qquad \text{if } t \in (t_n+\eta, t_{n+1}], \\ \dot{R}(t) &= r^iR\left(1 - \dfrac{R}{K_R^i}\right), \\ \dot{P}_r(t) &= \Lambda_p^i - \mu_{P_r}^iP_r. \end{cases} \tag{A.2}$$

Setting $L_1(t) = \dfrac{1}{M(t)}$ and integrating the first equation of systems (A.1) and (A.2) from t_n to t gives

$$M(t) = \begin{cases} M(t_n^+)e^{-\int_{t_n}^t C(m)dm} + \displaystyle\int_{t_n}^t \frac{\alpha_1(P(s))}{K_{L_1}}e^{-\int_s^t C(m)dm}ds \text{ if } t \in (t_n, t_n+\eta], \\ M((t_n+\eta)^+)e^{-\int_{t_n+\eta}^t C^i(m)dm} + \displaystyle\int_{t_n+\eta}^t \frac{\alpha^i(P(s))}{K_{L_1}^i}e^{-\int_s^t C^i(m)dm}ds \text{ if } t \in (t_n+\eta, t_{n+1}]. \end{cases} \tag{A.3}$$

Since $L_1(t_n + \eta^+) = \pi_{L_1} L_1(t_n + \eta)$, it comes that $M(t_n + \eta^+) = \dfrac{1}{\pi_{L_1}} M(t_n + \eta)$. Hence, from the second equation of (A.3), one can deduce that

$$\begin{aligned} M(t) &= \frac{1}{\pi_{L_1}}\left(M(t_n^+)e^{-\int_{t_n}^{t_n+\eta} C(s)ds} + \int_{t_n}^{t_n+\eta} \frac{\alpha_1(P(s))}{K_{L_1}} e^{-\int_s^{t_n+\eta} C(m)dm} ds\right) e^{-\int_{t_n+\eta}^{t} C^i(s)ds} \\ &+ \int_{t_n+\eta}^{t} \frac{\alpha^i(P(s))}{K_{L_1}} e^{-\int_s^t C^i(m)dm} ds, \text{ if } t \in (t_n + \eta, t_{n+1}]. \end{aligned} \tag{A.4}$$

Now, let us find $M(t_n^+)$.

Using the fact that $M(t_{n+1}^+) = \dfrac{1}{\psi_{L_1}} M(t_{n+1})$, it comes that $Z(t_{n+1}^+) = \dfrac{1}{\psi_{L_1}} Z(t_{n+1})$. Then, from Eq (A.4), it comes that

$$\begin{aligned} \psi_{L_1} M(t_{n+1}^+) &= \frac{1}{\pi_{L_1}} M(t_n^+) e^{-\int_{t_n}^{t_n+\eta} C(s)ds + \int_{t_n+\eta}^{t_{n+1}} C^i(s)ds} + \frac{1}{\pi_{L_1}} \int_{t_n}^{t_n+\eta} \frac{\alpha_1(P(s))}{K_{L_1}} e^{-\int_s^{t_n+\eta} C(w)dw + \int_{t_n+\eta}^{t_{n+1}} C^i(w)dw} ds \\ &+ \int_{t_n+\eta}^{t_{n+1}} \frac{\alpha^i(P(s))}{K_{L_1}} e^{-\int_s^{t_{n+1}} C^i(w)dw} ds. \end{aligned} \tag{A.5}$$

Searching for a fixed point for M gives

$$M(t_n^+) = \frac{\dfrac{1}{\pi_{L_1}} \displaystyle\int_{t_n}^{t_n+\eta} \frac{\alpha(P(s))}{K_{L_1}} \exp\left(-\left(\int_s^{t_n+\eta} C(m)dm + \int_{t_n+\eta}^{t_{n+1}} C^i(m)dm\right)\right) ds}{\psi_{L_1} - \dfrac{1}{\pi_{L_1}} \exp\left(-\left(\displaystyle\int_{t_n}^{t_n+\eta} C(s)ds + \int_{t_n+\eta}^{t_{n+1}} C^i(s)ds\right)\right)}. \tag{A.6}$$

Thus, the unique non-negative solution of the first equation of the system (A.1) is given by

$$M^*(t) = \begin{cases} \left(\dfrac{\dfrac{1}{\pi_{L_1}} \displaystyle\int_{t_n}^{t_n+\eta} \frac{\alpha(P(s))}{K_{L_1}} \exp\left(-\left(\int_s^{t_n+\eta} C(m)dm + \int_{t_n+\eta}^{t_{n+1}} C^i(m)dm\right)\right) ds}{\psi_{L_1} - \dfrac{1}{\pi_{L_1}} \exp\left(-\left(\displaystyle\int_{t_n}^{t_n+\eta} C(s)ds + \int_{t_n+\eta}^{t_{n+1}} C^i(s)ds\right)\right)}\right) \exp\left(-\displaystyle\int_{t_n}^{t} C(s)ds\right) \\ + \displaystyle\int_{t_n}^{t} \frac{\alpha(P(s))}{K_{L_1}} \exp(-\int_s^t C(m)dm)ds, \qquad \text{if } t \in [t_n, t_n + \eta], \\ \dfrac{1}{\pi_{L_1}} \left(\left(\dfrac{\dfrac{1}{\pi_{L_1}} \displaystyle\int_{t_n}^{t_n+\eta} \frac{\alpha(P(s))}{K_{L_1}} \exp\left(-\left(\int_s^{t_n+\eta} C(m)dm + \int_{t_n+\eta}^{t_{n+1}} C^i(m)dm\right)\right) ds}{\psi_{L_1} - \dfrac{1}{\pi_{L_1}} \exp\left(-\left(\displaystyle\int_{t_n}^{t_n+\eta} C(s)ds + \int_{t_n+\eta}^{t_{n+1}} C^i(s)ds\right)\right)}\right) \exp\left(-\displaystyle\int_{t_n}^{t_n+\eta} C(s)ds\right) \right. \\ \left. + \displaystyle\int_{t_n}^{t_n+\eta} \frac{\alpha(P(s))}{K_{L_1}} \exp\left(-\int_s^{t_n+\eta} C(m)dm\right) ds\right) \exp\left(-\int_{t_n+\eta}^{t} C^i(s)ds\right) \\ + \displaystyle\int_{t_n+\eta}^{t} \frac{\alpha^i(P(s))}{K_{L_1}} \exp\left(-\int_s^t C^i(m)dm\right) ds, \qquad \text{if } t \in [t_n + \eta, t_{n+1}]. \end{cases} \tag{A.7}$$

Then, one can show that

$$
\left|M(t)-M^*(t)\right| = \begin{cases} \left(\dfrac{\dfrac{1}{\pi_{L_1}}\displaystyle\int_{t_n}^{t_n+\eta}\dfrac{\alpha(P(s))}{K_{L_1}}\exp\left(-\left(\int_s^{t_n+\eta}C(m)dm+\int_{t_n+\eta}^{t_{n+1}}C^i(m)dm\right)\right)ds}{\psi_{L_1}-\dfrac{1}{\pi_{L_1}}\exp\left(-\left(\int_{t_n}^{t_n+\eta}A(s)ds+\int_{t_n+\eta}^{t_{n+1}}C^i(s)ds\right)\right)}\right)\exp\left(-\int_{t_n}^{t}C(s)ds\right), \\ \qquad\qquad\qquad\qquad\qquad\qquad\qquad\qquad\qquad\qquad\qquad\qquad \text{if } t\in[t_n,t_n+\eta], \\ \dfrac{1}{\pi_{L_1}}\left(\left(\dfrac{\dfrac{1}{\pi_{L_1}}\displaystyle\int_{t_n}^{t_n+\eta}\dfrac{\alpha(P(s))}{K_{L_1}}\exp\left(-\left(\int_s^{t_n+\eta}C(m)dm+\int_{t_n+\eta}^{t_{n+1}}C^i(m)dm\right)\right)ds}{\psi_{L_1}-\dfrac{1}{\pi_{L_1}}\exp\left(-\left(\int_{t_n}^{t_n+\eta}C(s)ds+\int_{t_n+\eta}^{t_{n+1}}C^i(s)ds\right)\right)}\right)\exp\left(-\int_{t_n}^{t_n+\eta}C(s)ds\right)\right. \\ \left.+\displaystyle\int_{t_n}^{t_n+\eta}\frac{\alpha(P(s))}{K_{L_1}}\exp\left(-\int_s^{t_n+\eta}C(m)dm\right)ds\right)\exp\left(-\int_{t_n+\eta}^{t}C^i(s)ds\right). \quad \text{if } t\in[t_n+\eta,t_{n+1}]. \end{cases}
$$

It is clear that $\left|M(t)-M^*(t)\right| \longrightarrow 0$ as $t\longrightarrow\infty$. Hence, one can deduce that $\left|L(t)-L^*(t)\right| \longrightarrow 0$ as $t\longrightarrow\infty$.

Integrating the second equation of systems (A.1) and (A.2) from t_n to t and from $t_n+\eta$ to t gives

$$
F(t) = \begin{cases} F(t_n^+)e^{-\int_{t_n}^{t}B(m)dm}+\displaystyle\int_{t_n}^{t}\beta(T(s))L_1^*(s)e^{-\int_s^t g(m)dm}ds, & \text{if } (t_n,t_n+\eta], \\ F((t_n+\eta)^+)e^{-\int_{t_n+\eta}^{t}B^i(m)dm}+\displaystyle\int_{t_n+\eta}^{t}\beta^i(T(s))L_1^*(s)e^{-\int_s^t B^i(w)dw}, & \text{if } t\in(t_n+\eta,t_{n+1}]. \end{cases} \tag{A.8}
$$

Using the fact that $F((t_n+\eta)^+)=\pi_F F(t_n+\eta)$, it comes that

$$
F(t) = \begin{cases} F(t_n^+)e^{-\int_{t_n}^{t}B(m)dm}+\displaystyle\int_{t_n}^{t}\beta(T(s))L_1^*(s)e^{-\int_s^t B(m)dm}ds, & \text{if } (t_n,t_n+\eta], \\ \left(\pi_F F(t_n^+)e^{-\int_{t_n}^{t_n+\eta}B(m)dm}+\pi_F\displaystyle\int_{t_n}^{t_n+\eta}\beta(s)L_1^*(s)e^{-\int_s^{t_n+\eta}B(m)dm}ds\right)e^{-\int_{t_n+\eta}^{t}B^i(m)dm}+ & \\ +\displaystyle\int_{t_n+\eta}^{t}\beta^i(T(s))L_1^*(s)e^{-\int_s^t B^i(w)dw} & \text{if } t\in(t_n+\eta,t_{n+1}]. \end{cases} \tag{A.9}
$$

Using the fact that $F(t_{n+1}^+)=\psi_F F(t_{n+1})$ and searching for a fix point for F, it comes that

$$
F(t_n^+) = \frac{\pi_F\psi_7\displaystyle\int_{t_n}^{t_n+\eta}\beta(s)L^*(s)e^{-\left(\int_s^{t_n+\eta}B(m)dm+\int_{t_n+\eta}^{t_{n+1}}B^i(m)dm\right)}ds+\psi_F\int_{t_n+\eta}^{t_{n+1}}\beta^i(s)L_1^*(s)\exp\left(-\int_s^{t_{n+1}}B^i(s)ds\right)}{1-\pi_F\psi_7 e^{-\left(\int_{t_n}^{t_n+\eta}B(m)dm+\int_{t_n+\eta}^{t_{n+1}}B^i(m)dm\right)}}
$$

Thus, the unique non-negative solution of the second equation of systems (A.1) and (A.2) is given by

$$
F^*(t) = \begin{cases} \left(\dfrac{\pi_F\psi_F\displaystyle\int_{t_n}^{t_n+\eta}\beta(s)L_1^*(s)e^{-\left(\int_s^{t_n+\eta}B(m)dm+\int_{t_n+\eta}^{t_{n+1}}B^i(m)dm\right)}ds+\psi_F\int_{t_n+\eta}^{t_{n+1}}\beta^i(s)L_1^*(s)\exp\left(-\int_s^{t_{n+1}}B^i(s)ds\right)}{1-\pi_F\psi_7 e^{-\left(\int_{t_n}^{t_n+\eta}B(m)dm+\int_{t_n+\eta}^{t_{n+1}}B^i(m)dm\right)}}\right) \\ \times e^{-\int_{t_n}^{t}B(m)dm}+\displaystyle\int_{t_n}^{t}\beta(T(s))L_1^*(s)e^{-\int_s^t B(m)dm}ds, \qquad \text{if } (t_n,t_n+\eta], \\ \left(\pi_F\left(\dfrac{\pi_F\psi_F\displaystyle\int_{t_n}^{t_n+\eta}\beta(s)L^*(s)e^{-\left(\int_s^{t_n+\eta}B(m)dm+\int_{t_n+\eta}^{t_{n+1}}B^i(m)dm\right)}ds+\psi_F\int_{t_n+\eta}^{t_{n+1}}\beta^i(s)L^*(s)\exp\left(-\int_s^{t_{n+1}}B^i(s)ds\right)}{1-\pi_F\psi_7 e^{-\left(\int_{t_n}^{t_n+\eta}B(m)dm+\int_{t_n+\eta}^{t_{n+1}}B^i(m)dm\right)}}\right)\right. \\ \left.\times e^{-\int_{t_n}^{t_n+\eta}B(m)dm}+\pi_F\displaystyle\int_{t_n}^{t_n+\eta}\beta(s)L_1^*(s)e^{-\int_s^{t_n+\eta}B(m)dm}ds\right)e^{-\int_{t_n+\eta}^{t}B^i(m)dm}+\int_{t_n+\eta}^{t}\beta^i(T(s))L_1^*(s)e^{-\int_s^t B^i(w)dw} \\ \qquad\qquad\qquad\qquad\qquad\qquad\qquad\qquad\qquad\qquad \text{if } t\in(t_n+\eta,t_{n+1}]. \end{cases} \tag{A.10}
$$

Then, one can show that

$$\left|F(t)-F^*(t)\right| = \begin{cases} \left(\dfrac{\pi_F\psi_F\int_{t_n}^{t_n+\eta}\beta(s)L_1^*(s)e^{-\left(\int_s^{t_n+\eta}B(w)ds+\int_{t_n+\eta}^{t_{n+1}}B^i(w)dw\right)ds}+\psi_F\int_{t_n+\eta}^{t_{n+1}}\beta^i(s)L_1(s)e^{-\int_s^{t_{n+1}}B^i(w)dw}}{1-\pi_F\psi_F e^{-\left(\int_{t_n}^{t_n+\eta}B(s)+\int_{t_n+\eta}^{t_{n+1}}B^i(w)dw\right)}}\right) \\ \times\exp\left(-\int_{t_n}^{t}g(w)dw\right) \text{ if } (t_n,t_n+\eta], \\ \pi_F\left(\dfrac{\pi_F\psi_F\int_{t_n}^{t_n+\eta}\beta(s)L_1^*(s)e^{-\left(\int_s^{t_n+\eta}B(w)ds+\int_{t_n+\eta}^{t_{n+1}}B^i(w)dw\right)ds}+\psi_2\int_{t_n+\eta}^{t_{n+1}}\beta^i(s)L_1^*(s)e^{-\int_s^{t_{n+1}}B^i(w)dw}}{1-\pi_2\psi_2 e^{-\left(\int_{t_n}^{t_n+\eta}B(s)+\int_{t_n+\eta}^{t_{n+1}}B^i(w)dw\right)}}\right) \\ \times\exp\left(-\int_{t_n}^{t}B^i(w)dw\right) \text{ if } t\in(t_n+\eta,t_{n+1}]. \end{cases}$$

It then comes that $|F(t)-F^*(t)|\longrightarrow 0$ as $t\longrightarrow\infty$.
Integrating the third equation of systems (A.1) and (A.2) from t_n to t and from $t_n+\eta$ to t gives

$$S(t)=\begin{cases} S(t_n^+)e^{-\int_{t_n}^{t}\mu_S(T(m))dm}+\int_{t_n}^{t}\nu_F(T(s))F^*(s)e^{-\int_s^t\mu_S(T(m))dm}ds, & \text{if } t\in(t_n,t_n+\eta], \\ S((t_n+\eta)^+) & \text{if } t\in(t_n+\eta,t_{n+1}]. \end{cases} \tag{A.11}$$

Using the fact that $S(t_n+\eta^+)=0$ and $S(t_{n+1}^+)=0$, one has that $S(t_n^+)=0$.
Thus, the unique non-negative solution of the second equation of systems (A.1) and (A.2) is given by

$$S^*(t)=\begin{cases} \int_{t_n}^{t}\nu_F(T(s))F(s)e^{-\int_s^t\mu_S(T(m))dm}ds, & \text{if } (t_n,t_n+\eta], \\ 0 & \text{if } t\in(t_n+\eta,t_{n+1}]. \end{cases} \tag{A.12}$$

With this in mind, one has that

$$\left|S(t)-S^*(t)\right|=\begin{cases} 0 \text{ if } (t_n,t_n+\eta], \\ 0 \text{ if } t\in(t_n+\eta,t_{n+1}]. \end{cases}$$

Then, $\left|S(t)-S^*(t)\right|\longrightarrow 0$ as $t\longrightarrow\infty$.
Setting $Z(t)=\dfrac{1}{R(t)}$ and integrating the fourth equation of systems (A.1) and (A.2) gives

$$Z(t)=Z((t_n+\eta)^+)e^{-r^i(t-(t_n+\eta)}+\frac{1}{K_R}(1-e^{-r^i(t-(t_n+\eta))}) \text{ if } (t_n+\eta,t_{n+1}]. \tag{A.13}$$

Using the fact that $Z((t_n+\eta)^+)=0$, it comes that

$$Z(t)=\frac{1}{K_R}(1-e^{-r^i(t-(t-t_n))}) \text{ if } (t_n+\eta,t_{n+1}]. \tag{A.14}$$

Thus, the unique non-negative solution of the fourth equation of systems (A.1) and (A.2) is given by

$$Z^*(t)=\frac{1}{K_R^i}(1-e^{-r^i(t-(t-t_n))}) \quad \text{if } (t_n+\eta,t_{n+1}]. \tag{A.15}$$

Then, one has that
$\left|Z(t)-Z^*(t)\right|\longrightarrow 0$ as $t\longrightarrow\infty$ and consequently $\left|R(t)-R^*(t)\right|\longrightarrow 0$ as $t\longrightarrow\infty$.

Using the same reasoning, one has that $\left|P_r(t) - P_r^*(t)\right| \longrightarrow 0$, where

$$P_r^*(t) = \begin{cases} \left(P_r(t_n) - \dfrac{\Lambda_p}{\mu_{P_r}}\right)e^{-\mu_{P_r}(t-t_n)} + \dfrac{\Lambda_p}{\mu_{P_r}}, & t \in (t_n, t_n+\eta], \\ \left[\phi_{P_r}\left(P_r(t_n) - \dfrac{\Lambda_p}{\mu_{P_r}}\right)e^{-\mu_{P_r}\eta} + \dfrac{\Lambda_p}{\mu_{P_r}}(\phi_{P_r}+1) - \dfrac{\Lambda_p^i}{\mu_{P_r}^i}\right]e^{-\mu_{P_r}^i(t-(t_n+\eta))} + \dfrac{\Lambda_p^i}{\mu_{P_r}^i}, & t \in (t_n+\eta, t_{n+1}], \end{cases} \tag{A.16}$$

with

$$P_r(t_n) = \frac{\phi_0\left[-\phi_{P_r}e^{-\mu_{P_r}\eta-\mu_{P_r}^i(T-\eta)}\frac{\Lambda_p}{\mu_{P_r}} + \left(\frac{\Lambda_p}{\mu_{P_r}}(\phi_{P_r}+1) - \frac{\Lambda_p^i}{\mu_{P_r}^i}\right)e^{-\mu_{P_r}^i(T-\eta)} + \frac{\Lambda_p^i}{\mu_{P_r}^i}\right]}{1-\phi_0\phi_{P_r}e^{-\mu_{P_r}\eta-\mu_{P_r}^i(T-\eta)}}.$$

A.2. Proof of Lemma 1

In this Appendix, we present the comprehensive results that serve as justification for our analysis.

Let $C = C([-\tau, 0], \mathbb{R})$ the Banach space of continuous mapping from $[-\tau, 0]$ to $\mathbb{R}$ equipped with the sup-norm. The nonnegative cone of C is defined by $C_+ = C([-\tau, 0], \mathbb{R}_+)$. By the fundamental theory of functional differential equations [41], we know that there exists a unique solution $(L(t), F(t), S(t), I(t), E(t), A(t), R(t), P_r(t))$ of systems (2.9)–(2.19) satisfying the initial conditions (2.10), (2.11), and (2.25).

Positivity of solutions

From the first equation of systems (2.9)–(2.19), one has that

$$\begin{cases} \dot{L}_1(t) &= C(t)L_1 - \dfrac{\alpha(P(t))}{K_L}L_1^2(t), & \text{if } t \in (t_n, t_n+\eta], \\ \dot{L}(t) &= C^i(t)L_1 - \dfrac{\alpha^i(P(t))}{K_{L_1}}L_1^2(t), & \text{if } t \in (t_n+\eta, t_{n+1}], \end{cases} \tag{A.17}$$

where $C(t) = \alpha(P(t)) - \mu_{L_1}(T(t))$ and $C^i(t) = \alpha^i(P(t)) - \mu_{L_1}^i(T(t))$.

Setting $L(t) = \dfrac{1}{M(t)}$ and integrating the first and second equations of system (A.17) from t_n to t and from $t_n + \eta$ to t gives

$$M(t) = \begin{cases} M(t_n^+)e^{-\int_{t_n}^t C(m)dm} + \int_{t_n}^t \dfrac{\alpha(P(s))}{K_{L_1}}e^{-\int_s^t C(m)dm}ds, & \text{if } t \in (t_n, t_n+\eta], \\ M(t_n+\eta^+)e^{-\int_{t_n+\eta}^t C^i(w)dw} + \int_{t_n+\eta}^t \dfrac{\alpha^i(P(s))}{K_{L_1}^i}e^{-\int_s^t C^i(w)dw} & \text{if } t \in (t_n+\eta, t_{n+1}]. \end{cases} \tag{A.18}$$

Using the initial condition (2.11), it comes that $M(t_n + \eta^+) = \dfrac{1}{\pi_{L_1}}M(t_n + \eta)$. Hence,

$$M(t) = \begin{cases} M(t_n^+)e^{-\int_{t_n}^t C(m)dm} + \int_{t_n}^t \dfrac{\alpha(P(s))}{K_{L_1}}e^{-\int_s^t C(m)dm}ds, & \text{if } t \in (t_n, t_n+\eta], \\ \dfrac{1}{\pi_{L_1}}\left(M(t_n^+)e^{-\int_{t_n}^{t_n+\eta} C(s)ds} + \int_{t_n}^{t_n+\eta}\dfrac{\alpha(P(s))}{K_{L_1}}e^{-\int_s^{t_n+\eta} C(m)dm}ds\right)e^{-\int_{t_n+\eta}^t C^i(s)ds} & \\ + \int_{t_n+\eta}^t \dfrac{\alpha^i(P(s))}{K_{L_1}^i}e^{-\int_s^t C^i(m)dm}ds, & \text{if } t \in (t_n+\eta, t_{n+1}]. \end{cases} \tag{A.19}$$

Using Eq (2.19), it comes that $M(t_{n+1}^+) = \dfrac{1}{\psi_{L_1}} M(t_{n+1})$, and

$$\begin{aligned}\psi_{L_1} M(t_{n+1}^+) &= \frac{1}{\pi_{L_1}} M(t_n^+) e^{-\int_{t_n}^{t_n+\eta} C(s)ds + \int_{t_n+\eta}^{t_{n+1}} C^i(s)ds} + \frac{1}{\pi_{L_1}} \int_{t_n}^{t_n+\eta} \frac{\alpha_1(P(s))}{K_{L_1}} e^{-\int_s^{t_n+\eta} C(w)dw + \int_{t_n+\eta}^{t_{n+1}} C^i(w)dw} ds \\ &+ \int_{t_n+\eta}^{t_{n+1}} \frac{\alpha^i(P(s))}{K_{L_1}^i} e^{-\int_s^{t_{n+1}} C^i(w)dw} ds.\end{aligned} \tag{A.20}$$

Searching for a fixed point for M gives

$$M(t_n^+) = \frac{\dfrac{1}{\pi_{L_1}} \displaystyle\int_{t_n}^{t_n+\eta} \frac{\alpha(P(s))}{K_{L_1}} \exp\left(-\left(\int_s^{t_n+\eta} C(m)dm + \int_{t_n+\eta}^{t_{n+1}} C^i(m)dm\right)\right) ds}{\psi_{L_1} - \dfrac{1}{\pi_{L_1}} \exp\left(-\left(\displaystyle\int_{t_n}^{t_n+\eta} C(s)ds + \int_{t_n+\eta}^{t_{n+1}} C^i(s)ds\right)\right)}. \tag{A.21}$$

Thus,

$$M(t) = \begin{cases} \left(\dfrac{\dfrac{1}{\pi_{L_1}} \displaystyle\int_{t_n}^{t_n+\eta} \frac{\alpha(P(s))}{K_{L_1}} \exp\left(-\left(\int_s^{t_n+\eta} C(m)dm + \int_{t_n+\eta}^{t_{n+1}} C^i(m)dm\right)\right) ds}{\psi_L - \dfrac{1}{\pi_{L_1}} \exp\left(-\left(\displaystyle\int_{t_n}^{t_n+\eta} C(s)ds + \int_{t_n+\eta}^{t_{n+1}} C^i(s)ds\right)\right)}\right) \exp\left(-\displaystyle\int_{t_n}^{t} C(s)ds\right) \\ + \displaystyle\int_{t_n}^{t} \frac{\alpha(P(s))}{K_{L_1}} \exp(-\int_s^t C(m)dm)ds, & \text{if } t \in [t_n, t_n+\eta], \\ \dfrac{1}{\pi_{L_1}} \left(\dfrac{\dfrac{1}{\pi_{L_1}} \displaystyle\int_{t_n}^{t_n+\eta} \frac{\alpha(P(s))}{K_{L_1}} \exp\left(-\left(\int_s^{t_n+\eta} C(m)dm + \int_{t_n+\eta}^{t_{n+1}} C^i(m)dm\right)\right) ds}{\psi_{L_1} - \dfrac{1}{\pi_{L_1}} \exp\left(-\left(\displaystyle\int_{t_n}^{t_n+\eta} C(s)ds + \int_{t_n+\eta}^{t_{n+1}} C^i(s)ds\right)\right)}\right) \\ \exp\left(-\left(\displaystyle\int_{t_n}^{t_n+\eta} C(s)ds + \int_s^{t_n+\eta} C(m)dm\right)\right) \\ + \dfrac{1}{\pi_{L_1}} \displaystyle\int_{t_n}^{t_n+\eta} \frac{\alpha(P(s))}{K_{L_1}} \exp\left(-\left(\int_s^{t_n+\eta} C(m)dm + \int_{t_n+\eta}^{t} C^i(m)dm\right)\right) ds \\ + \displaystyle\int_{t_n+\eta}^{t} \frac{\alpha^i(P(s))}{K_{L_1}} \exp\left(-\int_s^t C^i(m)dm\right) ds, & \text{if } t \in [t_n+\eta, t_{n+1}]. \end{cases} \tag{A.22}$$

From Eq (A.22), it comes that $M(t) > 0$ for all $t > 0$ and consequently $L(t) > 0$ for all $t > 0$.

From the second equation of systems (2.9) and (2.19), it comes that

$$\begin{cases} \dot{F}(t) = \beta(T)L_1 - g(t)F, & \text{if } t \in (t_n, t_n+\eta], \\ \dot{F}(t) = \beta^i(T)L_1 - g^i(t)F, & \text{if } t \in (t_n+\eta, t_{n+1}], \end{cases} \tag{A.23}$$

where

$$g(t) = \frac{\beta(T)}{K_F} L_1(t) + \mu_F(T) + \nu_F(T) \text{ and } g^i(t) = \frac{\beta^i(T)}{K_F} L_1(t) + \mu_F^i(T) + \nu_F^i(T).$$

Integrating the first and second equations of system (A.23) from t_n to t and from $t_n + \eta$ to t yields

$$F(t) = \begin{cases} F(t_n^+) e^{-\int_{t_n}^t g(m)dm} + \displaystyle\int_{t_n}^t \beta(T(s))L_1(s) e^{-\int_s^t g(m)dm} ds, & \text{if } t \in (t_n, t_n+\eta], \\ F((t_n+\eta)^+) e^{-\int_{t_n+\eta}^t g^i(m)dm} + \displaystyle\int_{t_n+\eta}^t \beta^i(T(s))L_1(s) e^{-\int_s^t g^i(m)dm}, & \text{if } t \in (t_n+\eta, t_{n+1}]. \end{cases} \tag{A.24}$$

Using the fact that $F((t_n+\eta)^+) = \pi_F F(t_n+\eta)$, it comes that

$$F(t) = \begin{cases} F(t_n^+)e^{-\int_{t_n}^{t} g(m)dm} + \int_{t_n}^{t} \beta(T(s))L_1(s)e^{-\int_{s}^{t} g(m)dm}ds, \ \text{ if } (t_n, t_n+\eta], \\ \left(\pi_F F(t_n^+)e^{-\int_{t_n}^{t_n+\eta} g(m)dm} + \pi_F \int_{t_n}^{t_n+\eta} \beta(s)L_1(s)e^{-\int_{s}^{t_n+\eta} g(m)dm}ds\right)e^{-\int_{t_n+\eta}^{t} g^i(m)dm} + \\ + \int_{t_n+\eta}^{t} \beta^i(T(s))L_1(s)e^{-\int_{s}^{t} g^i(w)dw} \qquad \text{if } t \in (t_n+\eta, t_{n+1}]. \end{cases} \tag{A.25}$$

Using the fact that $F(t_{n+1}^+) = \psi_F F(t_{n+1})$ and searching for a fix point for F, it comes that

$$F(t_n^+) = \frac{\pi_F\psi_7 \int_{t_n}^{t_n+\eta} \beta(s)L_1(s)e^{-\left(\int_{s}^{t_n+\eta} g(m)dm + \int_{t_n+\eta}^{t_{n+1}} g^i(m)dm\right)}ds + \psi_F \int_{t_n+\eta}^{t_{n+1}} \beta^i(s)L_1(s)\exp\left(-\int_{s}^{t_{n+1}} g^i(s)ds\right)}{1 - \pi_F\psi_7 e^{-\left(\int_{t_n}^{t_n+\eta} g(m)dm + \int_{t_n+\eta}^{t_{n+1}} g^i(m)dm\right)}}.$$

Thus,

$$F(t) = \begin{cases} \left(\dfrac{\pi_F\psi_7 \int_{t_n}^{t_n+\eta} \beta(s)L_1(s)e^{-\left(\int_{s}^{t_n+\eta} g(m)dm + \int_{t_n+\eta}^{t_{n+1}} g^i(m)dm\right)}ds + \psi_F \int_{t_n+\eta}^{t_{n+1}} \beta^i(s)L_1(s)\exp\left(-\int_{s}^{t_{n+1}} g^i(s)ds\right)}{1 - \pi_F\psi_7 e^{-\left(\int_{t_n}^{t_n+\eta} g(m)dm + \int_{t_n+\eta}^{t_{n+1}} g^i(m)dm\right)}}\right) \\ \times e^{-\int_{t_n}^{t} g(m)dm} + \int_{t_n}^{t} \beta(T(s))L_1(s)e^{-\int_{s}^{t} g(m)dm}ds, \qquad \text{if } (t_n, t_n+\eta], \\ \left(\pi_F\left(\dfrac{\pi_F\psi_7 \int_{t_n}^{t_n+\eta} \beta(s)L_1(s)e^{-\left(\int_{s}^{t_n+\eta} g(m)dm + \int_{t_n+\eta}^{t_{n+1}} g^i(m)dm\right)}ds + \psi_F \int_{t_n+\eta}^{t_{n+1}} \beta^i(s)L_1(s)\exp\left(-\int_{s}^{t_{n+1}} g^i(s)ds\right)}{1 - \pi_F\psi_7 e^{-\left(\int_{t_n}^{t_n+\eta} g(m)dm + \int_{t_n+\eta}^{t_{n+1}} g^i(m)dm\right)}}\right)\right. \\ \times e^{-\int_{t_n}^{t_n+\eta} g(m)dm} + \pi_F \int_{t_n}^{t_n+\eta} \beta(s)L_1(s)e^{-\int_{s}^{t_n+\eta} g(m)dm}ds\Big)e^{-\int_{t_n+\eta}^{t} g^i(m)dm} + \int_{t_n+\eta}^{t} \beta^i(T(s))L_1(s)e^{-\int_{s}^{t} g^i(w)dw} \\ \qquad \text{if } t \in (t_n+\eta, t_{n+1}]. \end{cases} \tag{A.26}$$

Hence, $F(t) > 0$ for all $t > 0$.

Integrating the last equation of system (2.19) gives

$$R(t) = \frac{1}{e^{-\int_{t_n+\eta}^{t} \alpha(s)ds}\left[\dfrac{1}{\gamma} + \dfrac{r}{K_R}\displaystyle\int_{t_n+\eta}^{t} e^{\int_{t_n+\eta}^{\tau} \alpha(s)ds}d\tau\right]}, \quad t \in (t_n+\eta, t_{n+1}],$$

where

$$\alpha(s) = r\left(1 - \mu_R - \frac{d^i I(s)}{D^i + I(s)}\right), \quad M = \exp\left(\int_{t_n+\eta}^{t_{n+1}} \alpha(s)ds\right), \quad J = \int_{t_n+\eta}^{t_{n+1}} e^{\int_{t_n+\eta}^{\tau} \alpha(s)ds}d\tau,$$

and

$$\gamma = \frac{M/\psi_R - 1}{\dfrac{r}{K_R}J}.$$

Hence, $R(t) > 0$, for $t \in (t_n+\eta, t_{n+1}] > 0$.

Using the last equation of systems (2.9) and (2.19) yields:

$$P_r(t) = \begin{cases} e^{A(t,t_n)}\phi_0 P_r(t_n) + \Lambda_P \displaystyle\int_{t_n}^{t} e^{A(t,s)}\,ds, & t \in (t_n, t_n+\eta], \\ e^{B(t,t_n+\eta)}\left[\phi_{P_r}\left(E_1\phi_0 P_r(t_n) + \Lambda_P I_1\right) + \dfrac{\Lambda_P}{\mu_{P_r}}\right] + \Lambda_P^i \displaystyle\int_{t_n+\eta}^{t} e^{B(t,u)}\,du, & t \in (t_n+\eta, t_{n+1}], \end{cases}$$

where

$$A(t,s) = \int_s^t \left(\frac{\sigma\nu L(u)}{K_P + L(u)} - \mu_{P_r}\right)du, \quad B(t,s) = \int_s^t \left(\frac{\sigma^i\nu^i L(u)}{K_P^i + L(u)} - \mu_{P_r}^i\right)du,$$

$$E_1 = e^{A(t_n+\eta,t_n)}, \quad E_2 = e^{B(t_{n+1},t_n+\eta)}, \quad I_1 = \int_{t_n}^{t_n+\eta} e^{A(t_n+\eta,s)}ds, \quad I_2 = \int_{t_n+\eta}^{t_{n+1}} e^{B(t_{n+1},u)}du,$$

and

$$P_r(t_n) = \frac{\phi_0\left[E_2\phi_{P_r}\Lambda_P I_1 + E_2\dfrac{\Lambda_P}{\mu_{P_r}} + \Lambda_P^i I_2\right]}{1 - \phi_0^2\phi_{P_r}E_1E_2}.$$

Hence, it comes that $P_r(t) > 0$, for all $t > 0$.

Now, assume there exists $t > 0$ such that $(S(t), I(t)) \notin \mathbb{R}_+^{*2}$.

Let

$$t_1 = \inf\{t > 0,\ (S(t), I(t)) \notin \mathbb{R}_+^{*4}\}.$$

Then, one has that $t_1 > 0$, since $E(0) > 0$ and $A(0) > 0$ and $E(t_1) = 0$ or $S(t_1) = 0$ or $I(t_1) = 0$ and for all $-\tau \le t \le t_1$, $E(t) > 0$, $A(t) > 0$, $S(t) > 0$ and $I(t) > 0$.

Assume $S(t_1) = 0$. Integrating the third equation of systems (2.9)–(2.19) gives

$$S(t_1) = \begin{cases} \left[S(t_n^+) - \displaystyle\int_{t_n-\tau_1}^{t_n} \frac{\gamma\psi A(s)S(s)}{N(s)} e^{\int_{t_n}^{s+\tau_1}\mu_S(T(m))dm}ds\right] e^{-\int_{t_n}^{t_1}\mu_S(T(m))dm} \\ + \displaystyle\int_{t_n}^{t}\left(\nu_F(T(s))F(s)e^{\int_{t_n}^{s}\mu_S(T(m))dm} - \frac{\gamma\psi A(s)S(s)}{N(s)}e^{\int_{t_n}^{s+\tau_1}\mu_S(T(m))dm}\right) \\ + \displaystyle\int_{t_1-\tau_1}^{t_1}\frac{\gamma\psi A(s)S(s)}{N(s)}e^{\int_{t_n}^{s+\tau_1}\mu_S(T(m))dm}ds, \quad \text{if } t_1 \in (t_n, t_n+\eta], \\ \\ \pi_S\left[S(t_n^+) - \displaystyle\int_{t_n-\tau_1}^{t_n}\frac{\gamma\psi A(s)S(s)}{N(s)}e^{\int_{t_n}^{s+\tau_1}\mu_S(T(m))dm}ds\right]e^{-\int_{t_n}^{t_n+\eta}\mu_S(T(m))dm} \\ +\pi_S\displaystyle\int_{t_n}^{t_n+\eta}\left(\nu_F(T(s))F(s)e^{\int_{t_n}^{s}\mu_S(T(m))dm} - \frac{\gamma\psi A(s)S(s)}{N(s)}e^{\int_{t_n}^{s+\tau_1}\mu_S(T(m))dm}\right) \\ +\pi_S\displaystyle\int_{t_n+\eta-\tau_1}^{t_n+\eta}\frac{\gamma\psi A(s)S(s)}{N(s)}e^{\int_{t_n}^{s+\tau_1}\mu_S(T(m))dm}ds, \quad \text{if } t_1 \in (t_n+\eta, t_{n+1}]. \end{cases} \tag{A.27}$$

Using the initial condition (2.10), one has that

$$S(t_n^+) > \int_{t_n-\tau_1}^{t_n}\frac{\gamma\psi A(s)S(s)}{N(s)}e^{\int_{t_n}^{s+\tau_1}\mu_S(T(m))dm}ds.$$

Assume that for all $t > 0$,

$$F(t) > \frac{\gamma\psi A(t)S(t)}{\nu_F(T(t))N(t)}e^{\int_t^{t+\tau_1}\mu_S(T(m))dm}.$$

Then, $S(t_1) > 0$, which contradicts the hypothesis.

Assume $I(t_1) = 0$.

Integrating the fourth equation of systems (2.9) and (2.19) gives

$$I(t_1) = \begin{cases} I(t_n^+)e^{\int_{t_n}^{t_1}\left(\mu_I+d\frac{A(m)}{D+I(m)}\right)dm} + \int_{t_n}^{t_1}\frac{\gamma\psi A(s-\tau_1)S(s-\tau_1)}{N(s-\tau_1)}e^{\int_{t_1}^{s}\left(\mu_I+d\frac{A(m)}{D+I(m)}\right)dm}ds, & \text{if } t_1 \in (t_n, t_n+\eta] \\ \pi_I I(t_n^+)e^{\int_{t_n}^{t_n+\eta}\left(\mu_I+d\frac{A(m)}{D+I(m)}\right)dm} + \pi_I\int_{t_n}^{t_n+\eta}\frac{\gamma\psi A(s-\tau_1)S(s-\tau_1)}{N(s-\tau_1)}e^{\int_{t_n+\eta}^{s}\left(\mu_I+d\frac{A(m)}{D+I(m)}\right)dm}ds, & \text{if} \\ t_1 \in (t_n+\eta, t_{n+1}]. \end{cases} \tag{A.28}$$

Using the fact that $I(t_{n+1}) = \pi_I I(t_{n+1})$ yields

$$I(t_n^+) = \frac{\pi_I\int_{t_n}^{t_n+\eta}\frac{\gamma\psi A(s-\tau_1)S(s-\tau_1)}{N(s-\tau_1)}e^{\int_{t_n+\eta}^{s}\left(\mu_I+d\frac{A(m)}{D+I(s)}\right)dm}ds}{1-\pi_I\psi_I e^{-\int_{t_n}^{t_n+\eta}\left(\mu_I+d\frac{A(m)}{D+I(m)}\right)dm}}. \tag{A.29}$$

Plugging Eq (A.29) into Eq (A.28) gives $I(t_1) > 0$, which is a contradiction.

The fifth and sixth equations of the system (2.9) can be written in the following compact form:

$$\dot{X} = g(X),$$

where $X = (x_1, x_2)^T$, and

$$g(X) = \begin{pmatrix} g_1(X) \\ g_2(X) \end{pmatrix} = \begin{pmatrix} \varepsilon a x_2\left(1-\frac{x_1}{K_L(T)+\lambda_1 N}\right) - (\nu_L(T)+\mu_L(T))x_1 \\ \nu_L(T)x_1 - \left(\frac{\mu_A(T)}{1+\lambda_2 N} - \frac{ed_1 I}{D+I}\right)x_2 \end{pmatrix}.$$

Note that $g_1(0, x_2) \geq 0$ and $g_2(x_1, 0) \geq 0$. Hence, every solution that starts in $\mathbb{R}^2_+$ remains in $\mathbb{R}^2_+$.

In the same way, one shows the positivity of L and A of the system (2.19).

Now, we prove the boundedness of solutions.

We first show that $L_1(t) \leq K_{L_1}$ for all $t \in (t_n, t_n+\eta]$.

Suppose there exists $t_0 \in (t_n, t_n+\eta]$ such that $L_1(t_0) > K_L$. By continuity, there exists $t_1 < t_0$ such that $L(t_1) = K_{L_1}$ and $L_1(t) > K_L$ for $t \in]t_1, t_0]$. Thus, if $L_1(t_1) = K_{L_1}$, one has that

$$\dot{L}_1(t) = -\mu_{L_1}(T)L_1(t_1) < 0.$$

Consequently, there exists $t^* \in]t_1, t_0[$ such that $L_1(t^*) < K_{L_1}$, which is absurd because $L_1(t) > K_{L_1}$, $\forall t \in]t_1, t_0]$. Thus, $L_1(t) \leq K_{L_1}$ for all $t \in (t_n, t_n+\eta]$. Additionally, one can show that $L_1(t) \leq K^i_{L_1}$, for all $t \in (t_n+\eta, t_{n+1}]$. Hence,

$$L_1(t) \leq K_{L_1} + K^i_{L_1} = M_0, \text{ for all } t \in (t_n, t_{n+1}]. \tag{A.30}$$

With a similar reasoning, one can demonstrate that

$$F(t) \leq K_F + K^i_F = M_1, \text{ for all } t \in (t_n, t_{n+1}]. \tag{A.31}$$

Adding the third and fifth equations of the system (2.9) gives

$$\dot{S}(t) + \dot{I}(t) \leq \nu_{F_{max}} M_1 - \min\{\mu_{S_{\min}}, \mu_I\}(S(t)+I(t)). \tag{A.32}$$

Applying the Gronwall lemma to Eq (A.29) yields

$$S(t)+I(t)\leq \frac{\nu_{F_{max}}M_1}{\min\{\mu_{S_{\min}},\mu_I\}}+\left(S(t_n^+)+I(t_n^+)-\frac{\nu_{F_{max}}M_1}{\min\{\mu_{S_{\min}},\mu_I\}}\right)\exp\left(-\min\{\mu_{S_{\min}},\mu_I\}(t-t_n)\right). \quad (A.33)$$

Taking the initial condition during the cropping season such that

$$S(t_n^+)+I(t_n^+)\leq \frac{\nu_{F_{max}}M_1}{\min\{\mu_{S_{\min}},\mu_I\}},$$

and the limit of Eq (A.33) when t tends to $+\infty$ gives

$$\lim_{t\to+\infty}\sup\left(S(t)+I(t)\right)\leq \frac{\nu_{F_{2max}}M_1}{\min\{\mu_{S_{\min}},\mu_{F_I}\}}=M_2.$$

In the same way, adding and integrating the third and fourth equations of the system (2.19) gives

$$\begin{aligned} S(t)+I(t) &= S((t_n+\eta)^+)+I((t_n+\eta)^+),\\ &\leq (\pi_S+\pi_I)M_2. \end{aligned} \quad (A.34)$$

Hence,

$$\lim_{t\to+\infty}\sup\left(S(t)+I(t)\right)\leq(\pi_S+\pi_I)M_2. \quad (A.35)$$

Then, for all $t\in[t_n,t_{n+1}]$ one has that

$$\lim_{t\to+\infty}\sup\left(S(t)+I(t)\right)\leq(1+(\pi_S+\pi_I))M_2=M_3.$$

We now show that $R(t)\leq K_R$ for all $t\in(t_n+\eta,t_{n+1}]$.

Suppose there exists $t_0\in(t_n+\eta,t_{n+1}]$ such that $R(t_0)>K_R$. By continuity, there exists $t_1<t_0$ such that $R(t_1)=K_R^i$ and $R(t)>K_R$ for $t\in]t_1,t_0]$. Thus, if $R(t_1)=K_R$, one has that

$$\dot{R}(t)=-\left(\mu_R+\frac{d^iI(t_1)}{D^i+I(t_1)}\right)<0.$$

Consequently, there exists $t^*\in]t_1,t_0[$ such that $R(t^*)<K_R$, which is absurd because $R(t)>K_R$, for all $t\in]t_1,t_0]$. Thus, $R(t)\leq K_R$ for all $t\in(t_n+\eta,t_{n+1}]$. Additionally, one can show that $R(t)\leq K_R$, for all $t\in(t_n+\eta,t_{n+1}]$. Hence,

$$R(t)\leq K_R,\ \text{for all } t\in(t_n+\eta,t_{n+1}]. \quad (A.36)$$

Using the same reasoning as for the case of the boundedness of L_1 or F, one can prove that $L(t)\leq K_{l_{\max}}+K^i_{L_{\max}}+\lambda_1M_3+\gamma_RK_R=M_4$, for all $t\in(t_n,t_{n+1}]$.

From the sixth equation of system (2.9), one has that

$$\dot{A}(t)\leq \nu_{L_{\max}}M_3-\left(\frac{\mu_{A_{\min}}}{1+\lambda_2M_2}-ed\right)A(t). \quad (A.37)$$

Integrating Eq (A.37) from t_n to t gives

$$A(t)\leq\left(A(t_n^+)-\frac{\nu_{L_{\max}}M_3(1+\lambda_2M_2)}{\mu_{A_{\min}}-ed(1+\lambda_2M_2)}\right)e^{-\left(\frac{\mu_{A_{\min}}}{1+\lambda_2M_2}-ed\right)(t-t_n)}+\frac{\nu_{L_{\max}}M_3(1+\lambda_2M_2)}{\mu_{A_{\min}}-ed(1+\lambda_2M_2)}. \quad (A.38)$$

Taking the initial condition such that $A(t_n^+) \leq \dfrac{\nu_{L_{\max}} M_3(1+\lambda_2 M_2)}{\mu_{A_{\min}} - ed(1+\lambda_2 M_2)}$ and the limit of the above equation when t tends to $+\infty$ gives

$$\lim_{t\to+\infty} \sup A(t) \leq \frac{\nu_{L_{\max}} M_3(1+\lambda_2 M_2)}{\mu_{A_{\min}} - ed(1+\lambda_2 M_2)}.$$

In the same way, integrating the sixth equation of the system (2.19) from $t_n + \eta$ to t yields

$$A(t) \leq \left(A(t_n+\eta^+) - \frac{\nu^i_{L_{\max}} M_3(1+\lambda_3 K_R)}{\mu^i_{A_{\min}} - e^i d^i(1+\lambda_3 K_R)}\right) e^{-\left(\frac{\mu^i_{A_{\min}}}{1+\lambda_4 K_R} - e^i d^i\right)(t-(t_n+\eta))} + \frac{\nu^i_{L_{\max}} M_3(1+\lambda_3 K_R)}{\mu^i_{A_{\min}} - e^i d^i(1+\lambda_3 K_R)}. \quad \text{(A.39)}$$

Taking the initial condition such that $A(t_n+\eta^+) \leq \dfrac{\nu^i_{L_{\max}} M_3(1+\lambda_3 K_R)}{\mu^i_{A_{\min}} - e^i d^i(1+\lambda_3 K_R)}$ and the limit of the above equation when t tends to $+\infty$ gives

$$\lim_{t\to+\infty} \sup A(t) \leq \frac{\nu^i_{L_{\max}} M_3(1+\lambda_3 K_R)}{\mu^i_{A_{\min}} - e^i d^i(1+\lambda_3 K_R)}.$$

Hence,

$$\lim_{t\to+\infty} \sup A(t) \leq \frac{\nu_{L_{\max}} M_3(1+\lambda_2 M_2)}{\mu_{A_{\min}} - ed(1+\lambda_2 M_2)} + \frac{\nu^i_{L_{\max}} M_3(1+\lambda_3 K_R)}{\mu^i_{A_{\min}} - e^i d^i(1+\lambda_3 K_R)} = M_5, \ \forall t \in [t_n, t_{n+1}]. \quad \text{(A.40)}$$

Applying the Gronwall Lemma to the last equations of systems (2.9) and (2.11) gives

$$\lim_{t\to+\infty} \sup P_r(t) \leq \frac{\Lambda_p}{\mu_p - \sigma\nu} + \frac{\Lambda^i_p}{\mu^i_p - \sigma^i\nu^i} = M_6, \ \forall \ t \in [t_n, t_{n+1}].$$

A.3. Variable and parameter values of systems (2.9) and (2.11)

Herein, we present the variable and the parameter values of systems (2.9) and (2.11).

Table A.1. Description variables of systems (2.9) and (2.11).

Symbols	Description
$L_1(t)$	Number of leaves at time t.
$F(t)$	Number of flowers at time t.
$S(t)$	Healthy fruits at time t.
$I(t)$	Infected fruits at time t.
$L(t)$	Number of immature females at time t.
$A(t)$	Number of mature females at time t.
$R(t)$	Natural reservoirs at time t.
$P_r(t)$	Parasitoids at time t.

Table A.2. Parameter values, units, and minimum/maximum bounds for plant components (leaves, flowers, and fruits).

	Parameter	Biological description	Unit	Value used	Min	Max	Source
			Leaf parameters				
α	Main season	Intrinsic growth rate	day^{-1}	0.45	0.01	0.80	[42]
α^i	Inter-cropping	Intrinsic growth rate	day^{-1}	0.08	0.01	0.80	[42]
K_{L_1}	Main season	Maximum carrying capacity	plant^{-1}	37.5	25.0	50.0	[21]
K_L^i	Inter-cropping	Maximum carrying capacity	plant^{-1}	27.5	25.0	50.0	[21]
μ_{L_1}	Main season	Mortality rate	day^{-1}	0.002	0.0010	0.59	[23]
$\mu_{L_1}^i$	Inter-cropping	Mortality rate	day^{-1}	0.02	0.0033	0.60	[23]
			Flower parameters				
β	main season	Intrinsic growth rate	day^{-1}	0.70	0.55	0.89	[42]
β^i	inter-cropping	Intrinsic growth rate	day^{-1}	0.07	0.01	0.80	[42]
K_F	main season	Carrying capacity limit	plant^{-1}	30.0	25.0	35.0	[21]
K_F^i	inter-cropping	Carrying capacity limit	plant^{-1}	20.0	15.0	35.0	[21]
μ_F	main season	Mortality rate	day^{-1}	0.05	0.0033	0.60	[23]
μ_F^i	inter-cropping	Mortality rate	day^{-1}	0.025	0.0033	0.60	[23]
ν_F	main season	Development rate	day^{-1}	0.75	0.66	0.80	[23]
ν_F^i	inter-cropping	Development rate	day^{-1}	0.45	0.36	0.70	[23]
			Fruit parameters				
μ_I	main season	Mortality rate (infected)	day^{-1}	$5 \cdot 10^{-3}$	0.00	0.99	[23]
μ_S	main season	Mortality rate (healthy)	day^{-1}	0.02	0.0033	0.073	[23]
τ	main season	Maturation period	day	25.0	1.0	40.0	[21]

Table A.3. Parameter values, units, and minimum/maximum bounds for insect and reservoir dynamics.

	Parameter	Biological description	Unit	Value used	Min	Max	Source
			Insect parameters				
μ_L	Main season	Mortality rate (immature Φ)	day^{-1}	0.02	0.010	0.99	[12]
μ_L^i	Inter-cropping	Mortality rate (immature Φ)	day^{-1}	0.025	0.010	0.19	[12]
μ_A	Main season	Mortality rate (mature Φ)	day^{-1}	0.05	0.010	0.75	[12]
μ_A^i	Inter-cropping	Mortality rate (mature Φ)	day^{-1}	0.025	0.010	0.19	[12]
a	Main season	Average eggs laid per female	$\text{eggs} \cdot \text{female}^{-1}$	80.0	1.0	600.0	[12]
a^i	Inter-cropping	Average eggs laid per female	$\text{eggs} \cdot \text{female}^{-1}$	30.0	1.0	600.0	[12]
ν_L	Main season	Development rate (eggs)	day^{-1}	0.30	0.15	0.45	[12]
ν_L^i	Inter-cropping	Development rate (immatures)	day^{-1}	0.29	0.27	0.65	[12]
			Reservoir parameters				
r	Main season	Intrinsic growth rate	day^{-1}	0.35	0.01	1.00	*
r^i	Inter-cropping	Intrinsic growth rate	day^{-1}	0.65	0.01	1.00	*
K_R	Inter-cropping	Carrying capacity limit	individuals	1500	500	2000	*
μ_R	Inter-cropping	Mortality rate	day^{-1}	0.23	0.01	1.00	*

* Assumed value.

A.4. Proof of convergence of variables $L_1(t)$, $F(t)$, $S(t)$, $R(t)$, and $P_r(t)$

Herein, we rigorously demonstrate the asymptotic convergence of the host-plant components (L_1, F, S), the environmental reservoir (R), and the parasitoid population (P_r).

Setting $E(t) = A(t) = 0$ for all $t > 0$ in systems (2.9) and (2.19) yields the following pest-free dynamics:

$$\begin{cases} \dot{L}_1(t) &= C(t)L_1 - \dfrac{\alpha(P(t))}{K_{L_1}}L_1^2(t), \\ \dot{F}(t) &= \beta(T)L_1 - B(t)F, \qquad \text{if } t \in (t_n, t_n + \eta], \\ \dot{S}(t) &= \nu_F(T(t))F - \mu_S(T(t))S, \\ \dot{P}_r(t) &= \Lambda_p - \mu_{P_r}P_r, \end{cases} \tag{A.41}$$

and

$$\begin{cases} \dot{L}_1(t) &= C^i(t)L_1 - \dfrac{\alpha^i(P(t))}{K_{L_1}}L_1^2(t), \\ \dot{F}(t) &= \beta^(T(t))L_1 - B^i(t)F, \\ \dot{S}(t) &= 0, \qquad \text{if } t \in (t_n + \eta, t_{n+1}], \\ \dot{R}(t) &= r^i R\left(1 - \dfrac{R}{K_R^i}\right), \\ \dot{P}_r(t) &= \Lambda_p^i - \mu_{P_r}^i P_r. \end{cases} \tag{A.42}$$

Setting $L_1(t) = \dfrac{1}{M(t)}$ and integrating the first equation of systems (A.41) and (A.42) from t_n to t gives

$$M(t) = \begin{cases} M(t_n^+)e^{-\int_{t_n}^t C(m)dm} + \int_{t_n}^t \dfrac{\alpha_1(P(s))}{K_{L_1}}e^{-\int_s^t C(m)dm}ds \text{ if } t \in (t_n, t_n + \eta], \\ M((t_n + \eta)^+)e^{-\int_{t_n+\eta}^t C^i(m)dm} + \int_{t_n+\eta}^t \dfrac{\alpha^i(P(s))}{K_{L_1}^i}e^{-\int_s^t C^i(m)dm}ds \text{ if } t \in (t_n + \eta, t_{n+1}]. \end{cases} \tag{A.43}$$

Since $L_1(t_n + \eta^+) = \pi_{L_1}L_1(t_n + \eta)$, it comes that $M(t_n + \eta^+) = \dfrac{1}{\pi_{L_1}}M(t_n + \eta)$. Hence, from the second equation of (A.43), one can deduce that

$$\begin{aligned} M(t) &= \frac{1}{\pi_{L_1}}\left(M(t_n^+)e^{-\int_{t_n}^{t_n+\eta} C(s)ds} + \int_{t_n}^{t_n+\eta} \frac{\alpha_1(P(s))}{K_{L_1}}e^{-\int_s^{t_n+\eta} C(m)dm}ds\right)e^{-\int_{t_n+\eta}^t C^i(s)ds} \\ &+ \int_{t_n+\eta}^t \frac{\alpha^i(P(s))}{K_{L_1}}e^{-\int_s^t C^i(m)dm}ds, \text{ if } t \in (t_n + \eta, t_{n+1}]. \end{aligned} \tag{A.44}$$

Now, let us find $M(t_n^+)$.

Using the fact that $M(t_{n+1}^+) = \dfrac{1}{\psi_{L_1}}M(t_{n+1})$, it comes that $Z(t_{n+1}^+) = \dfrac{1}{\psi_{L_1}}Z(t_{n+1})$. Then, from Eq (A.44), it comes that

$$\begin{aligned} \psi_{L_1}M(t_{n+1}^+) &= \frac{1}{\pi_{L_1}}M(t_n^+)e^{-\int_{t_n}^{t_n+\eta} C(s)ds + \int_{t_n+\eta}^{t_{n+1}} C^i(s)ds} + \frac{1}{\pi_{L_1}}\int_{t_n}^{t_n+\eta} \frac{\alpha_1(P(s))}{K_{L_1}}e^{-\int_s^{t_n+\eta} C(w)dw + \int_{t_n+\eta}^{t_{n+1}} C^i(w)dw}ds \\ &+ \int_{t_n+\eta}^{t_{n+1}} \frac{\alpha^i(P(s))}{K_{L_1}}e^{-\int_s^{t_{n+1}} C^i(w)dw}ds. \end{aligned} \tag{A.45}$$

Searching for a fixed point for M gives

$$M(t_n^+) = \frac{\frac{1}{\pi_{L_1}} \int_{t_n}^{t_n+\eta} \frac{\alpha(P(s))}{K_{L_1}} \exp\left(-\left(\int_s^{t_n+\eta} C(m)dm + \int_{t_n+\eta}^{t_{n+1}} C^i(m)dm\right)\right) ds}{\psi_{L_1} - \frac{1}{\pi_{L_1}} \exp\left(-\left(\int_{t_n}^{t_n+\eta} C(s)ds + \int_{t_n+\eta}^{t_{n+1}} C^i(s)ds\right)\right)}. \tag{A.46}$$

Thus, the unique non-negative solution of the first equation of the system (A.41) is given by

$$M^*(t) = \begin{cases} \left(\frac{\frac{1}{\pi_{L_1}} \int_{t_n}^{t_n+\eta} \frac{\alpha(P(s))}{K_{L_1}} \exp\left(-\left(\int_s^{t_n+\eta} C(m)dm + \int_{t_n+\eta}^{t_{n+1}} C^i(m)dm\right)\right) ds}{\psi_{L_1} - \frac{1}{\pi_{L_1}} \exp\left(-\left(\int_{t_n}^{t_n+\eta} C(s)ds + \int_{t_n+\eta}^{t_{n+1}} C^i(s)ds\right)\right)}\right) \exp\left(-\int_{t_n}^{t} C(s)ds\right) \\ + \int_{t_n}^{t} \frac{\alpha(P(s))}{K_{L_1}} \exp(-\int_s^t C(m)dm)ds, \qquad \text{if } t \in [t_n, t_n+\eta], \\ \\ \frac{1}{\pi_{L_1}} \left(\left(\frac{\frac{1}{\pi_{L_1}} \int_{t_n}^{t_n+\eta} \frac{\alpha(P(s))}{K_{L_1}} \exp\left(-\left(\int_s^{t_n+\eta} C(m)dm + \int_{t_n+\eta}^{t_{n+1}} C^i(m)dm\right)\right) ds}{\psi_{L_1} - \frac{1}{\pi_{L_1}} \exp\left(-\left(\int_{t_n}^{t_n+\eta} C(s)ds + \int_{t_n+\eta}^{t_{n+1}} C^i(s)ds\right)\right)}\right) \exp\left(-\int_{t_n}^{t_n+\eta} C(s)ds\right) \right. \\ \left. + \int_{t_n}^{t_n+\eta} \frac{\alpha(P(s))}{K_{L_1}} \exp\left(-\int_s^{t_n+\eta} C(m)dm\right) ds\right) \exp\left(-\int_{t_n+\eta}^{t} C^i(s)ds\right) \\ + \int_{t_n+\eta}^{t} \frac{\alpha^i(P(s))}{K_{L_1}} \exp\left(-\int_s^t C^i(m)dm\right) ds, \qquad \text{if } t \in [t_n+\eta, t_{n+1}]. \end{cases} \tag{A.47}$$

Then, one can show that

$$\left|M(t) - M^*(t)\right| = \begin{cases} \left(\frac{\frac{1}{\pi_{L_1}} \int_{t_n}^{t_n+\eta} \frac{\alpha(P(s))}{K_{L_1}} \exp\left(-\left(\int_s^{t_n+\eta} C(m)dm + \int_{t_n+\eta}^{t_{n+1}} C^i(m)dm\right)\right) ds}{\psi_{L_1} - \frac{1}{\pi_{L_1}} \exp\left(-\left(\int_{t_n}^{t_n+\eta} A(s)ds + \int_{t_n+\eta}^{t_{n+1}} C^i(s)ds\right)\right)}\right) \exp\left(-\int_{t_n}^{t} C(s)ds\right), \\ \qquad \text{if } t \in [t_n, t_n+\eta], \\ \\ \frac{1}{\pi_{L_1}} \left(\left(\frac{\frac{1}{\pi_{L_1}} \int_{t_n}^{t_n+\eta} \frac{\alpha(P(s))}{K_{L_1}} \exp\left(-\left(\int_s^{t_n+\eta} C(m)dm + \int_{t_n+\eta}^{t_{n+1}} C^i(m)dm\right)\right) ds}{\psi_{L_1} - \frac{1}{\pi_{L_1}} \exp\left(-\left(\int_{t_n}^{t_n+\eta} C(s)ds + \int_{t_n+\eta}^{t_{n+1}} C^i(s)ds\right)\right)}\right) \exp\left(-\int_{t_n}^{t_n+\eta} C(s)ds\right) \right. \\ \left. + \int_{t_n}^{t_n+\eta} \frac{\alpha(P(s))}{K_{L_1}} \exp\left(-\int_s^{t_n+\eta} C(m)dm\right) ds\right) \exp\left(-\int_{t_n+\eta}^{t} C^i(s)ds\right). \quad \text{if } t \in [t_n+\eta, t_{n+1}]. \end{cases}$$

It is clear that $\left|M(t) - M^*(t)\right| \longrightarrow 0$ as $t \longrightarrow \infty$. Hence, one can deduce that $\left|L(t) - L^*(t)\right| \longrightarrow 0$ as $t \longrightarrow \infty$.

Integrating the second equation of systems (A.41) and (A.42) from t_n to t and from $t_n + \eta$ to t gives

$$F(t) = \begin{cases} F(t_n^+)e^{-\int_{t_n}^{t} B(m)dm} + \int_{t_n}^{t} \beta(T(s))L_1^*(s)e^{-\int_s^t g(m)dm}ds, \ \text{ if } \ (t_n, t_n+\eta], \\ F((t_n+\eta)^+)e^{-\int_{t_n+\eta}^{t} B^i(m)dm} + \int_{t_n+\eta}^{t} \beta^i(T(s))L_1^*(s)e^{-\int_s^t B^i(w)dw}, \qquad \text{if } \ t \in (t_n+\eta, t_{n+1}]. \end{cases} \tag{A.48}$$

Using the fact that $F((t_n+\eta)^+) = \pi_F F(t_n+\eta)$, it comes that

$$F(t) = \begin{cases} F(t_n^+)e^{-\int_{t_n}^{t} B(m)dm} + \int_{t_n}^{t} \beta(T(s))L_1^*(s)e^{-\int_s^t B(m)dm}ds, \ \text{ if } (t_n, t_n+\eta], \\ \left(\pi_F F(t_n^+)e^{-\int_{t_n}^{t_n+\eta} B(m)dm} + \pi_F \int_{t_n}^{t_n+\eta} \beta(s)L_1^*(s)e^{-\int_s^{t_n+\eta} B(m)dm}ds\right)e^{-\int_{t_n+\eta}^{t} B^i(m)dm} + \\ + \int_{t_n+\eta}^{t} \beta^i(T(s))L_1^*(s)e^{-\int_s^t B^i(w)dw} \qquad \text{if } t \in (t_n+\eta, t_{n+1}]. \end{cases} \tag{A.49}$$

Using the fact that $F(t_{n+1}^+) = \psi_F F(t_{n+1})$ and searching for a fix point for F, it comes that

$$F(t_n^+) = \frac{\pi_F\psi_7 \int_{t_n}^{t_n+\eta} \beta(s)L^*(s)e^{-\left(\int_s^{t_n+\eta} B(m)dm + \int_{t_n+\eta}^{t_{n+1}} B^i(m)dm\right)}ds + \psi_F \int_{t_n+\eta}^{t_{n+1}} \beta^i(s)L_1^*(s)\exp\left(-\int_s^{t_{n+1}} B^i(s)ds\right)}{1-\pi_F\psi_7 e^{-\left(\int_{t_n}^{t_n+\eta} B(m)dm + \int_{t_n+\eta}^{t_{n+1}} B^i(m)dm\right)}}$$

Thus, the unique non-negative solution of the second equation of systems (A.41) and (A.42) is given by

$$F^*(t) = \begin{cases} \left(\dfrac{\pi_F\psi_F \int_{t_n}^{t_n+\eta} \beta(s)L_1^*(s)e^{-\left(\int_s^{t_n+\eta} B(m)dm + \int_{t_n+\eta}^{t_{n+1}} B^i(m)dm\right)}ds + \psi_F \int_{t_n+\eta}^{t_{n+1}} \beta^i(s)L_1^*(s)\exp\left(-\int_s^{t_{n+1}} B^i(s)ds\right)}{1-\pi_F\psi_7 e^{-\left(\int_{t_n}^{t_n+\eta} B(m)dm + \int_{t_n+\eta}^{t_{n+1}} B^i(m)dm\right)}}\right) \\ \times e^{-\int_{t_n}^{t} B(m)dm} + \int_{t_n}^{t} \beta(T(s))L_1^*(s)e^{-\int_s^t B(m)dm}ds, \qquad \text{if } (t_n, t_n+\eta], \\ \left(\pi_F\left(\dfrac{\pi_F\psi_F \int_{t_n}^{t_n+\eta} \beta(s)L^*(s)e^{-\left(\int_s^{t_n+\eta} B(m)dm + \int_{t_n+\eta}^{t_{n+1}} B^i(m)dm\right)}ds + \psi_F \int_{t_n+\eta}^{t_{n+1}} \beta^i(s)L^*(s)\exp\left(-\int_s^{t_{n+1}} B^i(s)ds\right)}{1-\pi_F\psi_7 e^{-\left(\int_{t_n}^{t_n+\eta} B(m)dm + \int_{t_n+\eta}^{t_{n+1}} B^i(m)dm\right)}}\right)\right. \\ \left. \times e^{-\int_{t_n}^{t_n+\eta} B(m)dm} + \pi_F \int_{t_n}^{t_n+\eta} \beta(s)L_1^*(s)e^{-\int_s^{t_n+\eta} B(m)dm}ds\right)e^{-\int_{t_n+\eta}^{t} B^i(m)dm} + \int_{t_n+\eta}^{t} \beta^i(T(s))L_1^*(s)e^{-\int_s^t B^i(w)dw} \\ \qquad \text{if } t \in (t_n+\eta, t_{n+1}]. \end{cases} \tag{A.50}$$

Then, one can show that

$$\left|F(t) - F^*(t)\right| = \begin{cases} \left(\dfrac{\pi_F\psi_F \int_{t_n}^{t_n+\eta} \beta(s)L_1^*(s)e^{-\left(\int_s^{t_n+\eta} B(w)ds + \int_{t_n+\eta}^{t_{n+1}} B^i(w)dw\right)ds} + \psi_F \int_{t_n+\eta}^{t_{n+1}} \beta^i(s)L_1(s)e^{-\int_s^{t_{n+1}} B^i(w)dw}}{1-\pi_F\psi_F e^{-\left(\int_{t_n}^{t_n+\eta} B(s) + \int_{t_n+\eta}^{t_{n+1}} B^i(w)dw\right)}}\right) \\ \times \exp\left(-\int_{t_n}^{t} g(w)dw\right) \ \text{ if } (t_n, t_n+\eta], \\ \pi_F\left(\dfrac{\pi_F\psi_F \int_{t_n}^{t_n+\eta} \beta(s)L_1^*(s)e^{-\left(\int_s^{t_n+\eta} B(w)ds + \int_{t_n+\eta}^{t_{n+1}} B^i(w)dw\right)ds} + \psi_2 \int_{t_n+\eta}^{t_{n+1}} \beta^i(s)L_1^*(s)e^{-\int_s^{t_{n+1}} B^i(w)dw}}{1-\pi_2\psi_2 e^{-\left(\int_{t_n}^{t_n+\eta} B(s) + \int_{t_n+\eta}^{t_{n+1}} B^i(w)dw\right)}}\right) \\ \times \exp\left(-\int_{t_n}^{t} B^i(w)dw\right) \ \text{ if } t \in (t_n+\eta, t_{n+1}]. \end{cases}$$

It then comes that $|F(t) - F^*(t)| \longrightarrow 0$ as $t \longrightarrow \infty$.

Integrating the third equation of systems (A.41) and (A.42) from t_n to t and from $t_n+\eta$ to t gives

$$S(t) = \begin{cases} S(t_n^+)e^{-\int_{t_n}^{t} \mu_S(T(m))dm} + \int_{t_n}^{t} \nu_F(T(s))F^*(s)e^{-\int_s^t \mu_S(T(m))dm}ds, \ \text{if } t \in (t_n, t_n+\eta] \\ S((t_n+\eta)^+) \qquad \text{if } t \in (t_n+\eta, t_{n+1}]. \end{cases} \tag{A.51}$$

Using the fact that $S(t_n + \eta^+) = 0$ and $S(t_{n+1}^+) = 0$, one has that $S(t_n^+) = 0$.

Thus, the unique non-negative solution of the second equation of systems (A.41) and (A.42) is given by

$$S^*(t) = \begin{cases} \int_{t_n}^{t} \nu_F(T(s))F(s)e^{-\int_s^t \mu_S(T(m))dm}ds, & \text{if } (t_n, t_n + \eta], \\ 0 & \text{if } t \in (t_n + \eta, t_{n+1}]. \end{cases} \tag{A.52}$$

With this in mind, one has that

$$\left|S(t) - S^*(t)\right| = \begin{cases} 0 \text{ if } (t_n, t_n + \eta], \\ 0 \text{ if } t \in (t_n + \eta, t_{n+1}]. \end{cases}$$

Then, $\left|S(t) - S^*(t)\right| \longrightarrow 0$ as $t \longrightarrow \infty$.

Setting $Z(t) = \dfrac{1}{R(t)}$ and integrating the fourth equation of systems (A.41) and (A.42) gives

$$Z(t) = Z((t_n + \eta)^+)e^{-r^i(t-(t_n+\eta)} + \frac{1}{K_R}(1 - e^{-r^i(t-(t_n+\eta))}) \text{ if } (t_n + \eta, t_{n+1}]. \tag{A.53}$$

Using the fact that $Z((t_n + \eta)^+) = 0$, it comes that

$$Z(t) = \frac{1}{K_R}(1 - e^{-r^i(t-(t-t_n))}) \text{ if } (t_n + \eta, t_{n+1}]. \tag{A.54}$$

Thus, the unique non-negative solution of the fourth equation of systems (A.41) and (A.42) is given by

$$Z^*(t) = \frac{1}{K_R^i}(1 - e^{-r^i(t-(t-t_n))}) \quad \text{if } (t_n + \eta, t_{n+1}]. \tag{A.55}$$

Then, one has that

$\left|Z(t) - Z^*(t)\right| \longrightarrow 0$ as $t \longrightarrow \infty$ and consequently $\left|R(t) - R^*(t)\right| \longrightarrow 0$ as $t \longrightarrow \infty$.

Using the same reasoning, one has that $\left|P_r(t) - P_r^*(t)\right| \longrightarrow 0$, where

$$P_r^*(t) = \begin{cases} \dfrac{\psi_{P_r}\phi_{P_r}\Lambda_p \exp(-\mu_{P_r}^i(\mathcal{T} - \eta))}{m(1 - \psi_{P_r}\phi_{P_r})\exp(-(\eta\mu_{P_r} + \mu_{P_r}^i(\mathcal{T} - \eta))} \exp(-\mu_{P_r}(t - t_n)), \text{ if } t \in (t_n, t_n + \eta], \\ \phi_{P_r}\left(\dfrac{\psi_{P_r}\phi_{P_r}\Lambda_p \exp(-\mu_{P_r}^i(\mathcal{T} - \eta))}{m(1 - \psi_{P_r}\phi_{P_r})\exp(-(\eta\mu_{P_r} + \mu_{P_r}^i(\mathcal{T} - \eta))} \exp(-\eta\mu_{P_r}) + \dfrac{\Lambda_p}{m}\right)e^{-\mu_{P_r}^i(t-(t_n+\eta)))}, \text{ if } t \in (t_n + \eta, t_{n+1}]. \end{cases} \tag{A.56}$$